# MAPPING PERMAFROST AND GROUND-ICE RELATED COASTAL EROSION ON HERSCHEL ISLAND, SOUTHERN BEAUFORT SEA, YUKON TERRITORY, CANADA

**Hugues Lantuit, Dept. of Geography, McGill University, Montréal**

**November, 2004**

**A thesis submitted to McGill University in partial fulfilment of the requirements of the degree of Masters of Science**

*Your file Votre référence*
*ISBN: 0-494-12481-4*
*Our file Notre référence*
*ISBN: 0-494-12481-4*

*"While there was a connection from the Island to the mainland, they called them Nuvuraqmiut (the "Point" people)... and after it became an island, they called it Qikiqtaruk (It is island)."*

Jean Tardiff

## ABSTRACT

Climate change and warming have been linked to enhanced coastal erosion in the arctic. Specifically, permafrost is believed to be thawing at greater rates, and wave dynamics are expected to increase in intensity. As a result, thermokarst activity, which includes the occurrence of retrogressive thaw slumps, will be more frequent along arctic coasts.

The availability of airborne and spaceborne imagery in the arctic over the last fifty years has made possible the temporal analysis of permafrost and ground ice-related erosion.
The objectives of this thesis are 1) the creation of a large scale database for horizontal coastal retreat on Herschel Island for the 1952-2000 timespan, 2) the investigation of retrogressive thaw slump activity over the same period and its relation to coastal erosion, and 3) the elaboration of stereophotogrammetric techniques to investigate retrogressive thaw slump activity volumetrically. Herschel Island, located on the northern coast of the Yukon Territory, was chosen as the study site for this research, because of the widespread presence of retrogressive thaw slumps and the lack of data for coastal erosion during the last fifty years.

Photogrammetric tools were used to create orthorectified and stereo-images of the Island for the years 1952, 1970, 2000 and 2004 from airphoto archives and Ikonos (1 m resolution) imagery. Coastal erosion was found to be stable or declining on Herschel Island except in the vicinity of retrogressive thaw slumps. In addition, retrogressive thaw slumps were identified on the imagery and observed to have increased in frequency for the 1952-2000 period.

Stereophotogrammetric analysis of two retrogressive thaw slumps showed that eroded sediment volumes from these landforms are considerable and should be included in future assessments of sediment release from arctic coasts to the oceanic shelves.

**RESUME**

L'érosion côtière grandissante dans l'arctique a été plusieurs fois corrélée aux changements climatiques et au réchauffement de la planète. Le pergélisol est ainsi sujet à des taux de fonte plus importants tandis que les plus récentes prédictions montrent que les vagues attaqueront le trait de côte de manière plus intense et prolongée.

L'existence de données aériennes et spatiales pour ces cinquante dernières années a rendu possible l'étude à long terme de l'érosion côtière en milieu à pergélisol et glace de sol. Les objectifs de cette thèse sont 1) le calcul des taux d'érosion côtiers sur l'île Herschel pour la période 1952-2000, 2) l'analyse de l'activité des écoulements régressifs de fonte au cours de la même période et leur relation avec l'érosion côtière, et 3) l'utilisation de techniques stéréophotogrammétriques dans le cadre de l'analyse volumétrique de l'activité des écoulements régressifs de fonte. L'île Herschel, située sur la côte septentrionale du Yukon, est un endroit propice à l'étude des dynamiques côtières arctiques de par l'omniprésence d'écoulements régressifs de fonte sur se côtes ainsi que le peu de données disponibles sur les taux d'érosion côtière pour ces cinquante dernières années. Cette île est donc le point central des divers sujets et études abordés dans cette thèse.

Des outils photogrammétriques ont permis de créer à partir de photos aériennes d'archive ou d'images Ikonos à haute résolution (1 m) des images orthorectifiées et des modèles numériques de terrain de l'île Herschel pour les années 1952, 1970, 2000 et 2004.

Les résultats de cette thèse montrent que l'érosion côtière a été stable ou en déclin au cours des cinquante dernières années, à l'exception notable de zones situées en contrebas d'écoulements régressifs de fonte, dans lesquelles les données ont décrit une augmentation conséquente des taux de retrait côtiers entre les périodes 1952-1970 et 1970-2000. Par ailleurs, les résultats suggèrent une augmentation importante du nombre d'écoulements régressifs de fonte le long des côtes de l'île Herschel au cours des cinquante dernières années du vingtième siècle. Enfin, l'analyse stéréophotogrammétrique de deux écoulements régressifs de fonte a pu montrer que les quantités de sédiments érodés sont considérables. Celles-ci devront donc être prises en compte au cours d'études futures visant à quantifier les volumes de sédiments érodés sur les côtes arctiques.

## ACKNOWLEDGEMENTS

I would like to express my gratitude to my supervisor, Dr. Wayne Pollard, whose expertise, understanding, and patience added considerably to my graduate experience. I appreciate his vast knowledge and skill in many areas (e.g., ground ice, permafrost, coastal dynamics, climate change, satellite imagery), the always renewed inspiration he provided for numerous projects in diverse fields (Mars, geophysics, field techniques, wildlife knowledge) and the considerable opportunities he provided me with by recommending me to worldwide conferences. I would like to thank the other member of my committee, Dr. Jonathan Seaquist for the friendship, assistance, encouragements and constructive reviews he provided at all levels of the research project. Dr. James Gray of Université de Montréal provided the external review of the thesis with many positive and encouraging comments.

A very special thanks goes out to the supporting staff of the department of Geography, McGill University, without whom I would not have achieved to complete the work required to finish this thesis. Maria Marcone, Pauline Nesbitt were fantastic when it came to overcome administrative hurdles. Paul Wrigglesworth, Ruilan Shi, Rosa Orlandini and Joanna Hobbins had to deal with my insatiable need for technical assistance and satellite imagery. Anastassia Khouri from the McGill Electronic Data Resources Service is the person who made this thesis truly possible by providing the funds necessary to the purchase of imagery. Mrs. Khouri didn't only provide the funds, but considerable encouragement, enthusiasm and support.

I must also acknowledge the discussions I had with several scientists I encountered either during conferences, courses or field trips (Steven Solomon, Volker Rachold, Rune Odegard, Frits Steenhuisen, Benoît Saint-Onge, etc.). These discussions were useful for both the practical and conceptual approach to my study. Alain Gagné from Geomatics Canada, Paul Budkewitsch from the Canadian Centre for Remote Sensing as well as the staff from the National Airphoto Library always provided me with great technical and theoretical help. Appreciation also goes out to the department faculty who trusted me and others in the undertaking of both teaching assistantship and the Geography Graduate Society. I am thinking in particular of Gordon Ewing, Jonathan Seaquist, Ludger Müller-Wille, Gail Chmura, Sherry Olson and Raja Sengupta. Graduate students from the department always brought laughter, smiles and happiness to the offices, lounges or corridors of Burnside Hall. I would like to thank especially Nicole Couture, Chad Davey and Sonja Klinsky for spending hours on editing my "frenglish". All these years will be difficult to forget. Andrew Carter, Mélanie Rousseau, Camellia Ibrahim, Delia Berrouard, Mark Brooks, Jamie Luce, Nancy Martineau and Muriel Abraham have always been there to share the good and bad moments. I would like to thank warmly Tim Haltigin, Greg De Pascale and Jennifer Turner, who had to endure my presence in the arctic and in arctic-related projects and spent a lot of time on writing proposals together with me. Roland and Pierre from the Herschel Island Territorial Park represented and integral part of our research project by providing an insight into the Park wildlife and supporting our study.

I would also like to thank my family for the support they provided me through my entire life (I was once a very annoying kid) and in particular, I must acknowledge my girlfriend and best friend, Ana-Maria, without whose love and encouragement, I would not have finished this thesis.

In conclusion, I recognize that this research would not have been possible without the financial assistance of the Government of Canada award from the International Council for Canadian Studies (ICCS), the Warren fellowship in Geographical Information Systems, the Centre for Climate and Global Change Research (CCGCR), the Geological Survey of Canada Atlantic, the Dept. of Geography, McGill University (Teaching Assistantships, Graduate Student stipend), the Polar Continental Shelf Project (PCSP) (Field expenses), The Climate Change Action Fund (CCAF) (Imagery), McGill Electronic Data Resources Services (EDRS) (Imagery), the International arctic Sciences Committee (IASC) (Travel funds) and the Alma Mater Travel Fund (Travel funds), and express my gratitude to those agencies.

## TABLE OF CONTENTS

# LIST OF FIGURES

## Chapters 1 & 2



## Chapter 3 - Manuscript #1



## Chapter 4 - Manuscript #2

## LIST OF TABLES

### Chapter 3 - Manuscript #1



### Chapter 4 - Manuscript #2

# CHAPTER 1 - INTRODUCTION

## 1.1 Introduction

The southern Beaufort Sea coast has received considerable attention in recent years because: (a) it is characterized by high rates of coastal retreat (both in the past and present), (b) it is one of the most ice-rich permafrost areas in the Canadian arctic, (c) it is an area where air temperatures are expected to rise by as much as 6°C (IPCC, 2001), and (d) it is an area with potential for hydrocarbon development.

Unconsolidated coasts in the Canadian, Russian and American arctic are believed to experience widespread and extensive erosion. Annual horizontal coastal retreat rates (herein referred to as coastal retreat rates or CRR) for these coasts, measured using archived airphotos range between 0.5 and 20 m/yr (Rachold *et al.*, 2003). In the southern Beaufort Sea sector, CRR oscillate between 1.0 and 5.0 m/yr (Solomon, 2004; Harper, 1990). On Herschel Island, CRR range between 0.3 and 2 m/yr (Lantuit and Pollard, 2005). Coastal erosion occurs during the open-water season, which is limited to approximately three months from mid-July to mid-October. Ocean freeze-up generally occurs in the second half of October and break-up in May-June. Most coastal processes including both erosion and deposition are inactive for the remaining 9 months, with the exception of "ice-push". Even during the open-water months, the development of wind-driven waves can be severely inhibited, depending on the concentration and distribution of floating pack ice.

These erosion rates (0.5 to 20 m/yr) are related to the presence of permafrost and ground ice in the coastal exposures (Rachold *et al.*, 2003). The loss of ground strength due to thawing of subaerial and sub-sea permafrost by warm air temperatures and solar radiation facilitate wave attack on coastal bluffs and the rapid removal of sediment from the nearshore zone.

Coastal retreat monitoring is a necessary component of studies that encompass coastal erosion in the arctic. Together with the knowledge of the rheological properties of specific materials, it makes possible the identification of critical parameters involved in coastal erosion. In addition, it helps to identify areas at risk for industry, community planners and aboriginal peoples. However, the remoteness of the arctic hampers the availability of direct observation and long-term datasets. Airphotos, which have been acquired over these regions since the early 1930's, are the only reliable source of information to reconstruct the magnitude of coastal erosion for many areas. Consequently, this study proposes to build the first dataset for coastal erosion on Herschel Island, Yukon Territory. Specifically, this project uses airphotos and satellite imagery to assess horizontal and volumetric coastal retreat.

### 1.2 Scientific Rationale

Most communities vulnerable to coastal erosion processes have already identified the threat to infrastructure and have constructed protective structures such as rip-rap rocks, sandbags and concrete mats. In Tuktoyaktuk, Northwest Territories, the threat to the community is relatively well understood and the community leaders have undertaken expansions of the current protected zones in response to scientific data on the huge rates of erosion (Johnson *et al.*, 2003). Even though increased sea level rise and changing climatic conditions might severely impact the community's shoreline, protective measures are already planned and implemented.

Nevertheless, the "equation" of coastal erosion is not a stable one. Changing climate can not be expressed as a direct cause for increasing CRR. Coastal erosion is often predicted to increase dramatically due to the changes associated with decreasing sea-ice extent, warming climate, sea-level rise, etc (IPCC, 2001). However, as shown by Solomon and Manson (2003) a decrease in sea-ice extent may not considerably effect changes in erosive activity on the shoreline. The length of the open-water season may prove a more direct influence. It is necessary to re-evaluate the factors associated with the occurrence of coastal erosion in arctic settings under changed regional climatic, oceanic and geomorphic conditions. This work focuses on the evolution of coastal erosion over the second half of the twentieth century and emphasizes the changes in coastal erosion evolution on Herschel Island. The presence of massive ground ice features were linked to greater rates of erosion during the 1970-2000 period, whereas other sections of the coast without these features experienced a decrease of coastal erosion. The role of ground ice has been identified in the literature, however, it is generally described as a factor that operates in close interaction with other variables (Dallimore *et al.*, 1996). This work shows that it can influence coastal erosion independently from other factors.

Under changing climate conditions the weight of any of the variables may change, or any single variable might become overwhelming in its significance. Thus, for communities like Tuktoyaktuk, who have already constructed coastal protective structures, a reassessment will be necessary. The integration of predicted changes into local studies is necessary. The added value of basic research towards the understanding of coastal erosion processes in arctic settings is knowledge that will provide more accurate solutions to the community planners concerned with local management.

Furthermore, several aspects of oil and gas development are subject to the impacts of coastal erosion processes. On the Beaufort Sea Shelf, for instance, a number of drilling platforms were built in the 1970's on artificial islands, made of unlithified sediments and protected by the same kinds of features used by arctic communities. These platforms are, due to their isolated position on the shelf and the nature of their constituting material, highly sensitive to coastal erosion (Gillie, 1988). A large number of studies (Gillie, 1988; McGillivray *et al.*, 1993; Maxwell, 1997) have been undertaken to assess the vulnerability of these platforms to both wave dynamics and ice scours, but a reassessment under changed climatic and oceanic conditions is necessary.

By their nature, arctic coastal environments are one of the most dynamic northern environments. Their complexity makes systematic modelling difficult and limited in application. By evaluating recent changes on arctic coasts, one can create a baseline upon which future changes can be both measured and predicted. The correlation of coastal change with climate change provides an important calibration for prediction models. Accordingly, there is an immediate need for such baseline studies. This thesis attempts to define a method for reconstruction of coastal change, and creates a detailed record for one of the most sensitive sections of the Beaufort Sea coast.

### 1.3 Objectives

The overall objective of this thesis is to document patterns (rates, spatial distribution and geomorphology) of coastal erosion on Herschel Island, Yukon Territory, over the past fifty years. This thesis will emphasize the role of permafrost and ground ice features in the erosive process using remotely sensed data. The specific aims of the thesis can be summarized as:

1) To create a large-scale database for horizontal coastal retreat on Herschel Island for the 1952-2000 timespan;

2) To investigate retrogressive thaw slump activity over the same period and assess its relation to coastal erosion;

3) To explore the application of stereophotogrammetric techniques to investigate retrogressive thaw slump activity volumetrically;

4) To quantify volumetric land surface losses and estimate sediment volumes released from retrogressive thaw slumps over the 1952-2004 period;

### 1.4 Organization of Thesis

This thesis is prepared as two manuscripts for publication following McGill University's Faculty of Graduate and Postdoctoral Studies guidelines. Chapter 3 (Manuscript #1) examines the evolution of coastal erosion and retrogressive thaw slump activity on Herschel Island between the years 1952 and 2000. Chapter 4 (Manuscript #2) investigates the potential use of stereophotogrammetric tools to quantify ice and sediment volume losses from two retrogressive thaw slumps on Herschel Island. Each of these manuscripts is considered as a separate entity. Therefore, there is unavoidable repetition of information (field description and methods) in the manuscripts. An additional literature review (Chapter 2) and a conclusion section (Chapter 5) have been included in the thesis to provide a more thorough discussion of coastal erosion issues that could not be included in the manuscripts.

Manuscript #1 will be submitted for publication in one of the following peer-reviewed journals: *Permafrost and Periglacial Processes*, *Earth Surface Processes and Landforms* or *Geomorphology*. Manuscript #2 will be submitted to *Natural Hazards and Earth Systems Science* (NHESS) for a special issue entitled "Landslides systems from triggering to characterization by DEM".

## 1.5 Contributions of Authors

Manuscript #1 authors: Hugues Lantuit and Wayne, H. Pollard. Dr. Wayne H. Pollard provided the historical accounts of retrogressive thaw slump activity over the past fifteen years as a result of long-term studies of retrogressive thaw slumps and coastal erosion on Herschel Island. In addition, Dr. Pollard provided assistance with the interpretation of surficial features on archived airphotos. As primary supervisor, Dr. Pollard provided guidance in constructing the framework and subsequent ideas presented in this manuscript. The Kinematic Differential Global Positioning System (KDGPS) control points were collected in the field during the summers of 2003 and 2004 by the primary author. The post-processing of the KDGPS control points and the orthorectification of the 80 airphotos and the Ikonos 2000 image were all done by the primary author in the Dept. of Geography, McGill University. The digitizing of the historical shorelines and of the retrogressive thaw slumps as well as the compilation of the related statistical outputs were also done by the primary author. The manuscript was entirely written by the primary author, however Dr. Pollard provided valuable advices and editing support.

Manuscript #2 authors: Hugues Lantuit and Wayne, H. Pollard. Dr. Pollard provided important observations of retrogressive thaw slump occurrence and ground ice contents during several years of field observations. In addition, Dr. Pollard helped with in situ KDGPS transect surveys. The primary author collected data in the field and post-processed the KDGPS points in the laboratory. In addition, the primary author conducted the stereophotogrammetric processing of the Ikonos panchromatic stereo-pair, the editing of the resulting DEM, the accuracy assessment of the DEM, and the volume calculations in the GIS Graduate Research Laboratory, McGill University.

# CHAPTER 2 - BACKGROUND

## 2.1 Permafrost Geomorphology

Permafrost is a contraction for "permanently frozen ground" (Muller, 1945) and is defined as "ground that remains at or below 0°C for at least two consecutive years" (Van Everdingen, 2002). It reflects a "thermodynamic balance between ground surface temperature, which is controlled by air temperature and the geothermal gradient" (Pollard, 1998). Permafrost *per se* is thus a thermal state. The geothermal gradient is the change of temperature in the Earth's crust, and from a permafrost perspective refers to the pattern of increasing temperatures with increasing depths (Fig.1).

The pattern of subsurface temperature varies depending upon the nature of the sediments (i.e. the thermal conductivity, structure and hydrogeology all of which influence the heat flux from the interior of the Earth). Concurrently, the ground undergoes temperature fluctuations at the Earth's surface due to changes in air temperature linked to climate, and to a lesser degree, soil moisture, vegetation cover and geomorphology (Pollard, 1998).

Permafrost underlies *ca* 26% of the Earth's land surface (Brown *et al.*, 1998) with 50% of Canada's and 70% of Russia's landmasses underlain by permafrost. Permafrost coverage is generally divided into two categories: continuous and discontinuous. Discontinuous permafrost is further divided into widespread and sporadic. These categories are based upon the spatial extent, the areal coverage and permafrost depth. The continuous zone refers to ubiquitous permafrost, except beneath deep water bodies, and extends to depths of 500-1000 m

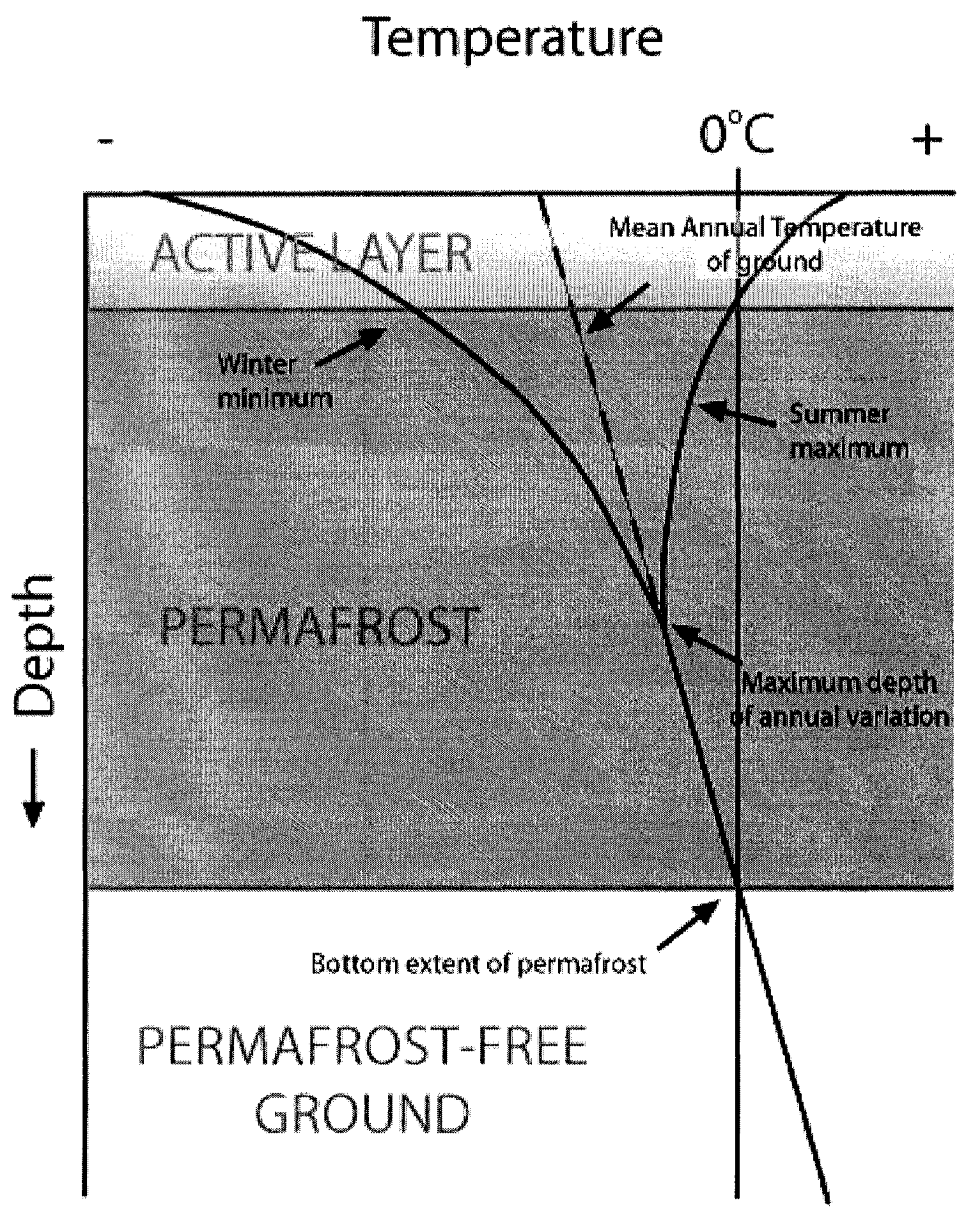


**Figure 1 – Ground temperature diagram for permafrost (after Williams and Smith, 1989)**

(Brown, 1970).The southern limit of the continuous zone is generally associated with the -6 to -8°C mean annual air temperature isotherm (Pollard, 1998). As one travels south, the distance between patches of permafrost increases, marking the progression between discontinuous and sporadic permafrost zones. In its most southern expression, permafrost is often controlled by local conditions and is only a few metres deep.

Permafrost is overlain by a surficial ground layer termed the *active layer*, which lies above the permafrost table and is subjected to periodic (decadal, seasonal or daily) climatic cycles. Active layer thickness ranges roughly from 10 to 20 cm in the continuous zone to 2 or 3 metres in the discontinuous zone.

### *2.1.1 Ground Ice*

Ground ice is a major component of permafrost. Through its aggradation and degradation it is responsible for the genesis of numerous landforms in the periglacial landscape. It is generally defined as "all forms of frozen water beneath the surface of the ground independent of its origin, transfer process and duration" (Pollard, 1998). Mackay (1972) identifies ten types of ground ice ranging from pore ice to segregated ice. It is noticeable that Mackay's classification closely parallels Shumskii and Vtyurin (1966) which includes buried ice deposits. In some cases ice aggradational processes generate ice contents that exceed saturated soil conditions, termed *excess ice*. Excess ice is defined by Williams and Smith (1989) as "ice present in excess of the volume of the soil pores". Excess ice yields supernatant water during the thawing process (i.e. water in excess of the volume of the soil pores) which induces thaw settlement of the soil.

The transition between liquid and solid states of pure water occurs at 0°C at a pressure of 1 atm. However, water is rarely pure and freezing occurs over a range of temperatures below 0°C. This phase change results a volume increase of 9%, which in return induces heaving pressures. Depending upon the soil texture, thermodynamic gradients associated with freezing can develop, resulting in water migration to the freezing front. This suction phenomenon induces the formation of ice inclusions larger than soil pore size. This process is termed ice segregation (Williams and Smith, 1989). Segregated often forms in subhorizontal layers (Williams and Smith, 1989). Ice segregation promotes frost heave (i.e. the expansion of the soil following the formation of segregated ice) which is reflected at the surface by the uplift of surficial sediments. Ground ice also occurs as intrusive ice (i.e. wedge ice, ice diapirs) or buried ice (buried snowbanks, buried glacier ice).

Massive ice, which is defined as "large masses of ground ice, including ice wedges, pingo ice, buried ice and large ice lenses" is constituted of ground ice having a gravimetric ice content >250%" (Mackay, 1971). Gravimetric ice content refers to the weight of water (ice) in a sample volume of sediment as a percentage of the dry sample weight. Because massive ice usually has a high excess ice content, it is thaw sensitive and can lead to dramatic thermokarstic events.

### *2.1.2 Thermokarst*

The term *thermokarst* refers to landforms resulting from the melting of all forms of ground ice (Van Everdingen, 2002). The term thermokarst was first introduced in 1932 by M. Ermolaev to depict the effects of melting ground ice on the northern Siberian landscapes (Shumskii, 1964, cited in Pollard, 1998). Although thermokarst topography can be similar in appearance to karst terrain, the processes by which it forms are completely different. Thermokarst designates the landforms resulting from the melting of all forms of ground ice.

The intensity of thermokarst activity is directly related to the evolution of the active layer and ground ice contents in the upper section of permafrost. It is triggered by human-induced or natural modification of the surface energy balance (i.e. the statement of the conservation of energy applied to a given surface). Its main components include the vertical fluxes of energy into or out of the surface due to net radiation, sensible heat, and latent heat, as well as the net


**Figure 2 – Massive ice exposure in a retrogressive thaw slump on the south-west shore of Herschel Island (2004).**

horizontal fluxes of energy in the subsurface. If ground ice is present then thermokarst processes can occur if thaw depths increase. Where excess ice is present the thermokarst will result in a net lowering of the ground surface proportional to the percent volume of excess ice.

The processes in the formation of thermokarst landforms include thermokarst subsidence and thermal erosion (Pollard, 1998). Thermokarst subsidence refers to the thaw settlement of flat low relief areas and often produces surface ponding and shallow depressions. Thermal erosion is a backwasting process which occurs on slopes where melting of exposed ground ice causes the slope face to retreat laterally (French, 1996). The most obvious expression of lateral thermokarst is the occurrence of retrogressive thaw slumps, which are bowl-shaped thaw structures, where ground ice is exposed in a retreating thaw face containing up to 13 m of massive ice (De Krom, 1990).

## 2.2 Coastal Dynamics

The ocean's coasts are complex systems. At the land-ocean interface they integrate a wide range of both offshore (deep water wave formation) and nearshore (wave refraction) processes. Coasts are broadly divided into two types based on the pattern of sea level change -- transgressive (where relative sea level rises) and regressive (i.e. emergent coasts) coasts. This study focuses on the transgressive coasts of the western Canadian Arctic.

### *2.2.1 Transgressive Coasts*

Long-term coastal erosion is often explained by a landward and upward translation of the subaqueous profile (portion of the profile below the water) as a result of relative sea level rise (Bruun, 1962). In a traditional erosive scenario, the upper shoreface undergoes erosive retreat into the backshore area, while the offshore zone and the adjacent seafloor is aggrading with the newly eroded material from the shoreface (Fig.3). In the transgressive scenario, the aggradation of the seafloor seaward of the erosive shoreface zone results in the widening of the nearshore platform (surf zone).

The action of the waves on the shoreline is the most important direct cause of coastal erosion. Waves attack at the base of the cliff and transport the eroded material away, exposing deeper sections of the cliff to erosion. If there is insufficient sediment to replace the material carried away from a shoreline, the shore will retreat or change shape so that it can better maintain its position against natural processes such as wave action. The energy expended by waves during a storm (i.e. wave power multiplied by time) is quantified using the following equation, modified after Komar (1998), where wave power is a product of wave frequency, wave amplitude, gravity and water density.

$$P = \frac{1}{2}\frac{\rho g^2 a^2}{4\pi f} \qquad [1]$$

where $P$ ($kW/m$) is the power, $\rho$ is the density of the water, $g$ is the acceleration due to gravity, $a$ is the amplitude of the wave and $f$ is the wave frequency. Storm waves cause erosion of sand and gravel from beaches, but material is often returned to the beach during fair weather.

It is possible to estimate the expected rate of erosion for a specific location using the transgressive model described by Bruun (1962). Critical parameters include height of the cliff, bluff profile (i.e. cliff angle), bluff sediment granulometry, water depth at the edge of the continental shelf, distance to the edge of the shelf, and relative sea-level rise. In the southern Canadian Beaufort Sea, sea level has risen by approximately 55 m over the last 15 000 years (Forbes, 1980, Hill *et al.*, 1993). It is presently estimated to be rising as much as 1-2 mm/yr (Forbes, 1980, Campeau *et al.*, 2000). Isostatic rebound in the area is limited due to its marginal position in relation to the Laurentide ice sheet at the last glacial maximum (Rampton, 1982). Eustatic sea level rise is not offset by isostatic adjustment, and relative sea level rise may therefore be equated with eustatic sea level fluctuations. Using Bruun's method, an erosion rate oscillating between 0.06 and 0.12 m/yr was determined for the northwestern shore of Herschel Island based upon representative (i.e. average) values present in the literature (Forbes, 1980; Campeau *et al.*, 2000). Most of the coasts in the Canadian Beaufort Sea are characterized by similar rates and magnitudes of erosion but different distances to the edge of the shelf (Harper, 1990). One should expect to observe erosion rates between 0.05 and 0.4 m/yr, depending on the location in relation to the edge of the shelf.

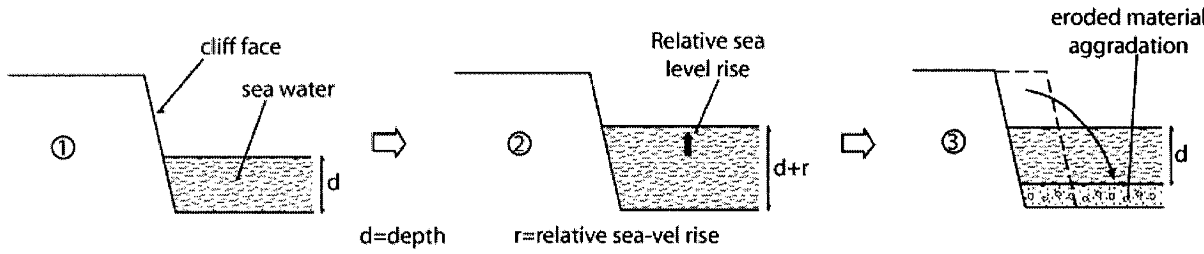


d=depth
r=relative sea level rise
(1) The cliff face is eroded in its original position by at the sealine level.The depth of the nearshore floor is d.
(2) Sea level rises and the depth of the nearshore increases of r.
(3) Erosion occurred and the material eroded is deposited in the nearshore area, so it recovers its original depth d.

**Figure 3 - Erosive sequence in a transgressive scenario (after Bruun, 1962)**

However, coastal retreat in the Beaufort Sea region has been documented for the second half of the twentieth century at rates largely exceeding those predicted by the transgressive scenario (Solomon, 2004). Bruun's theory also applies mainly to ice-free marine coasts which generally undergo year-long erosive processes. Since this is not the case for the western Beaufort coastline where the open-water season is only 3-4 months long, then it is clear that other processes are involved and that the higher than predicted rate of retreat is even more significant.

Arctic coasts are clearly a specific case, particularly in areas of regression and ice-rich permafrost. Several researchers have attempted to characterize the complex processes in these environments and explain the anomalous patterns of retreat (Aré, 1964, 1988; Mackay, 1960).

### *2.2.2 Arctic Coastal Erosion*

Permafrost plays a unique role in the development of Arctic coasts. Mackay (1986), Dyke (1991), and Dallimore *et al.* (1996) have suggested that the degradation of sub-sea permafrost by lowering the submerged profile (and therefore modifying the shoreface equilibrium following Bruun's 1962 theory) may accelerate coastal retreat. According to Dallimore *et al.* (1996), "volume reduction caused by thawing of both eroded and submerged sediments can result in a substantial decrease in sediment supply to the nearshore zone and deepening of the nearshore bathymetry". Héquette and Barnes (1990) suggested sea-ice processes are an additional factor for the lowering of nearshore profiles. Ice processes including ice gouging, ice pile-up, and ice enhanced current scour (Forbes and Taylor, 1994) are eroding the shoreface and nearshore area and are "significant contributors to rapid coastal erosion and to maintaining an equilibrium shoreface profile" (Héquette and Barnes, 1990). Reimnitz and Barnes (1987), Reimnitz *et al.* (1990) and Héquette *et al.* (2001) have also addressed the significance of these processes in the Beaufort Sea.

Thaw settlement and ice scour contribute to the lowering of the profile of the nearshore zone, but cannot explain entirely the excessive rates of erosion observed in the arctic. They contribute to the modification of the conditions by which thermal-mechanical processes (i.e. melting of the frozen bluff, wave attack, etc.) occur at the sea/land interface.

Aré (1988) provided a comprehensive review of thermal abrasion/denudation and mechanical erosion of arctic sea coasts. Aré suggests that erosion of frozen cliffs is a combination of thermal abrasion/denudation and mechanical erosion. Thermal abrasion plays a factor in the direct melting of ice in coastal bluffs, when those bluffs are in contact with sea water above 0°C. All sediments incorporated in the ground ice are released. Thermal denudation is the reduction of the strength in subaerial materials due to the presence of permafrost. Mechanical erosion is the action of incident waves on coastal bluffs. Thermal abrasion, combined with mechanical erosion induces an important undercutting of the coastal bluffs, which leads to the failure of the overlying cliffs. Kobayashi (1985), Kobayashi *et al.*,(1999) and Héquette and Barnes (1990) have demonstrated the sensitivity of frozen cliffs to the thermal-mechanical process particularly where higher ice contents lead to greater thermal erosion.

### *2.2.3 Storm Surges*

The greatest amount of coastal erosion occurs during storm induced wave activity and surge events. According to Solomon *et al.* (1994) and Solomon and Covill (1995), storm surge events in the southern Beaufort Sea account for most of the observed erosion. A storm surge is an unusually high stand of sea level produced by strong winds blowing water shoreward and by the ocean surface rising in response to low atmospheric pressure. Coastal cliffs are exposed to a wider wave-attack zone during storm surges. Storm surges can reach a height of 2.4 m in the Canadian Beaufort Sea (Forbes, 1989). A significant part of the wave energy and subsequent transport of sediment occurs during these low frequency high magnitude events. Harper and Penland (1982) estimate that over 20% of the wave energy is expended over only 2% of the open-water season. Ice-free fetch up to 200 kilometres during the open-water season allows the development of large waves which induce both mechanical and thermal processes at the land/sea interface. Melting of ground ice results in the addition of fine-grained sediment to the swash zone which is then transported along- or off-shore. Wave height, wave power, and ice contents are the critical variables influencing rates of coastal erosion during storm surges (Héquette and Barnes 1990; Solomon *et al.*, 1994). In the southern Canadian Beaufort Sea, waves observed during storm events generally originate from the north-west (Harper and Penland, 1982; Hudak and Young, 2002) and reach maximum heights of 2.4 m (Forbes, 1989).

Since the tidal range is small in the Canadian Beaufort Sea (0.3 to 0.5 m) and tidal currents are slow (generally less than 15 cm/s) tidal oscillations are not considered as a significant process to shoreline evolution in the Beaufort Sea (Harper, 1990)

### *2.2.4 Landforms in the Coastal Plain*

In the subaerial context, permafrost degradation occurs in different ways, depending upon the morphologic parameters of the cliff and on the amount of ground ice contained in the cliff sediments.

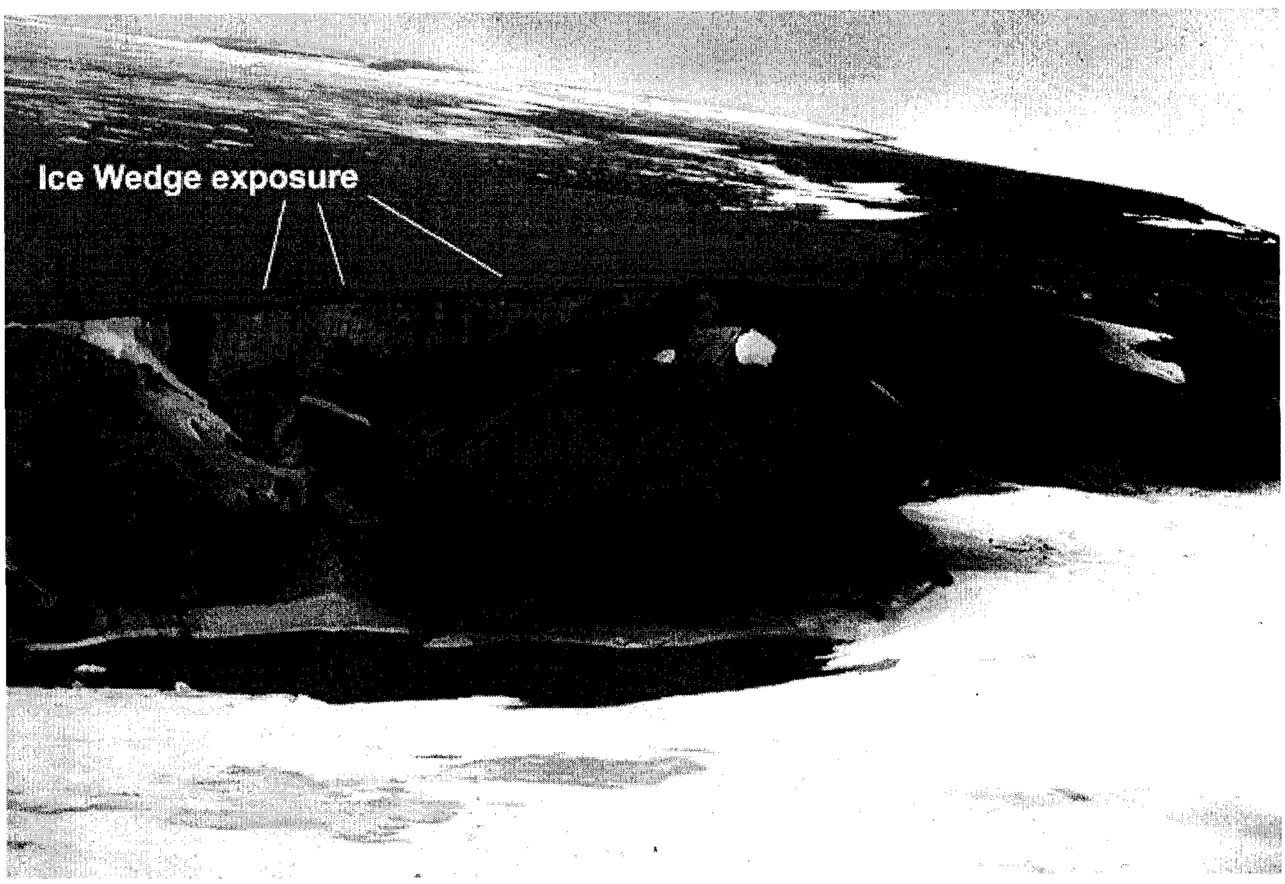


**Figure 4 - Block failure. The height of the cliff is approximately 20 m.**

Zones affected by an extensive coverage of and ice-wedge polygons in the subsurface are subject to block failure (Fig.4). Block failure involves the collapse of large blocks of sediment (from tens to thousands of cubic metres) characterized by angular edges which detach from the cliff under the influence of gravity. Block failures occur after: (1) the undercutting of the frozen cliff by thermal-mechanical-erosion and the formation of a thermo-erosional niche (Fig.5) and (2) the failure of blocks along ice wedge polygon boundaries, when the thermo-erosional niche extends to the point where overburden pressure exceeds the shear stress of the material. It seems likely that thermal contraction cracking associated with ice wedge formation plays a potential important role in this process (Hoque and Pollard, *in press*).

**Figure 5 - Thermoerosive niche at Komakuk Beach. Followed a moderate storm in August 2004. Thermoerosive niches up to 6 m were observed.**

When ground ice is present as massive tabular ice bodies, retrogressive thaw slumps develop by backwasting of exposed ice-rich sediments. Retrogressive thaw slumps are large landslide-like features that extend inland between 5 and 500 m and range between 5 and 1000 m wide. Retrogressive thaw slumps generally consist of three main components (De Krom, 1990;

Lewkowicz, 1987): (1) A vertical or sub-vertical headwall, comprised mostly of the active layer and ice-poor organic or non-organic materials, (2) a headscarp whose angle varies between 20 and 50° and which retreats by the ablation of ice-rich materials due to sensible heat fluxes and solar radiation and, (3) the slump floor, which consists of pooled water, fluid mudflow and plastic flow deposits that expand in a lobate pattern at the toe of the slump (Figure 6). If the exposed massive ice melts at rates that exceed the rates of thermal-mechanical erosion at the base of the cliff, then a retrogressive thaw slump is initiated (Lewkowicz, 1987). On Herschel Island, the headwalls of the retrogressive thaw slumps expose up to 13 m of ice (De Krom, 1990; Wolfe *et al.*, 2001). However, the thickness of the ground ice is probably greater since the lower portion of the ice is concealed by meltout debris that accumulates at the base of the retreating headwall.

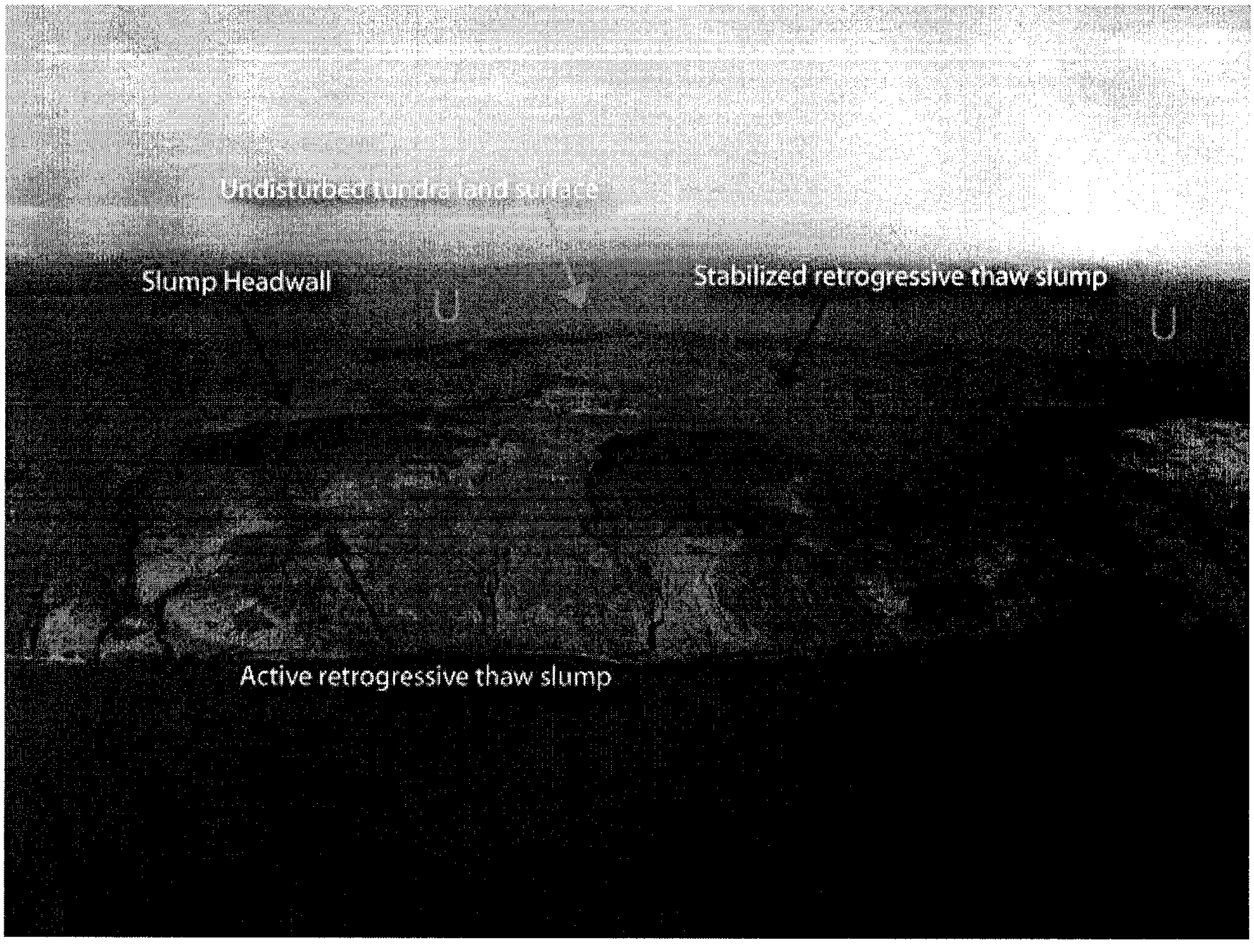


**Figure 6 - Polycyclic retrogressive thaw slumps in Thetis Bay, Herschel Island. August 2004.**

In coastal exposures, the rate of retrogressive thaw slump retreat is closely linked to the intensity of wave action, as the removal of retrogressive thaw slump debris by incident wave action or littoral drift aids in: (1) maintaining a steep headwall gradient and, (2) preventing the build-up of debris in front of the headwall and/or on the retrogressive thaw slump floor. Retrogressive thaw slumps do not require a removal of the debris to continue backwasting, since their expansion is driven mainly by massive ground ice melting or sublimation in the headwall related to solar radiation and positive air temperatures. However, the removal of debris by wave action and littoral drift helps sustain the thaw process and enhances retrogressive thaw slump activity. This type of positive feedback is most important during the initiation of coastal retrogressive thaw slumps (De Krom, 1990).

## 2.3 Climate Change

The gradual rise of the earth's surface temperature (i.e. global warming) is thought to be caused by the greenhouse effect and is responsible for changes in global climate patterns. It is predicted to occur at greater rates in northern latitudes, leading to dramatic changes in air temperatures (+2 to +6°C in the Arctic), increasing precipitation, and subsequent impacts on sea ice extent, permafrost thaw, sea surface temperatures, etc (IPCC, 2001).

Climate change is and will continue to strongly impact the arctic coasts. It has a direct influence on nearly all variables related to arctic coastal erosion, including permafrost temperature, sea surface temperature, sea salinity, sea level, storm frequency and intensity and sea ice conditions (McGillivray *et al.*, 1993). The seasonal and long-term pattern of ground surface temperatures is an important variable in the distribution of permafrost. They determine its presence and thickness as well as the near surface ground thermal regime, which in return affects the presence of ground ice.

Together with tidal variations, sea surface temperatures and salinity, ground temperatures determine the depth of the active layer along the beach/cliff profile. Melnikov *et al.* (1998) describe the indirect role played by changing sea temperature and salinity related to the inflow of Atlantic and Pacific ocean water to the Arctic Ocean through the Bering and the Fram straits in modifications of scour conditions in the nearshore zone. Deepening of the active layer can lead to the increased occurrence of retrogressive thaw slumps along coasts and in the backshore area (Kane *et al.*, 1991, Osterkamp and Romanovsky, 1999; Serreze *et al.*, 2000).

Arctic coastal erosion is driven by a combination of wave action and thermal degradation related to both air temperature and wind. Large waves are produced by high winds acting over a large area for prolonged periods of time. Normally, the short open-water season and limited area (fetch) over which the wind acts limits wave energy in arctic seas. However, any reduction in sea ice cover, combined with increased storm activity will certainly lead to greater coastal erosion. Chapman and Walsh (1993) found that arctic sea ice extent during the period 1953-1990 decreased by 3%. Most Global Climate Models (GCMs) predict an increase in the open water season from the current average of 60 days to about 150 days and increase the maximum extent of open water in summer from its present range of 150 - 200 km to 500 - 800 km (Carter *et al.*, 2000) (Fig.7).

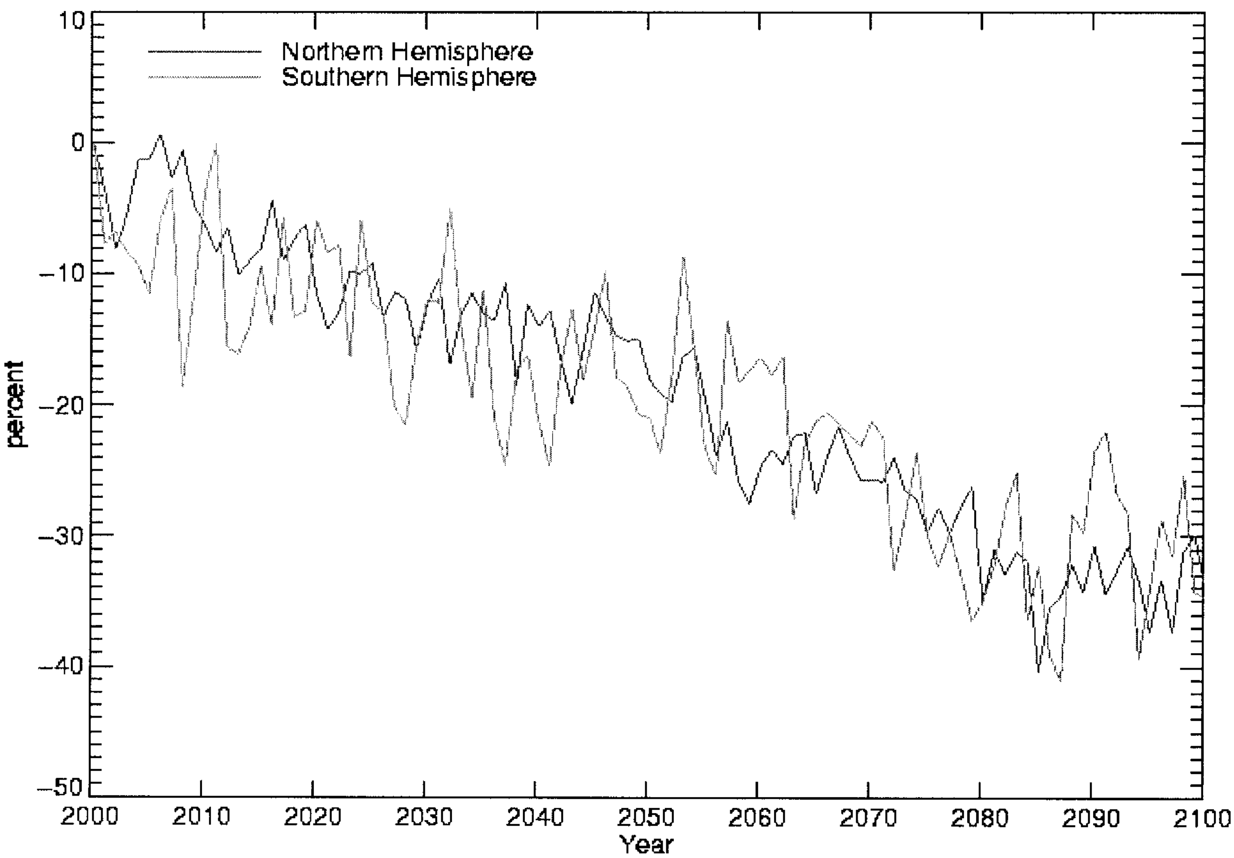


**Figure 7 - Annual average sea ice area change predicted from the Hadley Centre GCM (Global Climate Model). http://www.metoffice.com/research/hadleycentre/**

Solomon (2004) suggests that any trends for CRR in the southern Beaufort Sea are hard to detect. Solomon (2004) and Lantuit and Pollard (2005) suggest stable or possibly decreasing CRR in the southern Beaufort Sea. CRR "do not appear to be substantially affected by sea ice conditions" in the southern Canadian Beaufort Sea (Solomon and Manson, 2003, p 1). Solomon and Manson (2003) also point out that nearshore and onshore local geomorphology might be a more important limiting factor for coastal evolution than fetch. They note that the changes in sea ice extent predicted for the 21st century might not be as important for coastal evolution as changes in the duration of the open water season.

Coastal retreat is rapid and affects communities and infrastructure along the ice-rich coasts of Canada, the United States and the Russian arctic (Rachold *et al.*, 2003). Several small communities are located in ice-rich terrain along the Canadian southern Beaufort Sea coast. For example in Tuktoyaktuk, located in the Northwest Territories, coastal erosion has led to the destruction of several structures and the relocation of the school. Predicted coastal erosion in Tuktoyaktuk represents a threat for a third of the village over the next hundred years (Johnson *et al.*, 2003).

Heritage sites, such as burial graves or archaeological sites are also threatened by coastal erosion and sea-level rise when located on low-lying shores. Industry infrastructure in the arctic, particularly facilities linked to oil and gas, are also likely to be affected by changes in coastal erosion. Already, several structures in the Russian arctic have been threatened by coastal erosion, such as industry complexes in the Pechora Sea. (Ogorodov, 2003). Oil and gas drilling and exploration techniques are likely to be reconsidered under conditions of increased erosion (Maxwell, 1997). Artificial islands used for drilling on the Beaufort Sea Shelf are usually reinforced to resist sea-ice scouring and sea-ice pile-ups (Gillie, 1988). Although this may lead to reduced costs for drilling (because of the reduced presence of sea ice), new designs will be needed for offshore platforms to resist wave dynamics and storm surges and for future pipelines to accommodate both offshore and onshore permafrost enhanced melting (McGillivray *et al.*, 1993).

## 2.4 Conceptual approach to the study of coastal erosion

There are several different approaches to the study of coastal erosion in the arctic. For example, various aspects of coastal retreat and process can be measured through numerical models (Kobayashi *et al.*, 1999), field surveys and monitoring (Vassiliev *et al.*, 2004; De Krom, 1990) or by remote sensing (Solomon, 2004).

### *2.4.1 Coastal Modelling*

Even though there is considerable research involving the use of coastal numerical and stochastic models, they have seldom been derived for coastal erosion in arctic settings. Héquette and Barnes (1990) provided one of the first analyses of the statistical significance of processes involved in coastal erosion of frozen cliffs. Although they did not provide a numerical model *per se*, this study formed the basis of subsequent attempts to model coastal erosion of frozen cliffs. Héquette and Barnes (1990) ran linear regressions of horizontal and volumetric CRR versus a set of parameters (ice contents, grain size, wave height, wave power, cliff height and shoreface gradient) in order to determine the prevailing factors for coastal erosion on frozen cliffs. They assessed the sensitivity of erosion rates to wave height, wave power, grain size and ice content. Their results indicated that these parameters (except grain size) were strongly correlated to erosion. Kobayashi *et al.* (1999) developed a two-dimensional numerical model of erosion for frozen cliffs which includes both thermal and mechanical processes. The model was inspired by an earlier study by Kobayashi (1985) on the development of thermoerosive niches in frozen cliffs. The model established the crucial role of storm surge duration for the erosive process. Further development of the thermal component of coastal erosion was undertaken by Costard *et al.* (1999) and Makhoufi *et al.* (1999). They developed a process-based model that consisted of a block of ice placed in the middle of a flume, and ran sensitivity analyses for discharge, water temperature and ice temperature. They emphasized the importance of discharge and water temperature for the erosive process. No process-based models of permafrost erosion in fine-grained sediments has been reported in the literature to this date.

### *2.4.2 Surveys and Monitoring*

Field surveys and monitoring are frequently undertaken in the arctic. Russian researchers have maintained yearly measurement programs of coastal retreat for decades (Vassiliev *et al.*, 2004). In Canada such surveys are more recent, although coastal erosion rates were determined by Mackay as early as 1959 (Mackay, 1960). Mackay provided retreat rates for the Yukon Coast using anthropogenic features as landmarks on the coast, in particular a grave located near Kay Point. Currently, a wide range of tools exists for recording sea-level rise (tide gauges), meteorological data, nearshore bathymetry (single beam and recently multibeam sonar) (Blasco *et al.*, 2004), wave heights, etc. Measurements of coastal retreat rates and landslides require regular visits to the monitoring sites in order to maintain survey markers and to conduct measurements. Russian scientists have maintained such measurements for several sites in the Kara, Barents and the Laptev Sea  using geodetical tools (Rachold *et al.*, 2003). In Canada and the United States, similar techniques have been successfully employed (De Krom, 1990; Burn, 2000). However, few studies have maintained measurements over long timescales.

The Kinematic Differential Global Positioning System (KDGPS), which can achieve subcentimetre measurements, has considerably expanded the possibilities for researchers to record temporal changes with much less effort. Periodic measurements of the coastline can now be operated with little preparation in the field and with high mobility. When the required precision is submetric and the shoreline consists of flat terrain, the KDGPS device can be mounted on a motorized vehicle, and the operator can make measurements over extensive distances. The high precision of KDGPS also allows scientists to distinguish the different components of the shore in a rapid manner: cliff top, cliff bottom, and shoreline can be monitored in transversal and longitudinal surveys. Pollard *et al.* (2002) demonstrate the value of this approach to determine retrogressive thaw slump retreat on Herschel Island, Yukon territory. A slump, which had an inland extent of 450 m surveyed in 2000, provides a baseline for future studies on slump evolution.

KDGPS is a recent technique which has been used in the arctic only since the end of the twentieth century. Given that geodetic measurements have not been updated often enough to provide a baseline for change detection studies, future works will rely largely on remote sensing.

### *2.4.3 Remote Sensing*

Remote sensing is "the science and art of obtaining useful information about an object, area or phenomenon through the analysis of data acquired by a device that is not in contact with the object, area, or phenomenon under investigation" (Lillesand and Kiefer, 1979). The technique relies on devices such as cameras, lasers, radar systems and sonars, which are mounted on platforms operating from air, space or sea. We will be focusing on the techniques related to the use of satellite sensors and airphotos.

Airphotos were first produced in the 1930's, while satellite imagery became available in the early 1970's for northern Canada. Both represent potentially useful sources for temporal studies in the Canadian arctic. However, archival satellite imagery does not have the level of precision of airphotos, the Corona satellite, a "spy" satellite deployed in the early 1970's, achieves on a average basis a pixel resolution of 5 m, while Landsat-1 (1972) resolution was 80 m. Conversely, airphotos are constrained only by the grain of the photographic plate. Airphotos from the thirties still constitute a valuable tool for high resolution studies.

Presently, new high resolution satellites achieve spatial resolutions similar to the early airphotos. Ikonos has a pixel size of 1 m at nadir in the panchromatic channel (i.e. sensitive to the entire visible spectrum), and Quickbird has a resolution of 0.67 m at nadir. These sensors can replace airphoto datasets when the area of interest is limited (no greater than 500 $km^2$). When the area is greater, flying an airphoto mission becomes economically more feasible.

Scientists have long been interested in the potential of archived airphotos for calculations of CRR. In the Canadian Beaufort Sea, most CRR estimates to date have been based on these datasets (Harper, 1990, Solomon, 2004). Airphotos are used as either "raw" diapositives which include optical distortions from the camera and relief displacement attributed to the terrain, or as orthophotographs which correct for both distortions. The errors associated with "raw" airphotos can be quite dramatic and sometimes greater than the dimension of the geomorphologic process studied. The tedious work associated with the production of orthophotographs justified the use of "raw" images in the past. Photogrammetric techniques (i.e. techniques associated with the study and processing of photos, and by extension of airphotos) have progressed during the last two decades from a completely manual process involving large stereoplotters to the use of scanners and computerized tools, broadly termed *softcopy photogrammetry*. Softcopy photogrammetric techniques considerably reduce the time involved in the production of orthophotographs.

Consequently datasets obtained after softcopy photogrammetric processing can yield measurements that are very accurate.

Softcopy photogrammetric techniques can also be used to analyze elevational data. This information is generally stored as a DEM (Digital Elevation Model) and refers to the mean elevation of each pixel in the image. DEMs are also termed DSMs (Digital Surface Models), when they refer to the elevation of the bare surface (i.e. without human-built features). DEMs were initially created from the contour lines drawn by the operator of the stereoplotter. This technique results in large uncertainties since it relied on interpolation techniques based on statistical estimations adapted for this kind of operation. Presently, DEMs are constructed using *stereo-matching algorithms* implemented in softcopy photogrammetry software suites (Kasser and Egels, 2001). These algorithms compute the parallax for each pixel and consequently compute elevations for the overlapping areas of two contiguous airphotos.

Two requirements are crucial for the completion of this operation: 1) The availability of two images of the same location taken on the same day (if not the same hour) from different angles, and 2) the availability of an accurate and comprehensive set of control points (i.e. points for which coordinates in a given coordinate system, datum and ellipsoid are available). The first requirement is generally not fulfilled by the series of archive imagery from spaceborne sensors. Recent Earth observation satellites (Spot-5, Landsat-7, and Aster) can usually acquire two images the same day. However, the outputs are characterized by high uncertainty. High resolution satellites such as Quickbird and Ikonos also provide stereo-imagery (at high costs), which achieves accuracy close to that of stereophotogrammetric outputs from airphotos. Large scale studies that focus on temporal changes of locations in three dimensions rely on archived airphotos to obtain vertical information for pre-1990's locations.

The second condition (i.e. the availability of a dataset of accurate control points) is fundamental and directly influences the accuracy of the outputs of the stereophotogrammetric process. Control points are used directly into the stereophotogrammetric process. They form the basis for the success of the photogrammetric model, which is necessary for correctly aligning overlapping airphotos. Control points generally consist of geodetic points determined by national geodetic surveys, but are less accurate than KDGPS points. However, due to the recent interest in the civil uses of KDGPS, stereophotogrammetric outputs are very precise and can be used for monitoring coastal erosion. This recent improvement of absolute georeferencing techniques has a direct influence on georeferencing of archived imagery. It is common to be able to identify on archive imagery features which are geographically stable throughout the period of investigation. In arctic settings, where man-made features are rare, landforms such as tundra polygon edges are used. While tundra polygon edges are subject to small-scale movements (Williams and Smith, 1989), they can be ignored in the stereophotogrammetric process because they are less than the resolution of the DEM.

The production of DEMs can serve multiple purposes when used in the study of coastal erosion. The comparison of DEMs between different years can provide an estimate of volumetric losses along the coast (see manuscript #2). Three-dimensional coastal landform parameters such as slope and lateral extent can also be investigated. Consequently, a wide range of outputs can be expected from volumetric datasets. For example, when the volume fraction of a specific permafrost constituent (e.g. ground ice, soil organic carbon) is known, then detailed flux calculations are possible. Terrigenous carbon outputs to the ocean can be assessed for specific sections of coasts or for small scale calculations.

### *2.4.4 Synthesis*

Arctic scientists have used all three approaches (coastal modelling, surveys, and remote sensing) to understand and describe coastal erosion. However, when used together they provide a better understanding of both the scale and magnitude of processes. In the southern Beaufort Sea, researchers from the Geological Survey of Canada have developed and validated numerical models (Kobayashi *et al.*, 1999), undertaken numerous field surveys (Solomon and Covill, 1995, Dallimore *et al.*, 1996) and used remotely sensed imagery to characterize erosion rates and patterns during the last half of the twentieth century (Solomon, 2004). These approaches are inter-connected and provide spatial, multi-scale and temporal approaches to the study of coastal erosion. The present work documents coastal retreat rates and retrogressive thaw slump activity on Herschel Island for the 1952-2004 period, but can also support other types of scientific studies undertaken on the island (e.g. vegetation studies, park management, wildlife surveys, archaeology).

## 2.5 Study Area

Herschel Island, also known as Qikiqtaruk (meaning "it is island" in Inuvialuktun), is located in the northern part of the Yukon Territory, Canada. The island is situated at 69°36'N and at 139°04'W and lies approximately 60 km east of the boundary between Yukon and Alaska and 3 km north of the continental coast (Figure 8). Herschel Island covers an area of 108 $km^2$, is approximately 15 by 8 km, and has a maximum elevation of 185 m. The island is located in the southern Beaufort Sea and is part of the Yukon Coastal Plain physiographic region (Rampton, 1982). The Yukon Coastal Plain is bounded on the south by the Barn and British Mountains, on the east by the Mackenzie Delta and Richardson Mountains, and on the north by the Beaufort

Sea.

The Yukon Costal Plain extends nearly 200 km from the Mackenzie Delta to the Yukon/Alaska border where it becomes the Alaska North Slope. This plain is approximately 24 kilometres in width, and is an erosional surface covered by marine, fluvial and colluvial deposits of Pleistocene and Holocene age (Rampton, 1982). West of Firth River (i.e. to the west of Herschel Island), the plain consists of deltas and coalescing alluvial fans, while east of the river; it is covered by drift and numerous lakes and ponds (Rampton, 1982). This drift is composed of fluvial, marine, lacustrine and estuarine sediments (Rampton, 1982). The Yukon coastal plain extends offshore as the Beaufort Sea Shelf.

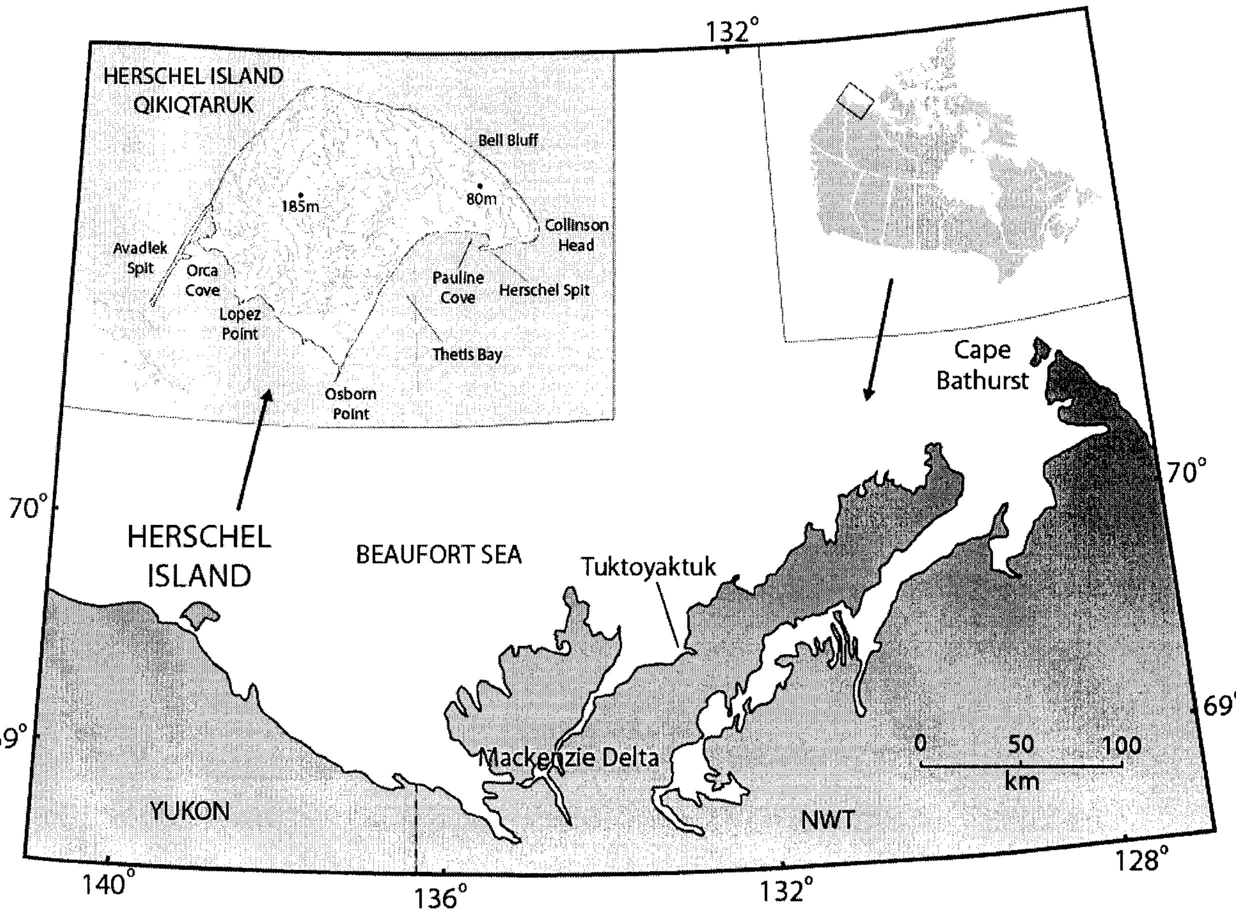


**Figure 8 - Study area**

Herschel Island was formed by glacial activity during the Pleistocene. Mackay (1959) suggested that Herschel Island could have been the result of glacial ice-thrusting by 1) noting its location at the limit of Pleistocene glaciation and, 2) by demonstrating that the volume of the island is "more-or-less" the same as the volume of sediment missing from Herschel Basin (Ptarmigan Bay). Rampton (1982) confirmed that the island was formed by the westward movement of a lobe of the Laurentide ice sheet during an early stage of the Wisconsin termed the Buckland Glaciation. The lobe ploughed frozen sediments, buckling and folding them to form a push moraine which today constitutes Herschel Island. The sediments of this ice-thrust feature are principally of marine, non-marine and mixed origin (Bouchard, 1974).

Bedrock is absent from the island. Bouchard (1974) reports that drilling to a depth of 35 m did not reach the base of the unconsolidated deposits. The postglacial sediments are deposits attributed to littoral or alluvial accumulation, accumulation of organic matter and mass movements. The glacial deposits include ice-push ridges, erratic boulders scattered over most of the island, and the gravel deposit presumed to be of fluvioglacial origin. Preglacial deposits are more complex; the marine sediments are either clays and clayey silts or clayey silts with sand laminae. The mixed sediments consist of sands with silt interbeds, sands with silt and fine sand laminae, and gravels. The non-marine sediments are generally found in beds of clayey silt and fine-grained sand, both rich in organic matter (Bouchard, 1974)

The island has a "rolling and fairly regular" topography (Bouchard, 1974). It is roughly divided in two main regions. The northern and eastern parts of the island are characterized by steep relief and high elevations, and the southern and western parts are characterized by lower elevation and more gentle slopes.

The northern and eastern parts of the island have the most relief (respectively 183 and 80 m). The northern edge of Herschel Island is dominated by rolling and hummocky push moraines which form a series of high parallel ridges and hills with narrow asymmetrical valleys in between. The ridges are breached by a series of deep gullies, which form steep valleys up to 46 m deep (Bouchard, 1974). The coastline of the northern edge is dominated by steep bluffs up to 50 m high fronted by very narrow to non-existent beaches. In this area, coastal retreat occurs mainly as large block failures (Fig. 4).

The southern and south-western shore sections of the Island are also characterized by low relief and rolling hills. Coastal morphologies are more complex; there are several aggrading spits composed of coarse gravel, sand and sandy silt, and containing boulders. The largest, Avadlek Spit, located on the south-western tip of Herschel Island is roughly 6 km long, while Herschel spit and Osborn Point are between 2-3 km in length (Fig. 8). Coastal slopes are subject to intense thermokarst activity and include numerous large retrogressive thaw slumps and active layer detachments. Retrogressive thaw slumps extend up to 500 m inland and reach a lateral extent of 1 km. Active layer detachments occur on steeper slopes and mudflows occur within stabilized floors of retrogressive thaw slumps. On the south-east side, the shoreline is mantled by a thick accumulation of supersaturated clays, clayey silts and organics, which are a residue of thermokarst activity. The shore sections are fronted by narrow beaches up to 10 m wide, which are covered by slump debris where retrogressive thaw slumps are occurring.

The active layer on Herschel Island penetrates the surface mantle of silty diamicton to depths of 15 cm to 45 cm, and up to 110 cm under the sand spits (Smith *et al.*, 1989). Ground ice is thought to underlay most of the island except under recent coastal landforms such as sand spits and sandy-pebbly beaches. It constitutes up to 60-70% of the upper 10-15 m of permafrost (Pollard, 1990; Pollard, *personal communication*). Bouchard (1974) showed that ice contents on Herschel Island were some 20% higher than ice contents on the rest of the Yukon Coastal Plain. Ground ice occurs in the form of ice-wedges, segregated ice lenses, pore ice, massive tabular ice bodies, buried snowbank and glacier ice (Pollard, 1989, 1990). Intrasedimental ice is the most common massive ground ice type (Pollard, 1990). The observed thickness of massive ice bodies ranges between 4 and 15 m (Pollard, 1990; Pollard, *personal communication*) but is probably greater since only the upper part of the ice body is exposed by retrogressive thaw slumps. Bouchard (1974) showed that the average depth of massive ice and ice-rich sediment is approximately 13 m.

## 2.6 Synthesis

The objective of the present work is therefore to pinpoint the specificity of the current coastal erosion and coastal thermokarst processes on Herschel Island using remote sensing methods. To do so, an exhaustive database of coastal erosion rates and retrogressive thaw slump activity is presented in chapter 3. Chapter 4 presents a focused study on two retrogressive thaw slumps located in the island coastal zone and provides quantitative data about the volume losses associated with these landforms.

# CHAPTER 3 – MANUSCRIPT #1

**Fifty years of coastal erosion and retrogressive thaw slump activity on Herschel Island, southern Beaufort Sea, Yukon Territory.**

Lantuit H and Pollard WH

**Abstract**

Keywords: *Coastal erosion, photogrammetry, retrogressive thaw slumps, climate change*

Arctic coasts experience high erosion rates (in the order of 1 to 5 m/yr in the southern Canadian Beaufort Sea) during the 4 to 5 month open-water season (June-October). Warming trends may increase sea level, increase wave energy and thaw earth materials, leading to enhanced coastal erosion. Since the southern Beaufort Sea region is one of the most ice-rich areas in the Canadian arctic, coastal erosion and retrogressive thaw slump activity may prove to increase dramatically. This paper provides an insight into the long-term dynamics of both coastal erosion and retrogressive thaw slumps on Herschel Island. Archived airphotos from 1952 and 1970 and a 2000 Ikonos image were orthorectified using softcopy photogrammetric tools corrected by Kinematic Differential Global Positioning System (KDGPS) control points. Shoreline and retrogressive thaw slumps were then digitized for each year. Mean annual coastal retreat rates changed from 0.74 m/yr over the 1952-1970 period to 0.55 m/yr over the 1970-2000 period. The highest coastal retreat rates are on shoreline sections exposed to the north-west, which is the main direction of storm attack in the region (Harper and Penland, 1982, Hudak and Young, 2002). Although generally decreasing, coastal retreat rates have been increasing on south, south-south-east and south-east exposed shoreline sections, which are marked by the greatest occurrence of ground-ice related features such as retrogressive thaw slumps. In addition, the discrepancy between annual headwall retreat rates of retrogressive thaw slumps and coastal retreat rates has led to the development of large polycyclic retrogressive thaw slumps on south, south-east and south-south-east exposed shoreline sections. The number and the total area of

these slumps as well as the proportion of *active* retrogressive thaw slumps have dramatically increased between 1952 and 1970 on Herschel Island (+125% and +160% respectively). Polycyclic retrogressive thaw slumps were observed to develop in a periodic fashion, illustrated by a general relationship between retrogressive thaw slump generation and maximum inland extent, constant throughout the last fifty years, despite the intensified presence of active retrogressive thaw slumps on south to south-east exposed shorelines.

## Introduction

Coastal retreat in arctic regions is an ongoing process that has become a major concern during the second half of the twentieth century. Arctic coasts experience high rates of erosion on the order of 1 to 5 m/yr in the southern Canadian Beaufort Sea (Solomon, 2004) during the 4 to 5 months when water is not frozen. Several community and industry infrastructures in the circum-Arctic have been relocated or destroyed due to coastal erosion (Solomon, 2002; Ogorodov, 2003; Johnson *et al.*, 2003).

Erosional dynamics are driven by a combination of geomorphological and climatological variables. For example, sea ice and permafrost extent are controlled by seasonal and long term patterns in temperature and to a lesser degree atmosphere and ocean air circulation. The mechanics of erosion are closely linked to wave action (wave height) and littoral drift which in both cases is controlled by winds, storm events, open water (fetch) and nearshore bathymetry and coastal profiles (Héquette and Barnes, 1990; Solomon *et al.*, 1994).

Erosion along arctic coasts reflects the complex interaction between geology and climate (material and permafrost properties, soil properties and coastal processes) (Aré, 1988; Mackay, 1960, 1963). Arctic coasts are mostly situated in the continuous permafrost zone (Brown *et al.*, 1998) and are highly vulnerable to global warming (McGillivray *et al.*, 1993). Warming trends may increase sea level along the coast, increase wave energy, and thaw earth materials, thereby predisposing the coast to erosion (McGillivray *et al.*, 1993). Melting ground ice may lead to thaw settlement of the nearshore zone (Dallimore *et al.*, 1996). This deepens the nearshore profile, thus allowing waves to approach closer to shore before breaking and thereby increasing breaking power. Ground ice may also be subject to greater thermal-mechanical processes at the base of coastal bluffs forming thermoerosional niches (Aré, 1988; Kobayashi *et al.*, 1999) and leading to the occurrence of block failures (Figure 2). Since the southern Beaufort Sea region is one of the most ice-rich areas in the Canadian arctic (Pollard and French, 1980), coastal erosion may increase dramatically.

In general, periodic and comprehensive datasets on coastal erosion in the arctic are rare, although Russian researchers have maintained yearly measurements of shoreline position in several locations for decades (Vassiliev, 2003). In the Canadian arctic, coastal erosion estimates rely primarily on remotely sensed data and in particular on airphoto archives. McDonald and Lewis (1973) documented average horizontal coastal retreat rates of 0.66 m/yr on Herschel Island, southern Canadian Beaufort Sea for the 1944-1970 period using archived airphotos. However, since 1980 few aerial missions have been flown and current estimations must be derived from high resolution optical satellites such as Ikonos or Quickbird. Solomon (2004) has produced an overall update of average coastal retreat rates for the southern Canadian Beaufort Sea but excludes Herschel Island. Coastal retreat rates for Herschel Island have been published for the 1954-2000 period (Lantuit and Pollard, 2003) using recent but non-orthorectified imagery. These estimates have a high degree of uncertainty; therefore it is necessary to provide accurate datasets of long-term erosion on arctic coasts.

The presence of ground ice on arctic shorelines can lead to the occurrence of retrogressive thaw slumps, which are major thermokarstic landslides. These landslides can lead to major volume losses on arctic coasts and represent a serious risk to coastal infrastructure (Lantuit and Pollard, *in press*). Retrogressive thaw slumps have three main elements: (1) a vertical or sub-vertical headwall, comprised mostly of the active layer and ice-poor organic or non-organic materials, (2) a headscarp whose angle varies between 20 to 50° and which retreats by the ablation of ice-rich materials due to sensible heat fluxes and solar radiation, and (3) the slump floor, which consists of a fluid mudflow and flow deposits that expand in a lobe pattern at the toe of the slump (Figure 3,4) (De Krom, 1990; Lewkowicz, 1987). On Herschel Island, slumps are initiated by wave erosion at the base of ice-rich coastal cliffs, which uncovers massive ice bodies and leads to ice ablation (De Krom, 1990) or by active layer detachments (a form of slope failure linked to deep thaw which may occur as coastal erosion oversteepens coastal slopes)(Lewkowicz, 1990). If the massive ice melts at rates that exceed the rates of erosion at the base of the cliff, then a retrogressive thaw slump is initiated (Lewkowicz, 1987). The headwalls of the retrogressive thaw slumps can expose up to 15m of ice (De Krom, 1990; Wolfe *et al.*, 2001; Pollard, *personal communication*), or more, depending on the thickness of the melted debris that accumulates at the base of the headwall.

The backwasting nature of retrogressive thaw slumps rarely removes all of a massive ice body. Varying thicknesses of massive ice are preserved in the floor of the slumps. Subsequent erosion (coastal, gully, retrogressive thaw slumping) may exhume this ice and trigger a new retrogressive thaw slump within the limits of the existing or stabilized form. The term polycyclicity is applied to this type of activity (Mackay, 1966; Wolfe *et al.*, 2001) (Figures 5 and 6). Polycyclic generations of retrogressive thaw slumps can coexist within the same slope. The newly activated thaw slumps eventually reach the headwall of the larger thaw slump. They can also contribute to the reactivation of slumps that have been stable for decades or even centuries.

For practical purposes, most current numerical models of coastal erosion consider wave attack on an idealized two-dimensional nearshore profile. Ground-ice related geomorphic landforms are ignored in most conceptual models. However, retrogressive thaw slumps, as described by Mackay (1966) and Burn and Lewkowicz (1990), are closely linked to coastal processes. Mackay (1966), Forbes and Frobel (1995), Harry *et al.* (1988) and Wolfe *et al.* (2001) qualitatively link coastal erosion rates and retrogressive thaw slumps. Quantitative assessments of the role of retrogressive thaw slumps to coastal erosion over long time periods are therefore necessary. In addition, retrogressive thaw slump activity over long time periods remains largely unknown. Since thermokarst activity is expected to increase dramatically in response to predictions of climate warming for the western Canadian arctic, long-term assessments of retrogressive thaw slump activities are needed to assess potential risks (Lewkowicz, 1991; Smith, 1993; Williams, 1995).

The general purpose of this study is to assess coastal recession on Herschel Island, Yukon Territory using archived airphoto imagery and a 2000 Ikonos image. Following the assessment of coastal retreat rates along the shoreline, this paper focuses on the spatial and temporal distribution of retrogressive thaw slumps along the island's shoreline. The specific aims of this paper are:

1) To document coastal retreat rates on Herschel Island for the 1952-2000 period.
2) To investigate the evolution of retrogressive thaw slump activity over the same period.
3) To document the relationship between coastal erosion intensity and retrogressive thaw slump activity.

**Study area**

Herschel Island is located in the northern part of the Yukon Territory, Canada. The island is situated at 69°36'N and at 139°4'W and lies approximately 60 km east of the boundary between Yukon and Alaska and 3 km north of the continental coast (Figure 1). The island is located in the southern Beaufort Sea and is part of the Yukon Coastal Plain physiographic region (Rampton, 1982). Herschel Island covers an area of 108 square kilometres (approximately 15 x 8 km) and has a maximum elevation of 183 m asl. (De Krom, 1990).

Herschel Island was formed by the westward movement of a lobe of the Laurentide ice sheet during an early stage of the Wisconsin termed the Buckland Glaciation, which ploughed up frozen sediments that were then buckled and folded to form a push moraine (Mackay, 1959;

Rampton, 1982). The sediments of this ice-thrust feature are principally marine, non-marine and of mixed origin (Bouchard, 1974).

The active layer is 15 cm to 45 cm thick in the silty diamicton that blankets most of the island and up to 110 cm under the sand spits which are located at the south-east and south tips of the island as well as under the Herschel settlement (Smith *et al.*, 1989). Ground ice underlies most of the island except under recent coastal landforms such as sand spits and sandy-pebbly beaches and constitutes up to 60-70% of the upper 10-15 m of permafrost (Pollard, 1990). Bouchard (1974) showed that ice contents on Herschel Island were 20% higher than ice contents for permafrost along the rest of the Yukon Coastal Plain. Ground ice occurs in the form of ice-wedges, segregated ice lenses, pore ice, buried snowbank and glacier ice and forms massive tabular ice bodies (Pollard, 1989, 1990). Massive ice is defined as "a mass of ground ice which has an ice content of at least 250 percent (on an ice-to-dry-soil weight basis)" (Mackay, 1971). On Herschel Island, massive ice is observed in coastal sections and slump-induced exposures, on south, south-east and north-west facing shores. Segregated (intrasedimental) ice is the most common massive ground ice type (Pollard, 1990). The observed thickness of massive ice bodies ranges between 4 and 15 m (Pollard, 1990; Pollard, *personal communication*) but is probably greater since only the upper part of the ice body is exposed by retrogressive thaw slumps. Bouchard (1974) showed that the average depth of massive ice and ice-rich sediment is approximately 13 m.

## Methods

*Geoprocessing of airborne and spaceborne imagery*

Photogrammetric processing of airphotos and Ikonos imagery was conducted to yield submetre accuracy images of the Herschel Island coastline for 1952, 1970 and 2000 so that coastal retreat rates could be estimated by comparing the respective years.

Photogrammetric operations (i.e. registration of control points and tie points, computation of the photogrammetric model and editing of the DEM) were conducted on an airphoto series from 1952 (A13470 series) and 1970 (A21921 series) and an Ikonos image of 2000. Before high resolution Global Positioning System (GPS) devices were introduced, georeferencing of digital images of Herschel Island used to rely on geodetic coordinates from the 1970's and on topographic maps at the 1:50,000 scale. Horizontal and vertical inaccuracies for these maps are estimated to be greater than 20 m in most cases in the area (Alain Gagné, Geomatics Canada, *personal communication*). Topographic maps at the 1:50,000 scale are available for the entire southern Beaufort Sea but are not reliable for precise positioning at large scales. Similarly, Ikonos panchromatic non-orthorectified products are considered by Space Imaging to be accurate only within a 50 m window (Valadan and Toosi, 2003). Therefore, 17 KDGPS (Kinematic Differential Global Positioning System) points were collected in the field during September 2003 and August 2004 using a Trimble 4700 differential GPS system in order to provide accurate georeferencing. The horizontal and vertical accuracy of the Trimble GPS is ± 2 cm. Such error is negligible when compared with the expected accuracy of stereophotogrammetric results. A set of stable landforms were determined on the three sets of imagery in generation to collect the GPS control points in the field. These points corresponded to intersections of polygon edges or to artificial features and were all located inland and on stable slopes. The point location was documented using field photography. An estimated error value of 0.50 m was however assigned to the eight GPS survey points in generation to account for the loss of accuracy due to the identification of features on the imagery by the operator. The 17 Ground control points collected in the field were distributed evenly on the island.

The 2000 panchromatic Ikonos image was acquired on September 18$^{th}$, 2000. Ikonos panchromatic images have, in theory, a 1 m ground pixel resolution. Depending on the nominal collection elevation and azimuth, the pixel resolution may vary. In this case, the actual pixel resolution ranged from 1.18 to 1.20 m.

A softcopy photogrammetric software program was used to perform orthorectification operations. Images were registered based upon the GPS ground control points, and a 1.1 m resolution DEM was created for the 1952 and 1970 airphoto series. Images were then orthorectified and mosaiced to produce 1.1 m pixel ground resolution images. The total Root Mean Square (RMS) error for ground control points and tie points was 2.16 m for the 1952 image series and 1.54 m for the 1970 image series. The Ikonos image was orthorectified using a rational function model implemented in the stereophotogrammetric software as described in similar studies (Toutin, 2001; Di *et al.*, 2003a). The rational function model was chosen over other methods because of its ease of use and its high vertical and horizontal accuracy (Valadan and Toosi, 2003). The total RMS for the ground control points was 1.58 m.

*Estimations of coastal retreat rates*

The digitizing of the shoreline and of the retrogressive thaw slumps as well as the estimation of coastal retreat rates were processed in Arc/Info® ESRI GIS software. Automated shoreline extraction procedures such as those described by Li *et al.* (2002), Di *et al.* (2003b) and Deneau (2002) were avoided as the shoreline of Herschel Island presents geomorphic features that could be misinterpreted by the algorithms (such as beaches of varying widths, presence of sloughing material in the shore zone). These procedures are also less efficient in shaded zones and on archived airphoto imagery because of interfering features which appear during image capture or scanning operations (Deneau, 2002).

The shoreline was digitized on the three datasets following Solomon (2004) who produced horizontal retreat measurements using a semi-automated procedure along the Mackenzie Delta shore and the Yukon Coastal Plain. Given the limited extent of our study area measurements were performed manually. However, measurement sites were determined using an automated procedure. Using the 1952 digitized shoreline, measurement sites were created every 300 m. Measurements were limited by the extent of the Ikonos panchromatic image, therefore the western part of the island has not been entirely incorporated (Figure 10). Previous studies on Herschel Island (MacDonald and Lewis, 1973; Lantuit and Pollard, 2003) used measurement sites separated by varying distances, up to 700 m. As a result, 132 measurement sites were used in this study (60 measurement sites for the aforementioned studies). Coastal retreat was calculated and divided by the number of years to provide annual coastal retreat rates. The south-west side of Herschel island ("Workboat Passage") is excluded in the present coastal retreat analysis because Hill (1990) showed that this section acts as a sediment sink within the broader littoral system of the Yukon coast, and is not subject to coastal erosion. The evolution of this section of the shoreline in the current study is related to the longshore movement of sediment in the beach face and to spit formation.

*Measurements of retrogressive thaw slumps*

Retrogressive thaw slumps and active layer detachments were also digitized on the three datasets using ArcGis software. Retrogressive thaw slumps were tentatively classified using two main criteria, (1) the level of activity, and (2) the generation of the retrogressive thaw slump. Measuring the level of activity for classification of retrogressive thaw slumps was implemented similar to the Wolfe *et al.* (2001) classification scheme. Active and stable retrogressive thaw slumps were discriminated against when digitizing. Active retrogressive thaw slumps were characterized by "exposed, icy headwall, thickest at maximum extent of retrogressive thaw slump and decreasing sideways; no established vegetation in slump" (Wolfe *et al.*, 2001, p.7) and stable retrogressive thaw slumps by the absence of a headwall and the presence of grass. The intermediate state between active and stable retrogressive thaw slumps described by Wolfe *et al.* (2001) was not incorporated in this study because of the uncertainty associated with the identification of these features on remotely sensed imagery. The identification of these classes on the 2000 image was aided by the use of photos acquired by helicopter late in the summer of 2003. The dimensions of the retrogressive thaw slumps were then calculated using automated functions (area) and manual measurements (inland extent) in the GIS software.

The numbering (hereafter referred to as "generation") of the retrogressive thaw slump is meant to describe the polycyclic dynamics and refers to the hierarchy of retrogressive thaw slump development. Retrogressive thaw slumps located within a slump floor were classified such that the larger retrogressive thaw slump was always assigned the number "1", the next largest retrogressive thaw slump located within it the number "2", and so on. The method is illustrated in Figure 6. The delineation of the respective generations was based on the shape of the retrogressive thaw slump and on the elevation differences between the different retrogressive thaw slump floors. The poor quality of the 1952 imagery and the low resolution due to flight line height could have resulted in an underestimate of the total number of digitized landslides.

Figure 12 examines the relationship between maximum inland extent and generation of retrogressive thaw slumps for the years 1952, 1970 and 2000. The 274 retrogressive thaw slumps documented from 1952, 1970 and 2000 were then aggregated to provide a general relationship between retrogressive thaw slump generation and maximum inland extent. This relationship is presented in Figure 13. A general pattern for polycyclicity can be deduced from the datasets.

## Results

### *Coastal erosion*

Coastal erosion rates were compiled for two periods: 1952-1970 and 1970-2000 (Figures 7 and 8). The average annual coastal retreat rate was found to be 0.61 m/yr for the 1952-1970 period and 0.45 m/yr for the 1970-2000 period (Table 1). Horizontal shoreline changes along exposed coastal areas for the 1952-1970 period varied from –59 m to +16 m (negative changes are erosional). The minimum and maximum for the 1970-2000 period were -54 m and +20 m, respectively.

### *Retrogressive thaw slump and active layer detachment activity*

The results summarized in Tables 2 and 3 suggest that, (1) the total landslide area as well as the total number of landslides have increased between 1952 and 2000, and (2) that the proportion of "active" retrogressive thaw slumps *vs.* other landslides (i.e. active layer detachments and stable retrogressive thaw slumps) has been consistently increasing. The increase is particularly obvious for the 1970-2000 time interval, during which the area of active retrogressive thaw slumps increased by a factor of 2.5. In comparison, total area of stable retrogressive thaw slumps has been decreasing in size during the 1970-2000 period. Despite this evidence, stable retrogressive thaw slumps constituted the bulk of the total area of the landslides observed in 2000 (65%).

*Polycyclicity*

The number of retrogressive thaw slumps of second and higher generations has been increasing consistently since 1952 (Table 4). There were 42, 59 and 79 episodes in 1952, 1970 and 2000, respectively. Since the total number of retrogressive thaw slumps has also been increasing, the proportion of the second and higher generation retrogressive thaw slumps has remained fairly constant during this time period (70% in 1952, 73% in 1970 and 68% in 2000). Their aggregated area remained remarkably stable as a proportion of the total retrogressive thaw slump area (21%, 25% and 26% in 1952, 1970, and 2000 respectively) as did their maximum inland extents (Table 4). The pattern presented in Table 4 and Figure 12 was found to remain fairly stable over a fifty year timespan, with average values of inland extent for each slump generation varying by only 25 m.

## Discussion

*Spatial pattern of coastal retreat*

The positive (aggradational) changes related to coastal evolution were related to littoral drift-driven depositional landforms such as Herschel Spit (a mobile sandy-pebbly spit) or to debris mudflows generated by major landslides (i.e. retrogressive thaw slumps or active layer detachments) along the shore. The distribution of coastal retreat rates shows that the greatest rates correspond to shorelines exposed to the north-west, north-north-west and north, which is consistent with the preferential occurrence of north-west-originating storms in the southern Beaufort Sea (Harper and Penland, 1982; Hudak and Young, 2002). Solomon (2004) demonstrates that the rest of the southern Canadian Beaufort Sea has undergone a limited increase in erosional processes and that the highest rates of retreat are generally associated with spits or low tundra bluffs which are exposed to waves and storm surges caused by the northwesterly wind storms (Solomon, 2004). Harper and Penland (1982) showed a secondary preferential orientation of storms (south-east and south-south-east) occurring in the Beaufort Sea. We found that south-east and south-south-east exposed shorelines on Herschel Island exhibit higher retreat rates than north-north-east, north-east, and south-west exposed shorelines. Turner *et al.* (2004) used a model developed by Kobayashi *et al.* (1999) to simulate erosion by storm surge occurrence during the 1970-2000 period by aggregating the number of storms by wind direction. This study found results on the same order of magnitude as the present study except for south, south-east and south-south-east exposed sections of the shoreline where modelled rates were lower than the ones presented here (0.30 m/yr vs. 0.83 m/yr).

A comparison of coastal retreat rates between the two periods shows a steady decrease for most sections of the coast (Table 1) except for south, south-east and south-south-east orientation. Neither the topography nor the lithology of the south-facing coasts can solely explain the local increase of coastal erosion. The presence of ground ice, and more specifically of massive ice in the coastal cliffs, potentially plays an important role in the observed increases. Solomon (2004) noted that coastal retreat rates could be higher for areas in which high ground ice content had been identified. Bouchard (1974) mapped ice-rich sediments on Herschel Island using borehole data and visual estimations in subaerial sections. The south, south-south-east and south-east exposed sections of the coast correspond to zones delineated as "ice-rich" while the north-east facing shore is not, and does not exhibit increasing erosional rates. Pollard (1990) showed that massive ice is not ubiquitous on the northern shore of the island, and that ground ice in this area probably occurs as isolated bodies of buried glacier ice together with pore ice. He noted that the south and south-east exposed sections of the coast (namely those located around Thetis Bay), and in particular the ones related to retrogressive thaw slump activity, exhibited large bodies of massive tabular ice. Massive tabular ice presence can be inferred remotely through the presence of retrogressive thaw slumps (Pollard and Couture, 2000), which are almost exclusively located on the south, south-south-east and south-east facing sides of the island (Figure 10). Table 1 shows that coastal erosion is amplified where retrogressive thaw slumps occur and is diminished where they are absent.

*Temporal pattern of coastal retreat*

The calculated rates of coastal retreat suggest a general decline in the intensity of coastal erosion during the twentieth century. This contradicts previous results (Lantuit and Pollard, 2003) which showed an increasing trend during the same period and differ slightly from results provided by McDonald and Lewis (1973). For the same section of coast, Lantuit and Pollard (2003) estimated a retreat rate of 0.67 m/yr for the 1954-1970 period and a rate of 1.03 m/yr for the 1970-2000 period. Calculated rates differ because: (1) the number of measurements in previous studies (n=60) was lower than the present study (n=132), (2) the distribution of measurement sites along the shoreline in previous studies was biased because of uneven spatial distribution, and (3) the use of unrectified airborne and satellite imagery, as acknowledged by Lantuit and Pollard (2003) introduced errors larger than the 15% uncertainty mentioned in the same study (McDonald and Lewis, 1973; Lantuit and Pollard, 2003). We found that for the same sites in both studies, measurements could differ by a factor of 1.41.

*Retrogressive thaw slump activity*

Retrogressive thaw slump occurrence and accelerated coastal erosion have been occurring on Herschel Island for the last fifty years and should be seen as interactive processes. While thermal inputs such as solar radiation impact equally south-west, south and south-east exposures, south-west facing sections of the shoreline have not experienced widespread retrogressive thaw slump activity, mainly because they are not exposed to high wave energy conditions. Our results suggest that, (1) the zones where large retrogressive thaw slumps occur on Herschel Island are exposed to wave activity and that, (2) the zones containing large retrogressive thaw slumps have exhibited increasing rates of coastal retreat during the last half of the twentieth century. The difference between the annual headwall retreat rates, shown by Lantuit *et al.* (*in press*) to be between 7.6 and 9.6 m/yr, and the rates of erosion calculated for the same segment of coast, demonstrate that headwall retreat rates outpace coastal retreat rates, allowing for the development of large retrogressive thaw slumps as well as for the activation of new retrogressive thaw slumps in the shore zone.

Table 3 shows that at decadal time scales there is no correlation between the occurrence of retrogressive thaw slumps and the presence of former active layer detachments. However, as hypothesized by de Krom (1990), active layer detachments can be considered a triggering mechanism at shorter time scales. De Krom (1990) also reported the triggering of retrogressive thaw slumps on Herschel Island by melt along ice-wedges, inducing failure and rapid exposure of the massive ice bodies, especially in zones affected by former thaw ponds. This hypothesis is confirmed by the widespread presence of drained thaw ponds just above the headwall of the retrogressive thaw slumps located inland from the coast. However, this hypothesis does not apply to the stable zones of a former retrogressive thaw slump. Ice in these sections exists primarily in the residual part of the massive ice body in the retrogressive thaw slump headwall (Burn, 2000). The reactivation of these zones is linked to their re-exposure. Reactivation in the coastal zone (i.e. at the cliff edge) can be attributed to the removal of stabilized mudflow debris by wave action (Aré, 1988). Reactivation in the retrogressive thaw slump floor is attributed to the removal of the overlying debris. This removal is the result of active layer slides within the retrogressive thaw slump floor, which leads to the initiation of retrogressive thaw slumps (Wolfe *et al.*, 2001), or of the gullying of the slump floor by the viscous flows which re-expose ice bodies (Lantuit and Pollard, *in press*). De Krom (1990) provides a striking example of the occurrence of a retrogressive thaw slump initiated "within an active layer slide" in a coastal zone of the island (Figure 14). There is no evidence in the imagery used in this study of this process, partly because the study was not conducted using annual or multiseasonal measurements. Further field base studies are therefore needed to investigate polycyclic retrogressive thaw slump triggering.

*Polycyclicity*

Figure 13 suggests that polycyclicity is only partly explained by the extent of the first generation retrogressive thaw slump and that the polycyclic pattern of the retrogressive thaw slump is based upon a decay function. Indeed, second and higher generation retrogressive thaw slumps occur primarily in the first 200 metres from the shoreline while first generation retrogressive thaw slumps can occur up to a distance of 506 m from the coast. This data suggests that polycyclicity on Herschel Island is a perennial phenomenon whose extent is steadily driven by the total area affected by slump activity. The aggregated area of second and higher generation slumps was observed at a proportion between 21 and 26% of the total area affected by slump activity. The validity of the general relationship presented in Figure 13 is restricted to Herschel Island and is based on site specific lithology, ice contents and topography. Also, the measured maximum inland extents have large variability (as the retrogressive thaw slump generation decreases) which clearly limits the applicability of this relationship. However, it is believed that the periodic pattern of polycyclic retrogressive thaw slumps is a common behaviour on Herschel Island, as illustrated in Figure 11.

**Conclusion**

The following conclusions arise from this study:

1) Shoreline erosion has decreased over the 1952-2000 period on Herschel Island, Yukon Territory. Mean annual coastal retreat rates decreased from 0.74 m/yr over the 1952-1970 period to 0.55 m/yr over the 1970-2000 period on the shorelines exposed to ocean dynamics. These results are consistent with recent estimates of coastal retreat rates in the southern Beaufort Sea by Solomon (2004).

2) The highest coastal retreat rates are on shoreline sections facing the northwest, which is the main direction of storm related wave attack in the region (Harper and Penland, 1982, Hudak and Young, 2002).

3) Although generally decreasing, coastal retreat rates have increased for south, south-south-east and south-east facing shorelines, which are marked by high ice contents (Pollard, 1990) and the highest density of ground-ice related features such as retrogressive thaw slumps.

4) The difference between annual headwall retreat rates of retrogressive thaw slumps and coastal retreat rates has led to the development of large polycyclic retrogressive thaw slumps on south, south-east and south-south-east facing shoreline sections.

5) The number and the total area of retrogressive thaw slumps have dramatically increased between 1952 and 1970 on Herschel Island (+125% and +160%, respectively) as well as the proportion of *active* retrogressive thaw slumps among all slumps.

6) Polycyclic retrogressive thaw slumps develop in a periodic fashion illustrated by a general relationship between retrogressive thaw slump generation and maximum inland extent, constant throughout the twentieth century, despite the intensified presence of active retrogressive thaw slumps on south to south-east exposed shorelines.

**Acknowledgements**

This research was supported by the Climate Change Action Fund (CCAF), and the Natural Science and Engineering Research Council of Canada (NSERC). Support from the Polar Continental Shelf Project (PCSP) and the Aurora Research Institute (ARI) for the field component was greatly appreciated. Hugues Lantuit is supported by the Warren fellowship in GIS and the Government of Canada Award Program administered by the International Council for Canadian Studies (ICCS) on behalf of the Department of Foreign Affairs and International Trade of Canada (DFAIT). Helpful discussions with Alain Gagné from Geomatics Canada and Paul Budkewitsch from the Canada Centre for Remote Sensing (CCRS) provided answers for processing and analysis of the imagery. The field assistance of Ms. N. Couture Ms. J. Turner and Mr. T. Haltigin is gratefully acknowledged. The authors wish to express sincere appreciation to the Yukon Territorial Government, to the Yukon Parks, the Yukon Department of Renewable Resources and to the Environmental Impact Screening Committee (EISC), Inuvialuit Renewable Resource Committees for their support and encouragement of this project. The authors also wish to thank N. Couture and C. Davey from McGill University for their helpful comments on this paper.

## References

Aré, FE. 1988. Thermal abrasion of sea coast. *Polar Geography and Geology* **12**. VH. Winston& Sons, 157 pp.

Bouchard M. 1974. *Géologie des dépôts meubles de l'île Herschel, Territoire du Yukon.* M.Sc. Thesis, Université de Montréal: Montréal, Québec; 70 pp.

Brown J, Ferrians Jr. OJ, Heginbottom JA and Melnikov ES. 1998. *Circum-Arctic Map of Permafrost and Ground-Ice Conditions*. Boulder, CO: National Snow and Ice Data Center/World Data Center for Glaciology. Digital Media

Burn CR. 2000. The thermal regime of a retrogressive thaw slump near Mayo, Yukon Territory. *Canadian Journal of Earth Sciences* **37**: 967-981.

Burn CR and Lewkowicz AG. 1990. Retrogressive thaw slumps. *The Canadian Geographer* **34** (3): 273-276.

Dallimore SR, Wolfe S and Solomon SM. 1996. Influence of Ground Ice and Permafrost on Coastal Evolution, Richards Island, Beaufort Sea Coast, NWT. *Canadian Journal of Earth Sciences* **33**: 664-675.

De Krom V. 1990. *Retrogressive thaw slumps and active layer slides on Herschel Island, Yukon.* M.Sc. Thesis, McGill University: Montréal, Québec; 157 pp.

Deneau D. 2002. Extracting 3D coastlines from remotely sensed data. *Report to AGRG and DFO.* Center of Geographic Sciences: Lawrencetown, Nova Scotia; 71 pp.

Di K, Ma R and Li R, 2003a. Geometric Processing of IKONOS-1 Geo Stereo Imagery for Coastal Mapping Applications. *Photogrammetric Engineering and Remote Sensing* **69** (8): 873-879.

Di K, Wang J, Ma R and Li R. 2003b. Automatic Shoreline Extraction from IKONOS-1 Satellite Imagery, *EOM*, **12** (7): 14-18.

Forbes DL and Frobel D. 1985. Coastal erosion and sedimentation in the Canadian Beaufort Sea. In *Current Research, Geological Survey of Canada*, Paper **85**-1B, 69-80.

Harper JR. 1990. Morphology of the Canadian Beaufort Sea Coast. *Marine Geology* **91**: 75-91.

Harper JR and Penland PS. 1982. Beaufort Sea sediment dynamics. *Technical Report for Geological Survey of Canada*. Woodward-Clyde Consultants: Victoria, British Columbia; 198 pp.

Harry DG, French HM and Pollard WH. 1988. Massive ice and ice-cored terrain near Sabine Point, Yukon Coastal Plain. *Canadian Journal of Earth Sciences* **25**: 1846-1856.

Héquette A and Barnes PW. 1990. Coastal retreat and shoreface profile variations in the Canadian Beaufort Sea. *Marine Geology* **91**: 113-132.

Hill PR. 1990. Coastal geology of the King Point area, Yukon Territory, Canada. *Marine Geology* **91**: 93-111.

Hudak DR. and Young JMC. 2002. Storm climatology of the southern Beaufort Sea. *Atmosphere-Ocean* **40**: 145-158.

Johnson K, Solomon SM, Berry D and Graham P. 2003. Erosion progression and adaptation strategy in a northern coastal community. *Proceedings - 8th International Conference on*

*Permafrost, Zurich, Switzerland, July 20-25, 2003*. Edited by . Phillips, S.M. Springman and L.U. Arenson; International Permafrost Association **8**: 489-494.

Kobayashi N, Vidrine JC, Nairn RB and Solomon SM. 1999. Erosion of frozen cliffs due to storm surge on Beaufort sea coast. *Journal of coastal research* **15**: 332-344.

Lantuit H and Pollard WH. 2003. Remotely sensed evidence of enhanced erosion during the twentieth century on Herschel Island, Yukon Territory. **443**: 54-59.

Lantuit, H. and Pollard, W.H. Temporal stereophotogrammetric analysis of retrogressive thaw slumps on Herschel Island, Yukon Territory. *Natural Hazards and Earth System Science, in press.*

Lantuit, H., Couture, N., Pollard, W.H., Haltigin, T., De Pascale, G. and Budkewitsch, P.: Short-term evolution of coastal polycyclic retrogressive thaw slumps on Herschel Island, Yukon Territory. *Berichte zur Polar- und Meeresforschung (Reports on Polar and Marine Research), in press.*

Lewkowicz AG. 1987. Headwall retreat of ground-ice failures, Banks Island, Northwest Territories. *Canadian Journal of Earth Sciences* **24**: 1077-1085.

Lewkowicz AG. 1990. Morphology, frequency and magnitude of active layer detachment slides, Fosheim Peninsula, Ellesmere island, N.W.T. *Proceedings of the Fifth Canadian Permafrost Conference*. Quebec City, Université Laval; 111-118.

Lewkowicz AG. 1991. Climatic Change and the Permafrost Landscape. In Woo MK and Gregor DJ. 1991. *Arctic Environment: Past, Present and Future*, proceedings of a symposium, Nov 14-15, 1991, Dpt. Of Geography, McMaster University, Hamilton; 91-104.

Li D, Ma R and Di K. 2002. Digital Tide-Coordinated Shoreline. *Marine geodesy* **25**: 27-36.

Mackay JR. 1959. Glacier ice-thrust features of the Yukon coast. *Geographical Bulletin*. **13**: 5-21.

Mackay JR. 1960. Notes on small boat harbours of the Yukon Coast. *Geography Bulletin* **15**: 19-30.

Mackay JR. 1963. Notes on the shoreline recession along the coast of the Yukon Territory. *Arctic* **16**: 195-197.

Mackay JR. 1966. Segregated epigenetic ice and failures in permafrost, Mackenzie Delta area, N.W.T. *Geographical Bulletin* **8**: 59-80.

Mackay JR. 1971. The origin of massive icy beds in permafrost, western arctic coast, Canada. *Canadian Journal of Earth Sciences* **8** (4): 397-422.

McDonald BC and Lewis CP. 1973. *Geomorphologic and Sedimentologic Processes of Rivers and Coast, Yukon Coastal Plain*. Environmental-Social Committee, Northern Pipelines, Canada; Rept. No. 73-39, 245 pp.

McGillivray DG, Agnew TA, McKay GA, Pilkington GR. and Hill MC. 1993. Impacts of climatic change on the Beaufort sea-ice regime: Implications for the arctic petroleum industry. *Climate Change Digest CCD 93-01*, Environnement Canada: Downsview, Ontario; 36 pp.

Ogorodov SA. 2003. Coastal dynamics in the Pechora Sea under technogenic impact. *Berichte zur Polar- und Meeresforschung (Reports on Polar and Marine Research)* **443**: 74-80.

Pollard WH. 1989. Buried snowbank ice in the central and northern Yukon Territory. *Proceedings, Twenty-Fifth Eastern Snow conference*, Québec; 292-297.

Pollard WH. 1990. The nature and origin of ground ice in the Herschel Island area, Yukon Territory. *Proceedings, Fifth Canadian Permafrost Conference*, Québec; 23-30.

Pollard WH and French HM. 1980. A first approximation of the volume of ground ice, Richards Island, Pleistocene Mackenzie Delta, N.W.T. *Canadian Geotechnical Journal* **17**: 509-516.

Pollard WH and Couture N. 2000. Application of morphological methods to estimation of ground ice content at selected sites along the Beaufort Sea coast. Report for Geological Survey of Canada (Atlantic), 39 pp.

Rampton VN. 1982. Quaternary geology of the Yukon coastal plain. *Geological Survey of Canada, Bulletin* **317**, 49pp.

Smith MW. 1993. Climate Change and permafrost. In *Canada's Cold Environments*, French HM and Slaymaker O (ed); 292-311.

Smith CAS, Kennedy CE, Hargrave AE and McKenna KM. 1989. Soil and vegetation of Herschel Island, Yukon Territory. *Yukon Soil Survey Report No. 1*. Land Resource Research Centre, Agriculture Canada: Ottawa.

Solomon SM. 2002. *Tuktoyaktuk Erosion Risk Assessment Report*. Geological Survey of Canada, Natural Resources Canada.

Solomon SM. 2004. Spatial and temporal variability of shoreline change in the Beaufort-Mackenzie region, Northwest Territories, Canada. *Geo-Marine Letters. Online edition.*

Solomon SM, Forbes DL and Kierstead B. 1994. Coastal Impacts of Climate Change: Beaufort Sea Erosion Study. *Canadian Climate Centre, Report 94-2* Environment Canada: Downsview, Ontario, Canada; 34 pp.

Toutin T. 2001. Geometric Processing of IKONOS-1 Geo Images with DEM. *Proceedings of ISPRS Joint Workshop "High Resolution Mapping from Space" 2001,* 19-21 September, Hanover, Germany

Turner JD, Pollard WH and Hoque MD. 2004. Numerical modeling of thermal-mechanical niche formation and block failure on Herschel Island, Yukon Territory, Canada. *Eos Transactions. Joint Assembly of the CGU, AGU, SEG and EEGS, Montreal, Canada, May 17-21, 2004.* **85** (17): OS33A-01.

Valadan Z and Toosi, KN. 2003. Rigorous and non-rigorous photogrammetric processing of IKONOS-1 geo image *Proceedings Joint ISPRS Workshop "High resolution mapping from space 2003"*, October 2003, Hannover, Germany, 6pp, (on CD-ROM).

Vasiliev, A. 2003 "Permafrost controls of coastal dynamics at the Marre-Sale key site, Western Yamal." *Proceedings - 8th International Conference on Permafrost, Zurich, Switzerland, July 20-25, 2003.* Edited by . Phillips, S.M. Springman and L.U. Arenson; International Permafrost Association **2**: 1173-1178.

Williams PJ. 1995. Permafrost and climate change: geotechnical implications. *Philosophical Transactions, Royal Society of London* **352** (1699): 347-358.

Wolfe SA, Kotler E and Dallimore SR. 2001. Surficial characteristics and the distribution of thaw landforms (1970 to 1999), Shingle Point to Kay Point, Yukon Territory. *Open File 4088.* Geological Survey of Canada.

**Table 1. Coastal retreat rates (m/yr).**
Subdivided by orientation of the shoreline and by proximity to retrogressive thaw slumps. Negative changes are erosional

| | Shoreline exposition/type | | | | | | | | | | | | | |
|---|---|---|---|---|---|---|---|---|---|---|---|---|---|---|
| | NW | NNW | N | NNE | NE | ENE | E | ESE | SE | SSE | S | Overall | Presence of slumps (within a 10m radius) | No presence of slumps (within a 10m radius) |
| CRR 1952-1970 (m/yr) | -1.16 | -1.82 | -1.01 | -0.66 | -0.97 | x | -1.32 | -0.35 | -0.36 | -1.04 | -0.43 | -0.61 | -0.32 | -0,93 |
| CRR 1970-2000 (m/yr) | -0.82 | -0.73 | -0.64 | -0.44 | -0.35 | x | -0.61 | -0.10 | -0.58 | -1.04 | -0.86 | -0.45 | -0.60 | -0,51 |
| Evolution (%) | -29 | -60 | -37 | -33 | -64 | x | -54 | -71 | +61 | 0 | +100 | -26 | +88 | -45 |

*x = No data available*

**Table 2 Area and count of landslides by type (active and stable slumps and active layer detachments) for the years 1952, 1970 and 2000**

| | 1952 | 1970 | 2000 |
|---|---|---|---|
| Areas (m²) | | | |
| Total landslide area | 1556103 | 1713783 | 1783714 |
| Active slumps | 185837 | 189300 | 484037 |
| Stable slumps | 1234835 | 1324742 | 1158777 |
| Active layer detachments | 135431 | 199741 | 140901 |
| Areas (%) | | | |
| Total landslide area | 100 | 100 | 100 |
| Active slumps | 12 | 11 | 27 |
| Stable slumps | 79 | 77 | 65 |
| Active layer detachments | 9 | 12 | 8 |
| Count | | | |
| Total | 80 | 134 | 164 |
| Active slumps | 46 | 68 | 75 |
| Stable slumps | 15 | 31 | 40 |
| Active layer detachments | 19 | 35 | 49 |
| Count (%) | | | |
| Total | 100 | 100 | 100 |
| Active slumps | 57 | 51 | 46 |
| Stable slumps | 19 | 23 | 24 |
| Active layer detachments | 24 | 26 | 30 |

**Table 3 Identification of zones precluding active slump occurrence**

Type of landslide (active or stable slump and active layer detachments) in the preceding measurement year (1952 for 1970 and 1970 for 2000)
Each active slump in 2000 is attributed the type of landslide occurring at the same location in 1970
The same operation is repeated with the year 1952 for 1970

| | Proportion of active slumps located in: | | |
|---|---|---|---|
| Measurement year | Previously active slumps (%) | Previously stable slumps (%) | Previously active layer detachment (%) |
| 1970 | 19 | 76 | 5 |
| 2000 | 48 | 42 | 10 |

**Table 4 Retrogressive thaw slump generation and corresponding morphologic parameters for the years 1952, 1970, and 2000**

| | 1952 | | | 1970 | | | 2000 | | |
|---|---|---|---|---|---|---|---|---|---|
| Slump generation | Mean inland extent (m) | Mean Area ($m^2$) | Number of slumps | Mean inland extent (m) | Mean Area ($m^2$) | Number of slumps | Mean inland extent (m) | Mean Area ($m^2$) | Number of slumps |
| 1 | 226 | 61707 | 18 | 164 | 36652 | 31 | 174 | 33005 | 37 |
| 2 | 98 | 8323 | 33 | 86 | 6469 | 41 | 103 | 6295 | 56 |
| 3 | 55 | 2471 | 7 | 69 | 4997 | 19 | 82 | 3348 | 19 |
| 4 | 54 | 933 | 2 | 60 | 1767 | 7 | 55 | 1559 | 3 |
| 5 | x | x | 0 | 60 | 331 | 2 | 48 | 1610 | 1 |

**Fig.1 Herschel Island location in the southern Beaufort Sea. Top left hand inset: toponimy of the Herschel Island area.**

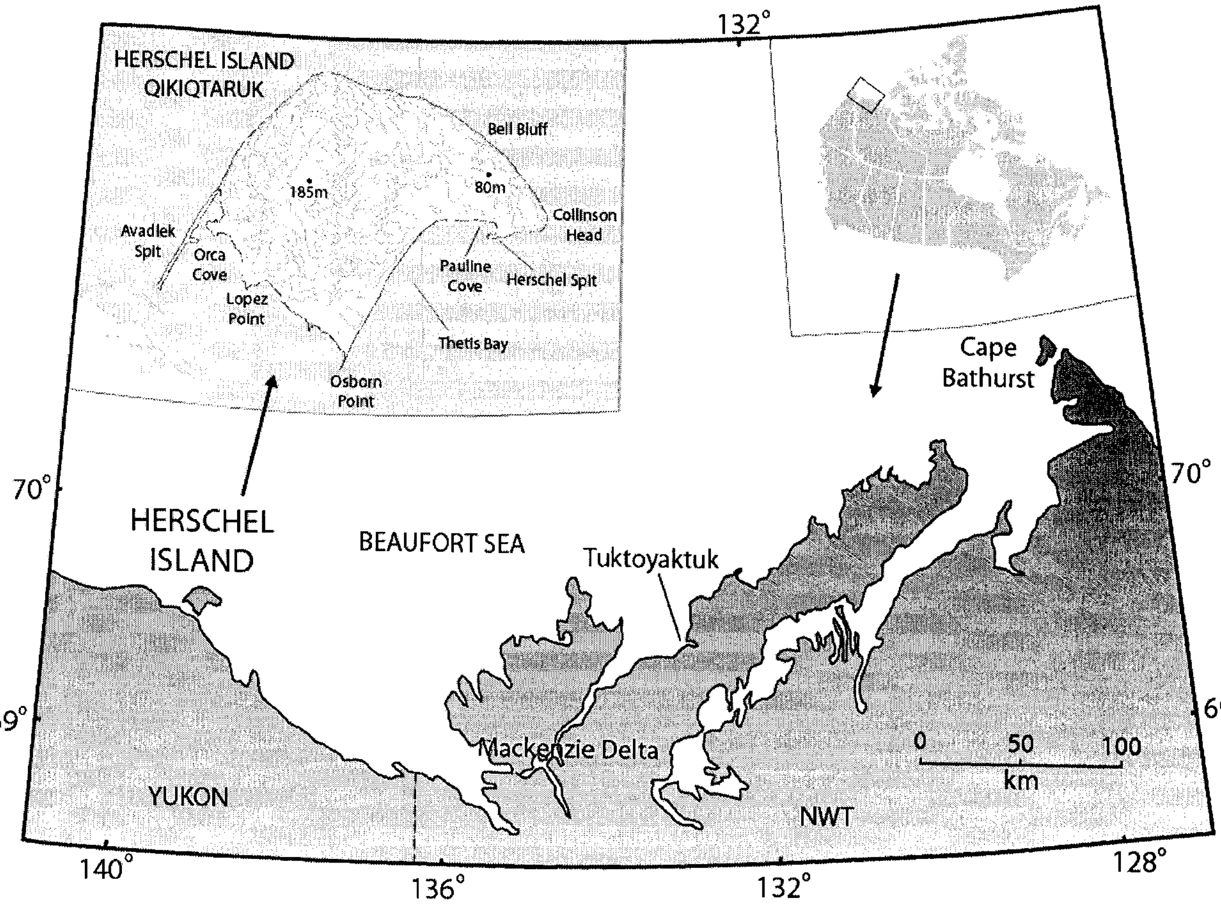

**Fig.2 Block failure, May 1986.** Cliff is approximately 20m high.

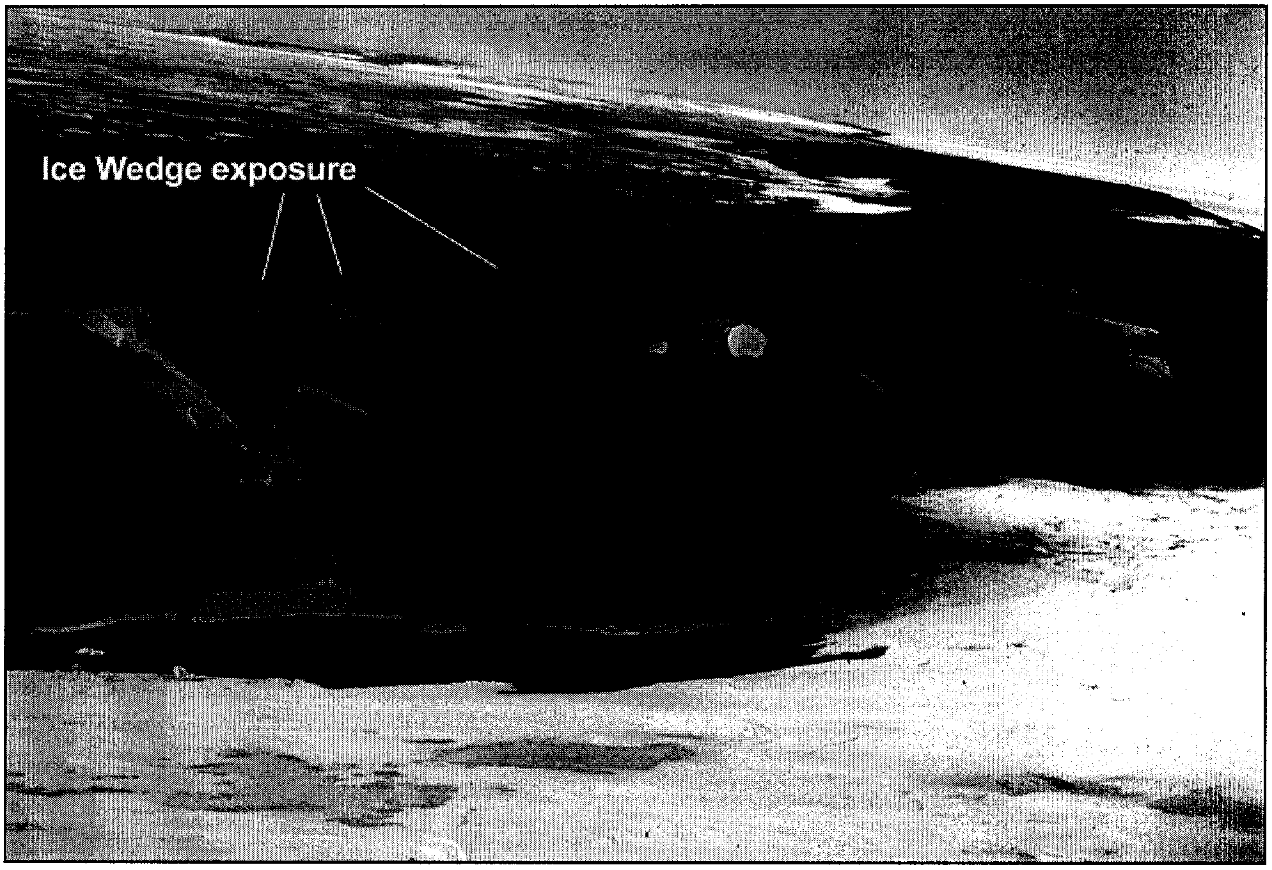

**Fig.3 Retrogressive thaw slump in Thetis Bay, Herschel Island, July 1986.**
Note the typical bowl shape of the slump and the former slump scar surrounding the current headwall.

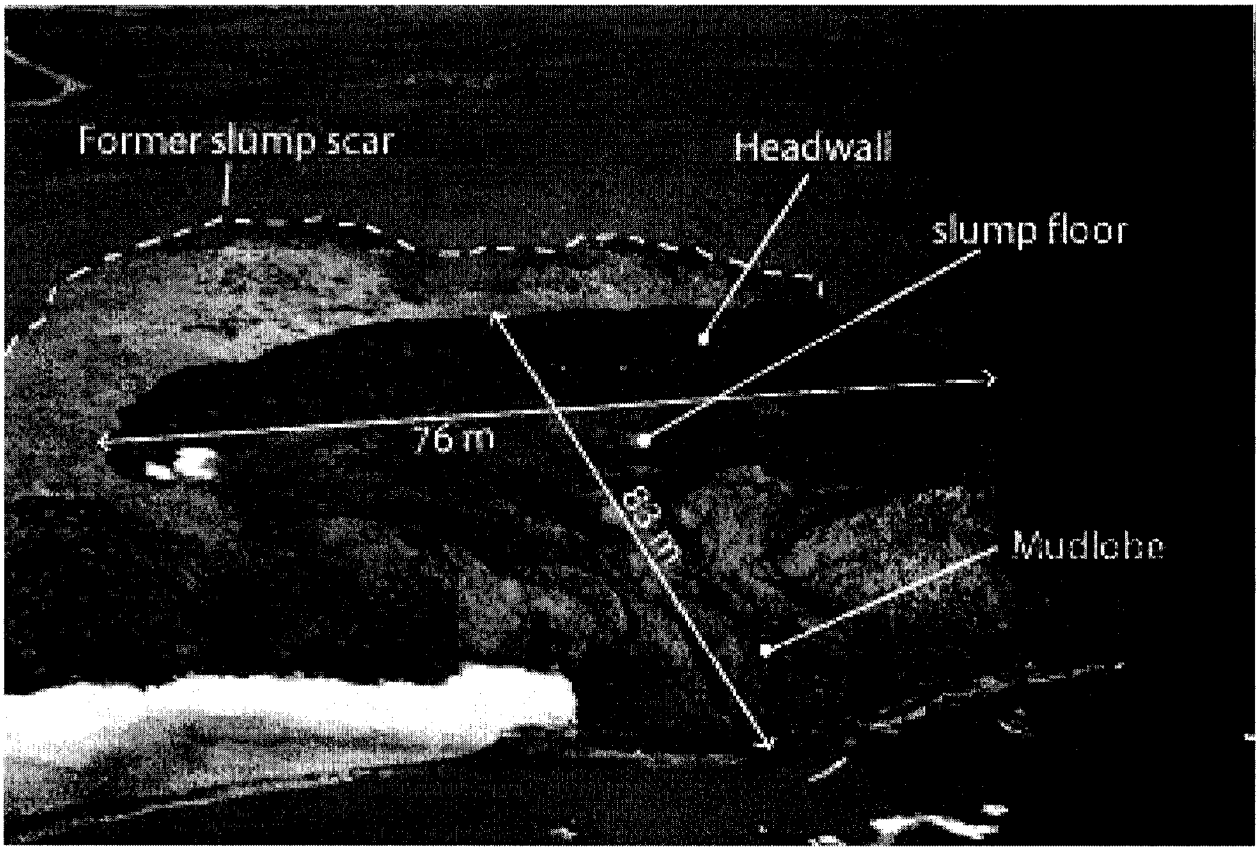

**Fig.4. Functional scheme of retrogressive thaw slump..**

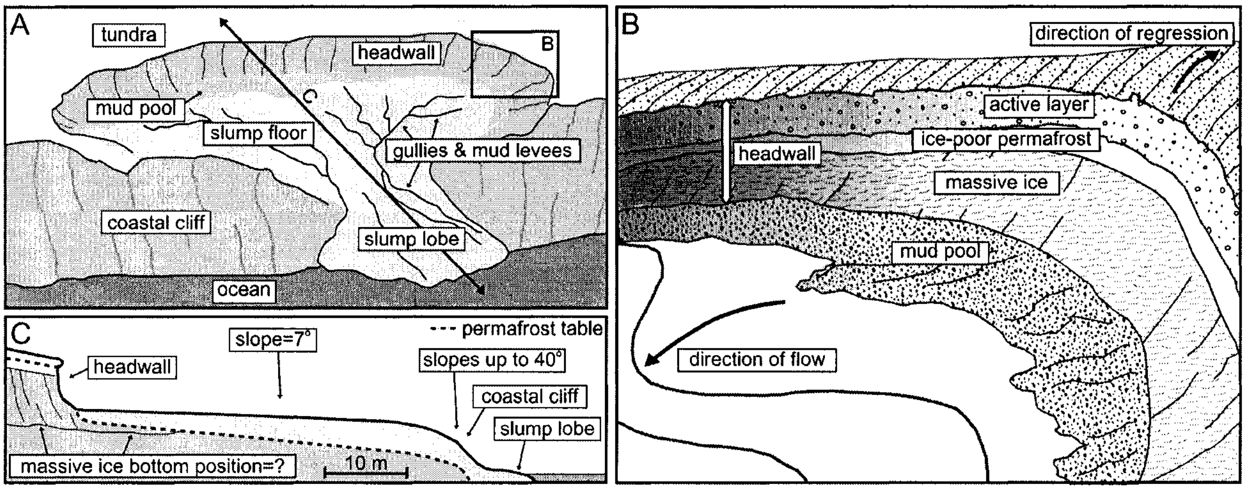

**Fig.5 Helicopter view of a polycyclic slump in Thetis Bay, Herschel Island, August 2004.**

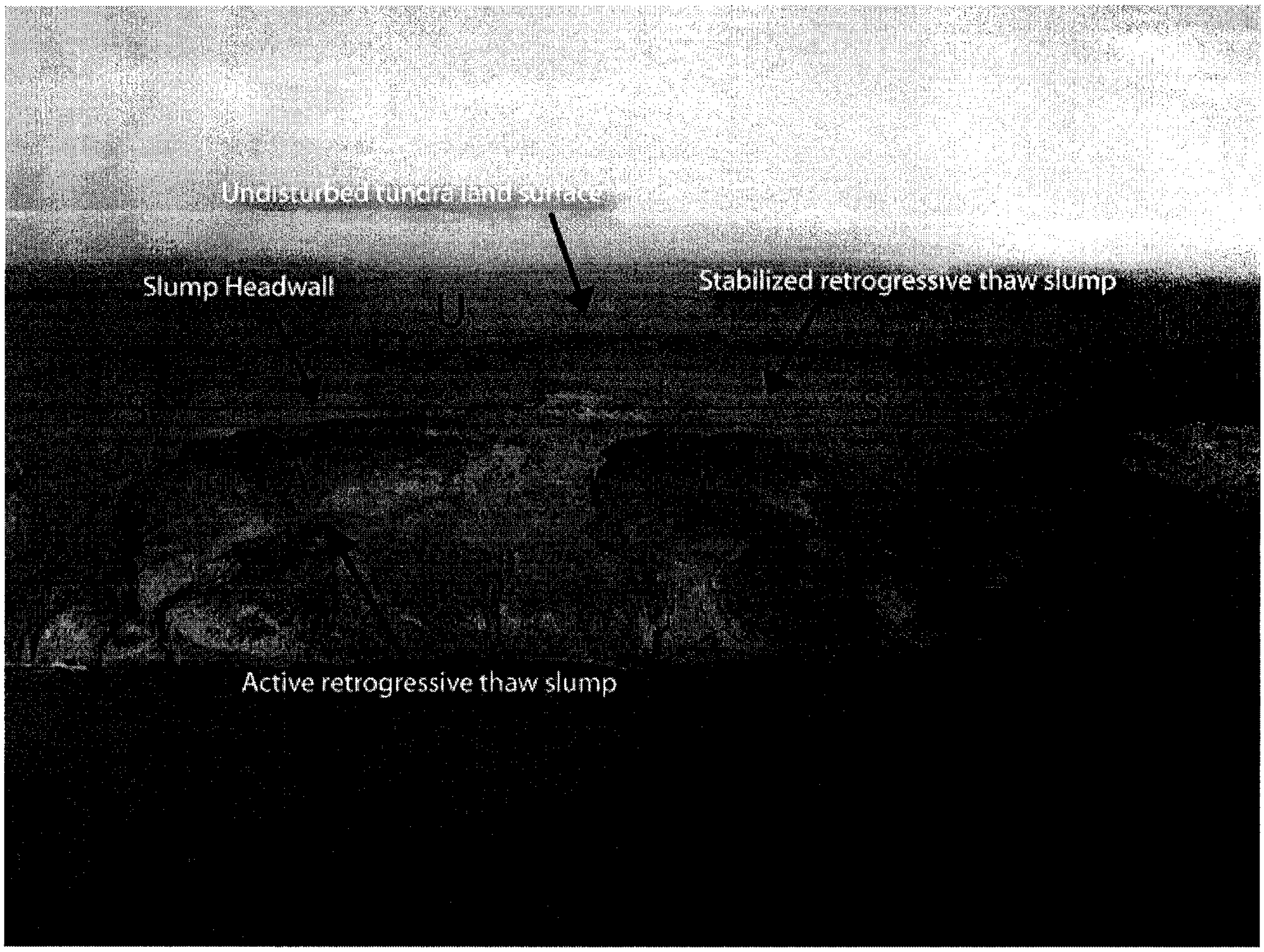

**Fig.6 Conceptual illustration of the methodology for slump generation classification.**
Background image for contextualisation

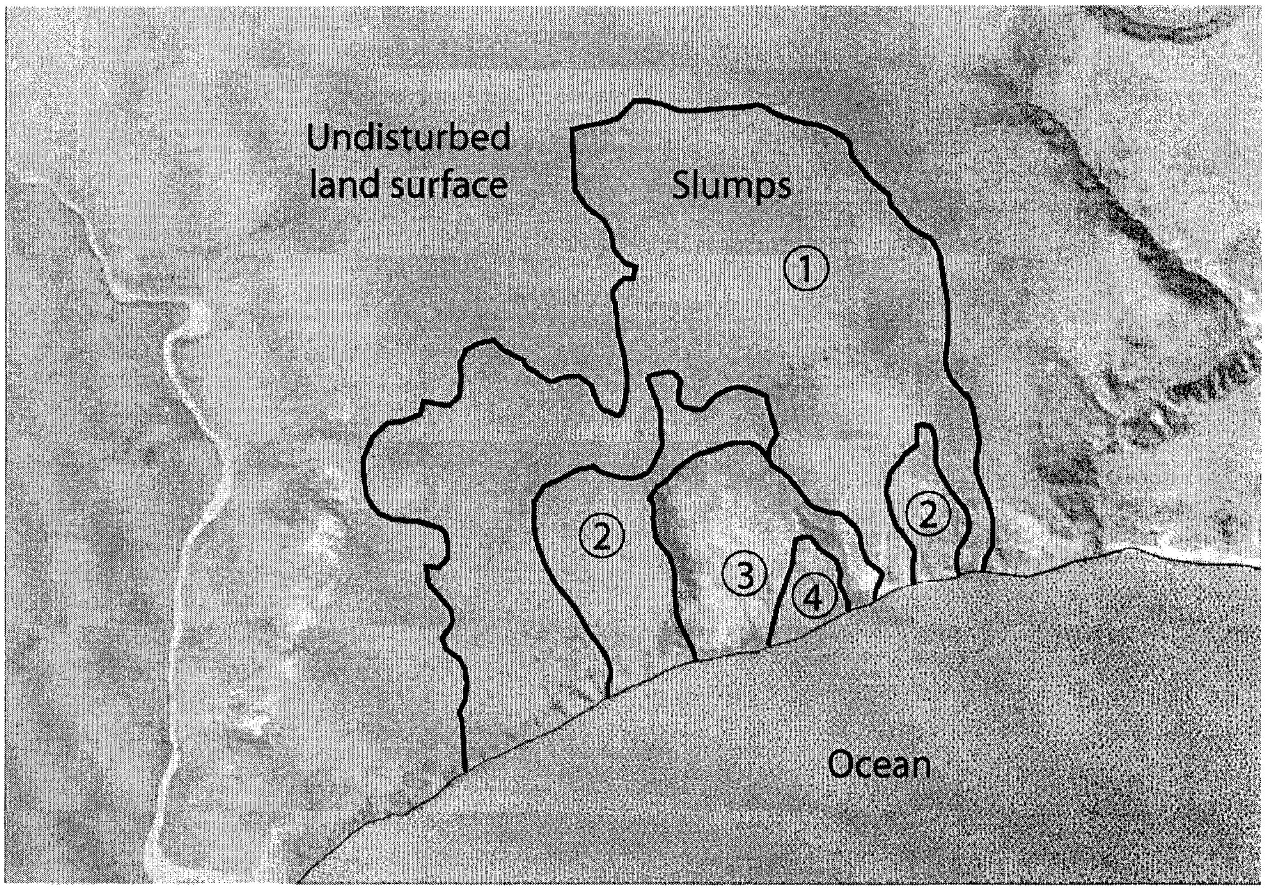

**Fig.7 Coastal retreat rates, 1952-1970, Herschel Island.**

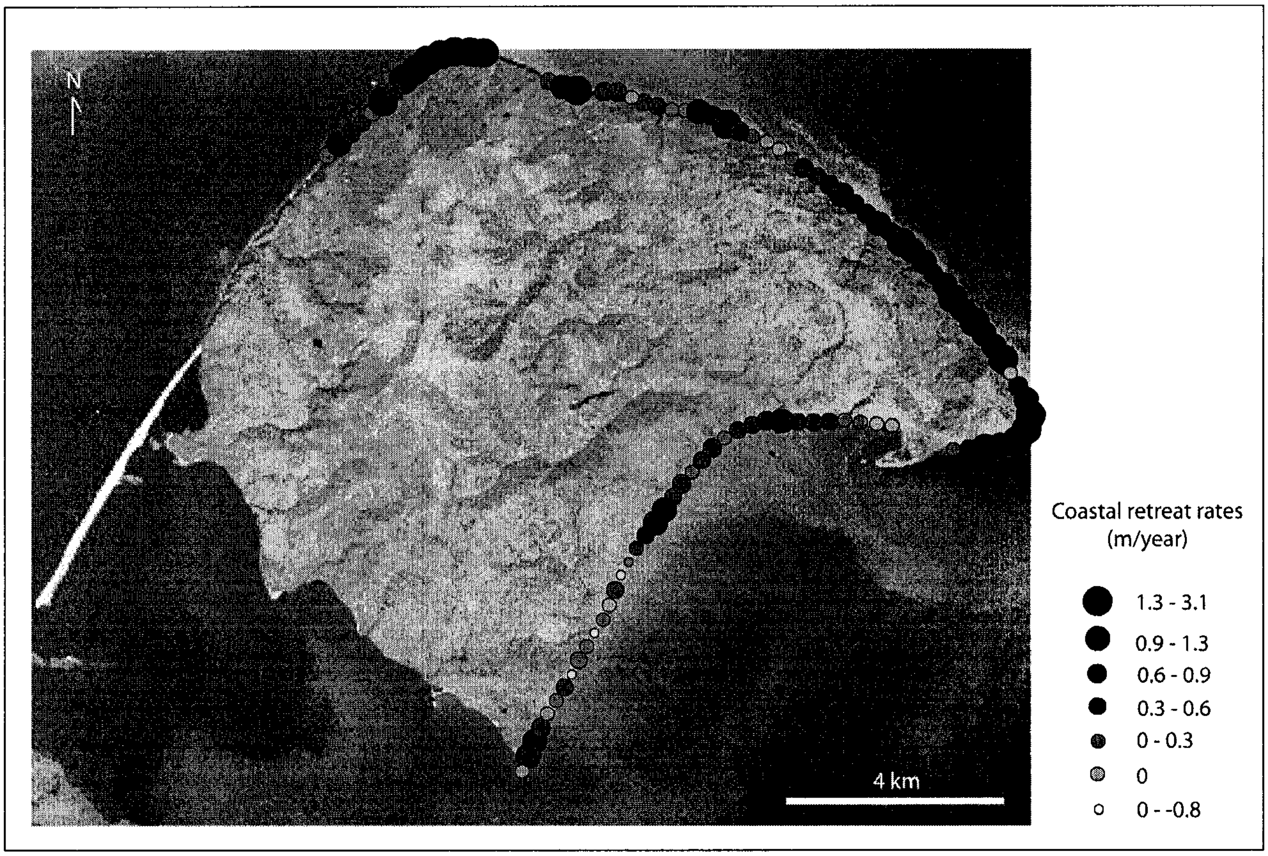

**Fig.8 Coastal retreat rates, 1970-2000, Herschel Island.**

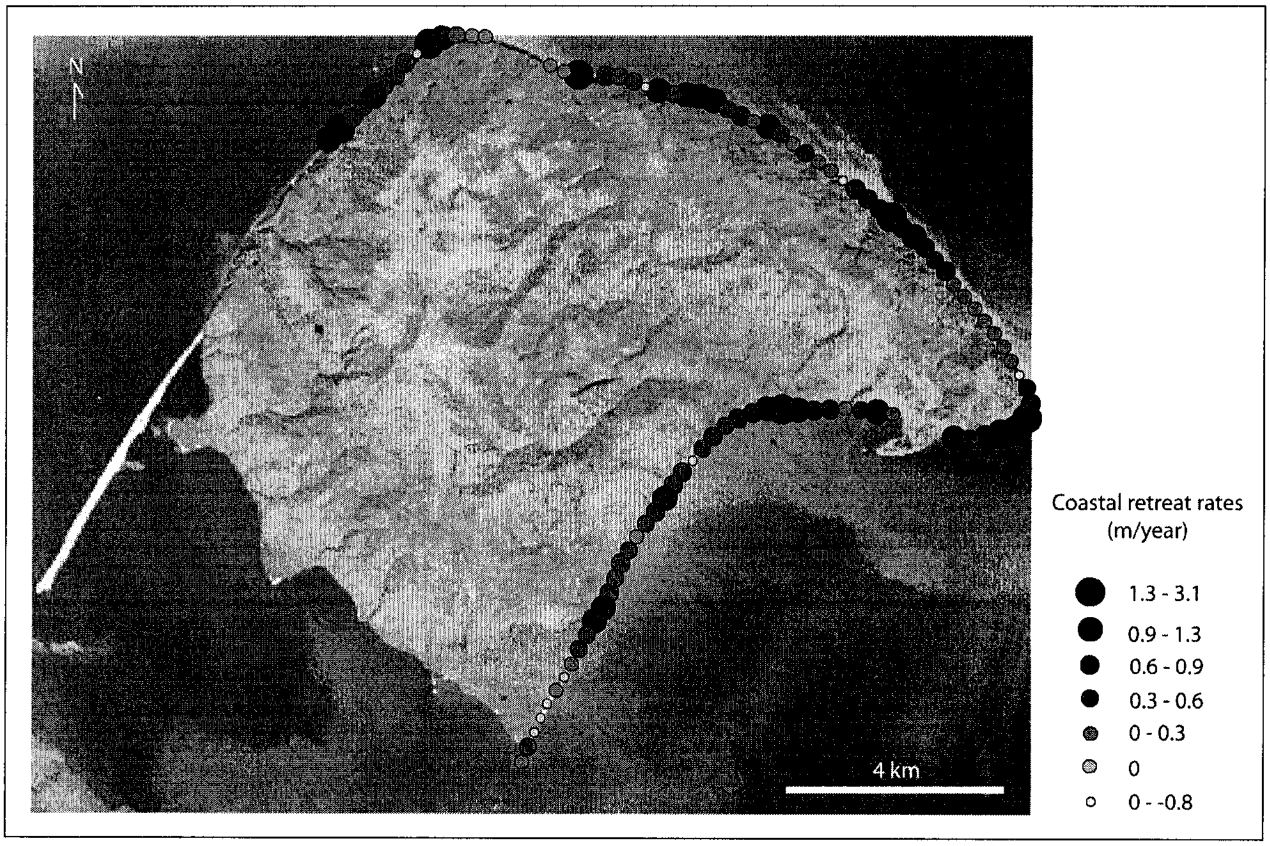

**Fig.9 Coastal retreat rates evolution between the 1952-1970 and 1970-2000 periods, Herschel Island.**

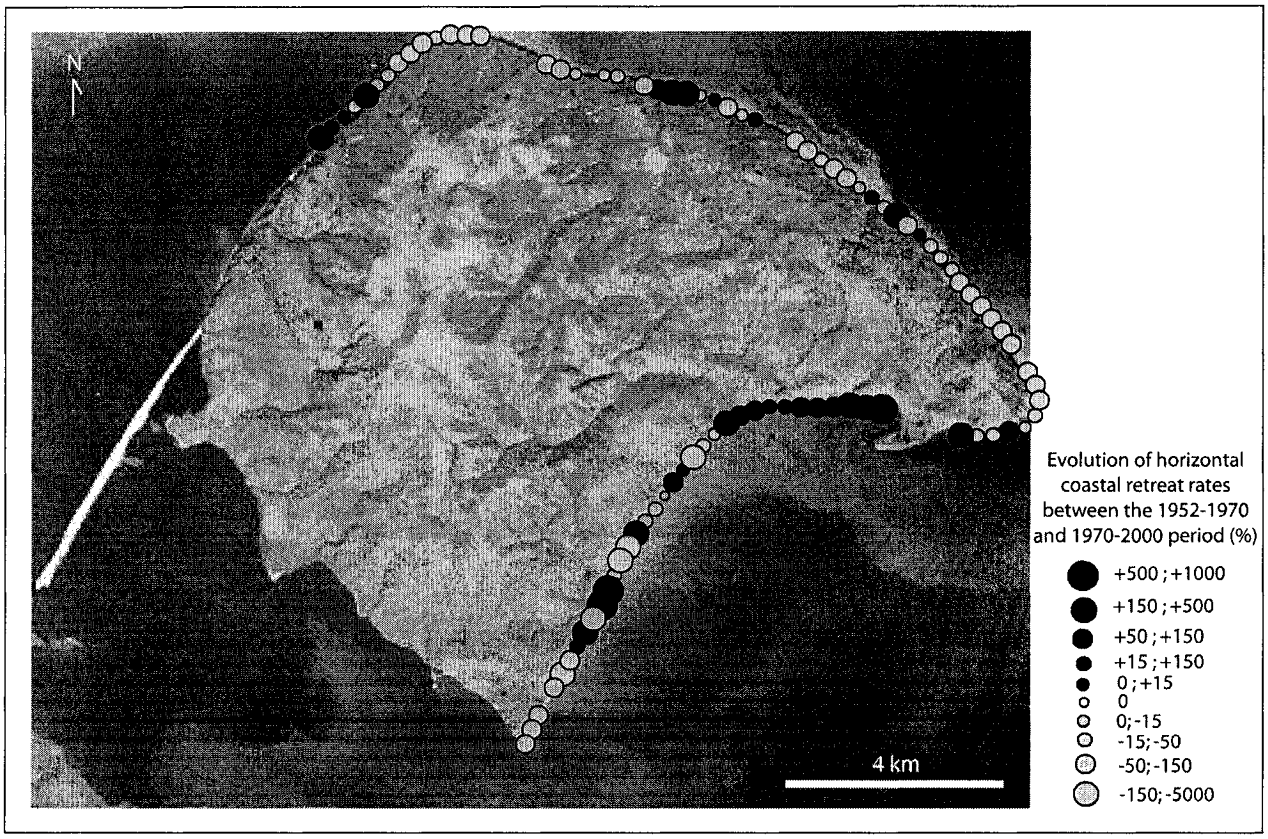

**Fig.10 Slumps locations in 2000, Herschel Island.**
Note that the western part of the island is not included in the study.

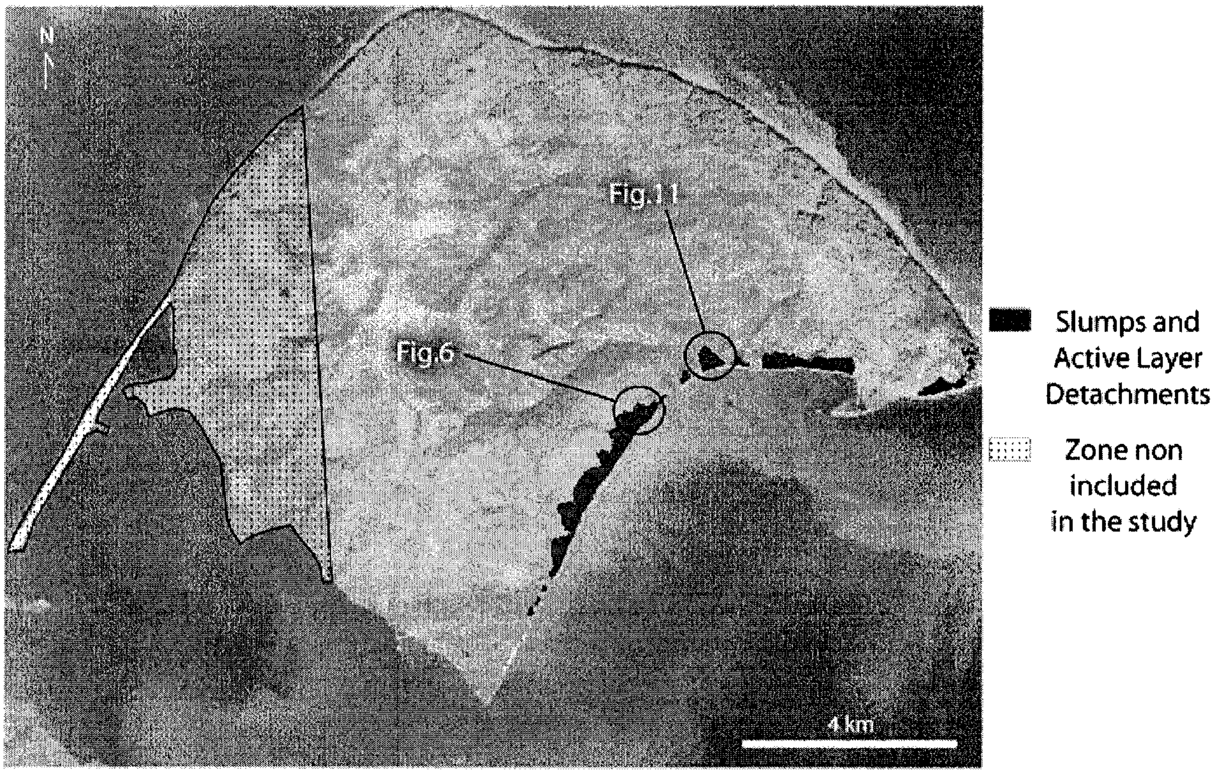

**Fig.11 Retrogressive thaw slump in Thetis Bay. Years 1952, 1970 and 2000.**
Second and higher order slumps have developed in the main slump floor.

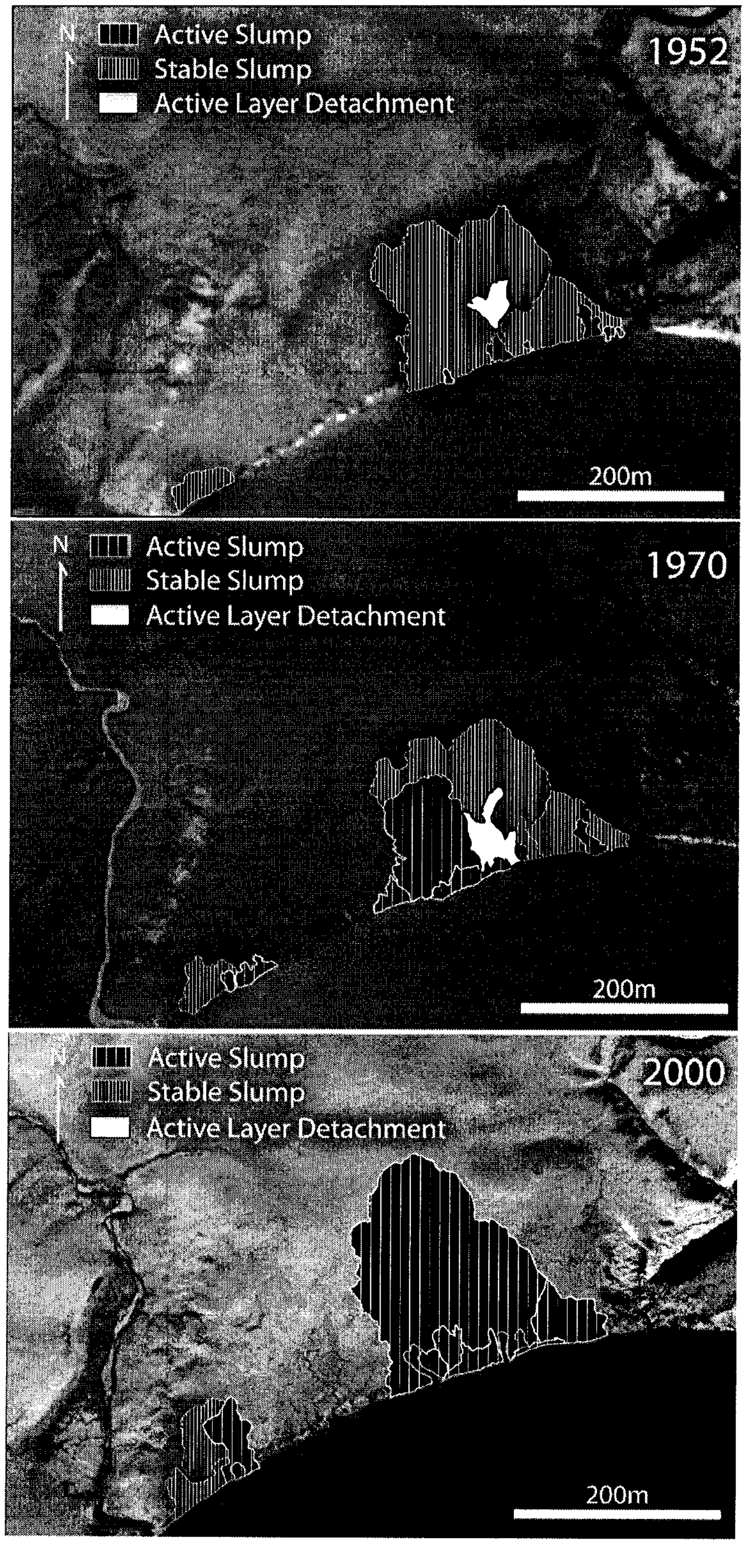

**Fig.12 Maximum inland extent and slump generations for the years 1952, 1970 and 2000, Herschel Island.**

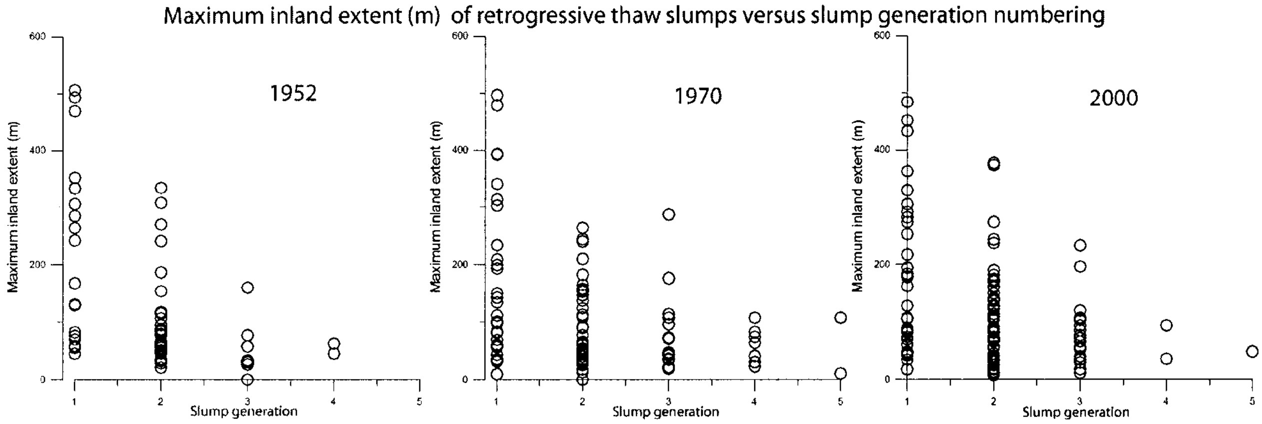

**Fig.13. General relation between slump generation and mean and median maximum slump inland extent, Herschel Island.**
Number of considered slumps = 274.

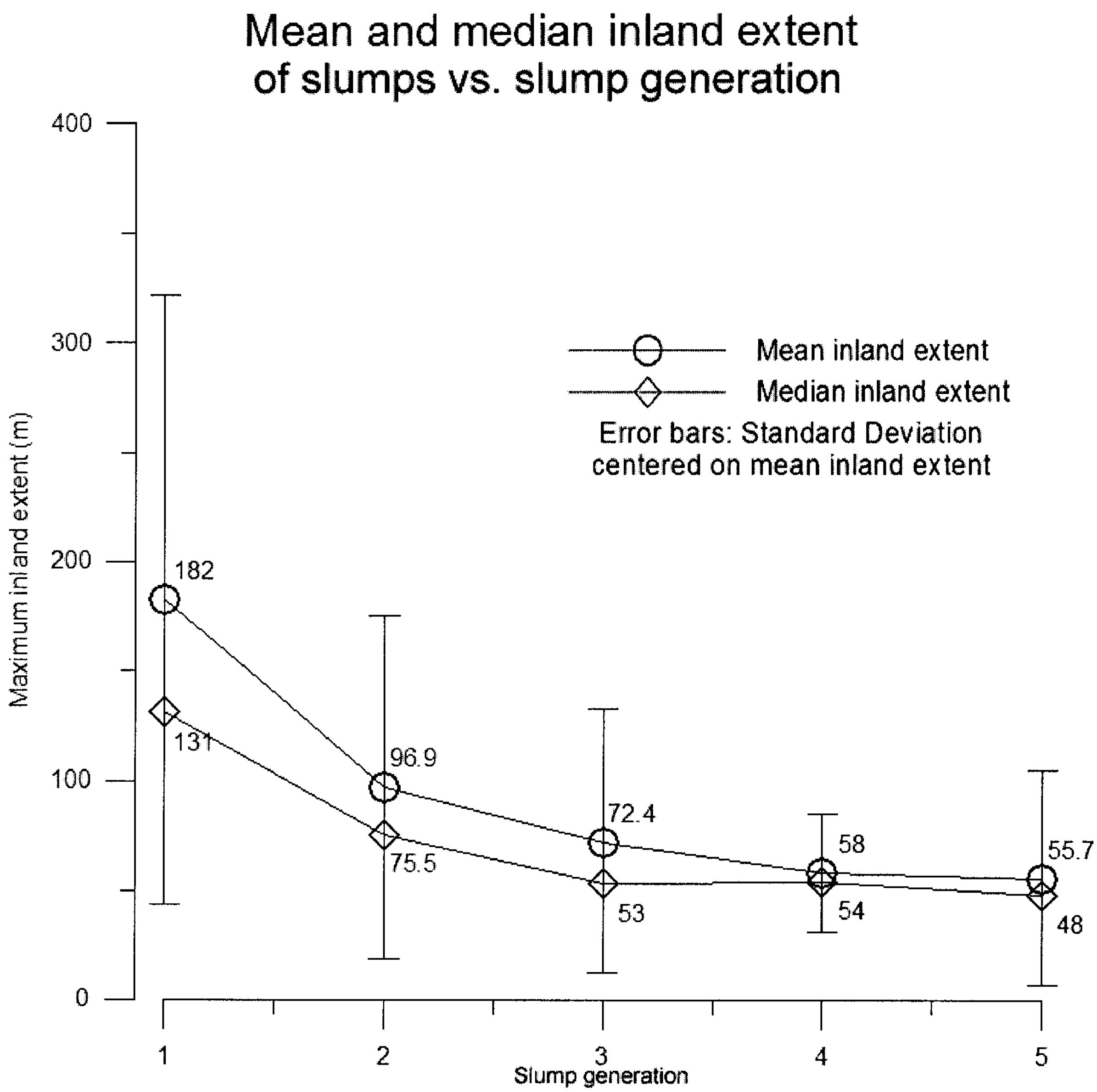

**Fig.14 Retrogressive thaw slump development within the floor of an active layer detachment, Herschel Spit area, Herschel Island, Summer 1986.**
After De Krom (1990)

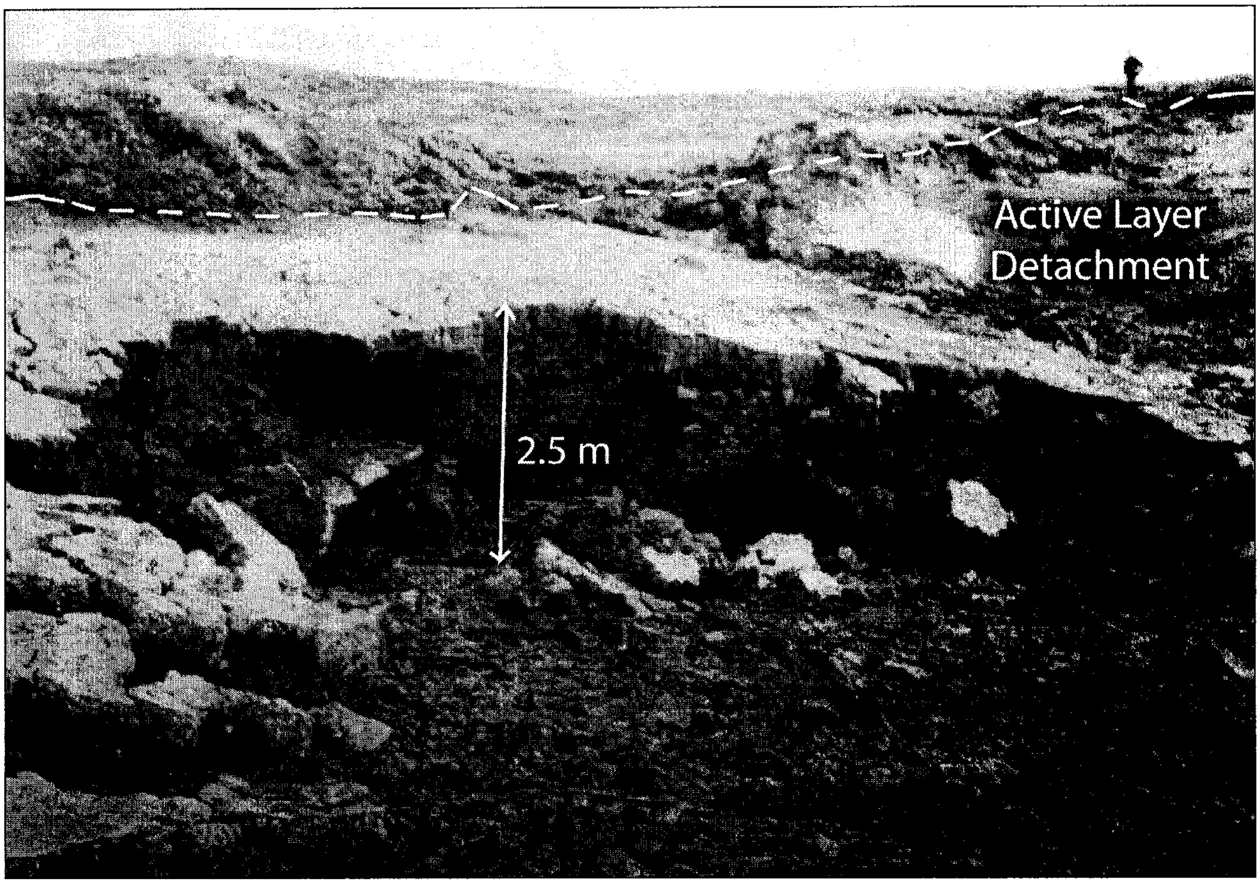

# CHAPTER 4 – MANUSCRIPT #2

**Temporal stereophotogrammetric analysis of retrogressive thaw slumps on Herschel Island, Yukon Territory**

H. Lantuit and W.H. Pollard

## Abstract

The western Canadian Arctic is vulnerable to global warming, leading to enhanced coastal erosion and thermokarst activity. Retrogressive thaw slumps, a major form of backwasting thermokarst, are common along Herschel Island coasts and have been increasing in number due to enhanced thawing of massive ice and coastal erosion. The volumes of sediment eroded through slump activity and subsequent release of organic carbon to the nearshore zone, which ultimately contribute to the global carbon cycle, are largely unknown. In response, two retrogressive thaw slumps located on the western shore of Herschel Island were analyzed using stereophotogrammetric methods in order to (1) provide the first three-dimensional analysis of these landforms, and (2) provide an estimation of the volume of sediment eroded through slump activity. Digital Elevation Models (DEMs) were extracted for the years 1952, 1970 and 2004 and validated against Kinematic Global Positioning System (KDGPS) points collected in the field. Estimations of eroded sediment from retrogressive thaw slumps showed that the volume of sediment can vary greatly from one slump to another. For slump A, eroded volumes of sediment and ice measured approximately 1 560 000 $m^3$ for the 1970-2004 period. For the same period and slump, eroded volumes of sediment alone were estimated at about 360 000 $m^3$. These volumes of sediment eroded through slump activity were observed to be larger than volumes of eroded sediment observed in typical cliff erosion. The temporal analysis of the DEMs showed that predictions of future occurrences of second generation retrogressive thaw slumps within the floor of a larger polycyclic retrogressive thaw slump are possible.

## 1 Introduction

Most arctic coasts are situated in the continuous permafrost zone and are therefore vulnerable to thaw-related warming processes (Brown *et al.*, 1998; Serreze *et al.*, 2000). Warming will cause sea level rise, increased exposure to wave activity, and thawing of earth materials, leading to enhanced coastal erosion and greater thermokarst activity (McGillivray *et al.*, 1993). Retrogressive thaw slumps, a form of backwasting thermokarst, are common along arctic coasts and are characterized by the presence of massive ground ice. Since the southern Beaufort Sea region is one of the most ice-rich areas in the Canadian Arctic (Pollard and French, 1980), retrogressive thaw slumps are expected to occur on a more frequent basis (Lantuit and Pollard, 2005).

Using high resolution imagery, polycyclic retrogressive thaw slumps (slumps within former slumps) are easy to identify (Lantuit and Pollard, 2005). However, there has been no attempt thus far to use a three-dimensional analysis to predict future occurrences of retrogressive thaw slumps within former slumps. Furthermore, in order to assess volumetric losses of sediment from retrogressive thaw slumps, a three-dimensional analysis of digital images is required.

The quantity of sediments removed by retrogressive thaw slump activity is used to estimate the contribution of organic carbon from arctic coasts into the Arctic Ocean, based on the volume fraction of soil organic carbon measured for permafrost soils (Rachold *et al.*, 2003). Under various climate change scenarios, thermokarst processes are expected to increase, but since there are no long-term studies of thaw-related volume losses or estimates of carbon content, the potential contribution is unknown (Lewkowicz, 1991).

Retrogressive thaw slump headwalls are often hundreds of metres long and occasionally over a kilometre wide, and retreat at average rates up to 9.6 m/yr (Lantuit *et al.*, *in press*). This magnitude of landscape change constitutes a major hazard for human-built structures (Huscroft *et al.*, 2003). Since the western Canadian arctic is one of the most ice-rich and populated arctic areas, it is likely that many communities in the region will undergo increasing threat due to this type of thermokarst activity. Since the prediction of new retrogressive thaw slump occurrence remains difficult due to the variable nature of ground ice, new tools and techniques are needed to monitor and predict the progression of these landforms once they begin.

## 2 Objectives

The goals of this paper are (1) to assess the value of stereophotogrammetric methods in mapping volume losses associated with two retrogressive thaw slumps on Herschel Island between 1952 and 2004, (2) to estimate the total volume of sediment and ice lost for two retrogressive thaw slumps, and (3) to map the morphological evolution of these slumps and the possibilities of future occurrence of second or third generation retrogressive thaw slumps.

## 3 Background

The Yukon Coastal Plain and Mackenzie Delta are underlain by continuous permafrost up to 1000 m deep (Young and Judge, 1986). Permafrost is ground that remains at or below 0°C for a minimum of two years (Everdingen, 2002). Permafrost conditions in the western Arctic reflect the complex pattern of glacial events during the Pleistocene and the development of Holocene permafrost. Typically areas of Pleistocene permafrost are much thicker than areas of more recent permafrost aggradation.

Ground ice is a common constituent of permafrost. Since ground ice includes all forms of frozen moisture it varies greatly in character. If the volume of ice in the ground exceeds the total pore volume, the volume in excess of saturation is termed "excess ice". Upon thawing, a soil containing excess ice will consolidate, releasing vast quantities of thawed water, termed supernatant water.

Excess ice occurs in various forms (segregated ice, reticulated ice, buried glacier ice, buried snowbank ice, massive tabular ice, wedge ice) (Mackay, 1972). The term massive ice refers to "a mass of ground ice which has an ice content of at least 250 percent (on an ice-to-dry-soil weight basis)" (Mackay, 1971).

The degradation of massive ice leads to thermokarst, which is "the process by which characteristic landforms result from the thawing of ice-rich permafrost or the melting of massive ice (Everdingen, 2002)". Retrogressive thaw slumps are backwasting thermokarst features that sometimes extend as much as 500 m inland and 1 km laterally (Lantuit and Pollard, 2005) (Figure 1). Retrogressive thaw slump morphology includes, (1) a vertical "headwall" comprised of the active layer and ice-poor organic and mineral materials, (2) a "headscarp" comprised of a steeply inclined (20 to 50°) exposure of ice-rich sediment that retreats by the ablation due to sensible heat fluxes and solar radiation, and (3) the slump floor, consisting of a mud pool at the base of the headscarp followed by a zone of fluid mud forming levees and flow deposits that expand in a lobe pattern at the toe of the slump (Figures 1 and 2) (De Krom, 1990; Lewkowicz, 1987). Retrogressive thaw slumps are initiated by erosion of a thermally protected layer and exposure of ice-rich materials. For example, waves at the base of ice-rich coastal cliffs may uncover a massive ice body leading to ice ablation (De Krom, 1990). If the exposed massive ice melt rate exceeds the rate of erosion at the base of the cliff, then a retrogressive thaw slump is initiated and sustained (Lewkowicz, 1987).

In some coastal locations, the frequency of retrogressive thaw slump activity is linked to the intensity of wave action at its base. The removal of retrogressive thaw slump debris at its toe by wave action or littoral drift aids in maintaining a steep shore gradient. This facilitates the removal of sediment and prevents the build-up of debris at the base of the headwall or on the retrogressive thaw slump floor. Retrogressive thaw slumps are also often polycyclic in nature. This refers to the formation of new retrogressive thaw slumps within the floor of an older retrogressive feature (Mackay, 1966; Wolfe *et al.*, 2001). The older slump can be active or stable. The new retrogressive thaw slump will develop a similar shape to its parent. It is not uncommon to find several generations of retrogressive thaw slumps co-existing within the same slump. Renewed retrogressive thaw slumps eventually reach the headwall of the larger retrogressive thaw slump.

## 4 Study area

### *4.1 Location and physiographic setting*

Herschel Island lies approximately 60 km east of the Yukon / Alaska border, 160 km west of the Mackenzie Delta and 3 km north of the continental coast (Figure 3). It is part of the Yukon Coastal Plain physiographic region, which is an erosional surface in the bedrock that has been covered by marine and fluvial deposits. Herschel Island is believed to be a push moraine caused by late Pleistocene fluctuations of the Laurentide ice sheet (ca. 40 000 BP) (Rampton, 1982).

Ice contents in the permafrost on Herschel Island are up to 20% higher than elsewhere on the Yukon Coastal Plain (Pollard, 1990). Ground ice underlies most of the island except under recent coastal landforms such as sand spits and sandy-pebbly beaches, and constitutes up to 60-

70% of the upper 10-12 m of permafrost (Pollard, 1990). Massive ice is widely observed on the island in coastal sections and landslide-induced exposures, on south, south-east and north-west facing shores (Figure 4). The thickness of massive ice has been observed to range between 4 and 13 m but is probably greater since only the upper part of the ice body is visible in coastal exposures(Pollard, 1990; De Krom, 1990).

### *4.2 Slump activity on Herschel Island*

The retrogressive thaw slumps on Herschel Island are among the largest and most numerous encountered in the Canadian Arctic (De Krom, 1990). The rates of coastal erosion observed on the island range between 0.3 and 2 m/yr and contribute to the development of retrogressive thaw slumps (Lantuit and Pollard, 2005). In addition, coastal erosion is often observed to increase following the occurrence of thaw slumps (Lantuit and Pollard, 2005).

Retrogressive thaw slump frequency has been increasing on Herschel Island during the 1952-2000 period and is expected to continue to increase due to generally warmer conditions in the Canadian arctic (Lewkowicz, 1991; Lantuit and Pollard, 2005).

Figures 5a and 5b illustrate two retrogressive thaw slumps (Slump A and Slump B) occurring in a sample area characterized by shore sections known to be susceptible to intense erosion (Lantuit and Pollard, 2005). Slump A is a large polycyclic retrogressive thaw slump that has been active since at least 1952, while Slump B is a simple bowl-shaped retrogressive thaw slumps which appears only on post-1970 imagery. Slump A extends 600 m laterally and Slump B is of much smaller size. Both slumps have massive ice bodies up to 20 m thick exposed in the headwall.

## 5 Methods

The calculation of soil volume losses relies on the creation of three-dimensional surface or DEM (Digital Elevation Model) for different periods. The creation of these surfaces is completed using a combination of geodetic surveys, high resolution GPS surveys and stereophotogrammetric methods. While the first two methods provide a higher accuracy for three-dimensional measurements, they require extensive surface coverage for good accuracy. Stereophotogrammetric methods, although relying largely on the accuracy of ground control points, can be used to build three-dimensional surfaces over much larger areas. In remote locations like the arctic, ground-based surveys can not be completed with any frequency so stereophotogrammetric analyses are a complementary alternative.

In this study, softcopy stereophotogrammetric tools are used to compile airphoto archives of Herschel Island for 1952 and 1970, and Ikonos panchromatic stereo-pairs for 2004.

### *5.1 Georeferencing controls for remotely sensed imagery*

The first step in processing datasets is to acquire a common georeferencing database. Given the remote location of Herschel Island, it is difficult to achieve this by relying on publicly available datasets. Georeferencing of digital images of Herschel Island were based on aerotriangulated coordinates from the 1970's and on topographic maps at the 1:50,000 scale. Topographic maps at the scales of 1:50,000 are available for the entire southern Beaufort Sea, but are not reliable for precise positioning at large scales. Differences in georeferencing between topographic maps and positions determined by submetre GPS are often greater than 40 m. Geodetic control points are more accurate but are limited along the Yukon Coastal Plain. We therefore used survey-grade positioning systems to georeference our imagery. Post-processed

Kinematic KDGPS (Kinematic Differential Global Positioning System) points were collected in the field during September 2003 and August 2004 using a Trimble 4700 GPS system in order to provide accurate absolute georeferencing. The horizontal and vertical accuracy of the outputs are within 2 cm when the collected points are rigorously postprocessed. An error of this magnitude is negligible when compared with the expected accuracy of stereophotogrammetric analyses. A 0.5 m resolution was assumed when locating ground control points in photo space. A set of stable landforms were identified on the three sets of imagery in order to collect the GPS control points in the field. These points, referred to polygon edges intersections or artificial features, and were all located inland and on stable slopes. The point location was documented using field photography. Changes related to either thaw subsidence or isostatic adjustment were not considered because: 1) their magnitude is likely very small for the location and 2) there are insufficient long-term data to make these corrections. The points chosen are equally distributed over the island. In addition, a KDGPS survey of the slump headwalls and the slump floors was completed on August 8$^{th}$, 2004, three days after the image was acquired by the Ikonos sensor in order to assess the quality of the extracted DEM.

*5.2 Stereophotogrammetric processing of remotely sensed imagery.*

Softcopy photogrammetric software was used to create the DEMs. Airphoto blocks were georeferenced according to the KDGPS survey points and DEMs were produced using the stereomatching algorithm of the softcopy photogrammetric software. The total Root mean square (RMS) error for the 17 ground control points after bundle adjustment was 1.69 m for the 1952 image series, and 1.58 m for the 1970 image series. The DEM spatial resolution was adopted from the scanning resolution used for the airphotos. Airphotos from 1952 (Aug. 28$^{th}$, 1:60,000) were scanned at 1600 dpi and produced an effective resolution of 1 m while airphotos from 1970 (Aug. 20$^{th}$, 1:13,000) were scanned at 800 dpi and produced an effective resolution of 0.3 m, later resampled to 1 m. The 2004 DEM was extracted from an Ikonos panchromatic stereo-pair (1 m resolution) acquired on August 5$^{th}$, 2004 using the method described by Toutin *et al.* (2001) and implemented in the softcopy photogrammetric software. Resulting DEMs were then edited and mosaiced to produce 1 m pixel ground resolution DEMs of the zones surrounding the retrogressive thaw slumps. The subtraction of both DEMs gave us a GIS layer for differential volume erosion over the 1952-1970 and 1970-2004 periods (Figures 5a, 5b). Pixels corresponding to losses of sediment were aggregated and used to calculate volume erosion.

### *5.3 Accuracy assessment*

The KDGPS points collected in the field three days after the acquisition of the Ikonos stereo-pair were used to assess the accuracy of the computed DEMs. The KDGPS points have an estimated accuracy of ± 2 cm, which is sufficient for the type of accuracy typically associated with DEMs extracted from Ikonos stereo-pairs (Valadan and Toosi, 2003). Two transects from the headwall to the lobe were conducted within the floors of the retrogressive thaw slumps. Due to the pattern of mudflows present within the slumps floors, transects could not be performed along a perfectly straight line (Figures 5a, 5b). They were, however, kept as straight as possible. Once processed in the softcopy photogrammetric software, DEMs were overlaid and compared to the KDGPS points. The resulting profiles are shown in Figures 6 and 7. The DEMs computed for the years 1952 and 1970 were controlled using KDGPS checkpoints collected during the summer of 2004. These checkpoints were located on tundra polygon edges or closed thaw ponds chosen for their stability between 1952 and 2004. Volume losses associated with retrogressive thaw slump occurrence were computed for the 1952-1970 and for the period of 1970-2004 on slump A and for the 1970-2004 on slump B. On slump A measurements were performed on a 600 m section of coast extending 200 m inland, excluding volume losses associated with coastal erosion. On slump B, volume losses were estimated on a 100 m long strip of coast extending 100 m inland for the 1970-2004 period.

### *5.4 Sediment erosion calculations*

In order to assess the amount of sediment eroded from the slumps that is then transported into the nearshore zone, it is necessary to consider any bias in the calculations from the large quantities of ground ice associated with retrogressive thaw slumps. Typically, massive ice bodies in retrogressive thaw slump headwalls are exposed from the base of the overburden to the slump floor. The overburden consists of the active layer and a metre thick of ice-poor material. Its lower limit is associated with the hypsythermal observed elsewhere in the area by Harry et al. (1988). The lower part of the massive ice section is generally concealed by the mud pools present at the base of the headwall. The amount of volumetric ice in these massive bodies has been measured up to 90% on Herschel Island (Pollard, 1990). The resulting proportion of sediment in these bodies can therefore be estimated to 10% of the remaining fraction of the total volume extending below the active layer. The active layer ranges from 15 to 90 cm (Kokelj *et al.*, 2002; N. Couture, Dept. of Geography, McGill University, unpublished data), depending on the location of the sampling site. Undisturbed tundra surfaces are generally characterized by a shallow active layer up to 45 cm thick, while that for former slump floors (now stabilized) can be characterized by depths up to 90 cm. Since Slump A and Slump B occur in areas of former slump activity we chose to assign a constant active layer depth of 90 cm (Lantuit and Pollard, 2005).

Massive ice is covered by an overburden layer that includes the active layer and the upper part of permafrost. The lower part of the overburden is constituted of perennially frozen material where excess ice is present in negligible quantities (Pollard, 1990). The overburden can therefore be considered free of excess ice and assigned a volumetric ice content of 0%. Observations in the field on August 8th, 9th and 10th of 2004 showed that the total thickness of the overburden is 1.5 m on average.

The total volume of sediment enclosed within the ice and released to the nearshore zone through the slumping process was estimated using equation (1),

$$V_{Sice} = \sum_{i=1}^{n} \left[ \left( (A_i \cdot \Delta h_i) - Z_o \right) (1 - \theta) \right] \tag{1}$$

where $V_{Sice}$ is the total volume of eroded sediment from the ice (m³) through the slumping process , $A_i$ is the area (m²) of the pixel, $\Delta h_i$ the computed difference (m) of elevation between the DEMs, $Z_o$ is the mean overburden depth (m), $\theta$ the volume ice content (%) for massive ice bodies and $n$ the total number of pixels considered in the calculation.

In addition, the total volume of sediment eroded from the active layer was calculated using equation (2);

$$V_{So} = \sum_{i=1}^{n} (A_i \cdot Z_o) \tag{2}$$

where $V_{So}$ is the total volume of sediment eroded from the overburden through the slumping process. The addition of both (1) and (2) led to the estimation of the total volume of sediment eroded from the slump ($V_S$) as noted in (3). The equation presented in (3) was solved using a Geographic Information System (GIS) to estimate the resulting sediment volumes for both slumps.

$$V_s = \sum_{i=1}^{n} \left[ \left( (A_i \cdot \Delta h_i) - Z_o \right) (1 - \theta) + (A_i \cdot Z_o) \right] \quad (3)$$

## 6 Results

### *6.1 Accuracy assessment*

The elevations extracted from the Ikonos stereo-pair and the archived airphotos must be consistent with KDGPS elevations to provide accurate measurements of volume losses.
The elevations obtained from the 2004 DEM at the transect locations within the two slump floors were consistently lower than the KDGPS profiles by an average of 1.2 m in slump A and 1.7 m in Slump B. Single deviations never exceeded 3 m, and in the case of Slump A were within 2 m 98% of the time. Overall, the shapes of the profile were quite similar. A simple regression analysis between KDGPS and DEM elevations was run for the two slumps (Figures 8 and 9) and showed a strong correlation for both slumps (0.996 for Slump A and 0.961 for Slump B) as well as regression slopes close to 1 (1.02 and 0.94 respectively. The hypothesis $H_0$ (regression slope = 1) was tested against $H_1$ (regression slope $\neq 1$) and found to be significant for both regression analyses with an $\alpha$ of 0.05. The elevations extracted from the 1952 and 1970 DEMs were observed to be within 1.2 m of the checkpoint elevations. A checkpoint located 50 m inland from the slump headwall location in 2004 showed a deviation of 0.9 m with the 1952 DEM and of 1.1 m for the 1970 DEM. The latter deviations corresponded to an underestimation of the elevations by the DEM stereo-matching algorithm. Given the consistent underestimation of elevation by the DEM algorithm throughout the years ,we chose to use the raw values uncorrected for volume calculations.

### *6.2 Eroded sediment volumes*

Eroded sediment volumes are presented in Table 1. Results are summarized by period and type of volume loss (i.e. total volume loss, total eroded sediment, eroded sediment from the overburden, eroded sediment from massive ice). Since Slump B started after 1970, no values are recorded for the 1952-1970 period. Volume losses for the two slumps varied greatly. While Slump B can be considered a "small" slump, Slump A is a large slump marked by considerable volumes of sediment and ice loss. Volume losses in Slump A have increased by 300% (585 953 $m^3$ to 1 566 909 $m^3$) between the 1952-1970 and the 1970-2004 periods. In addition, the difference in volume of eroded sediment between Slump A and Slump B was observed to differ by a factor of 16 (355 042 $m^3$ *vs.* 22 246 $m^3$ respectively).

Volumes of eroded sediment from the overburden were always greater or similar to the ones eroded from massive ice. This is especially true in the case of Slump A for the period 1970-2004 (222 294 $m^3$ - 63% - of sediments from the overburden vs. 132 748 $m^3$ - 37% - of sediments from massive ice), during which sediment volumes originating from massive ice accounted for only 37% of the total volume of sediment eroded. The total volume of sediment roughly accounted for half of overburden sediments - 51% - and half of sediments enclosed in massive ice - 49% - during the former period. In Slump B, which is a slump expanding in a typical bowl-shaped fashion, sediment eroded from massive ice accounted roughly for 42% of the total sediment loss.

### *6.3 Mapping thermokarst volumes*

The spatial pattern of retrogressive thaw slump occurrence is illustrated in Figures 10, 11 and 12. Slump A expands along a east-west axis but retains the same shape. The main zones of erosion for both periods are located in the centre of the main headwall. Lateral exposures are generally not associated with the largest erosion values, which emphasizes the fact that the greatest losses are occurring mostly in the centre of the headwall. The retreat process is illustrated best where the greatest erosion values for the 1970-2004 layer are compared to those for the 1952-1970 layer. The main erosion zone (where vertical difference $\Delta h_i$ exceeds 15 m) has tripled in size between the two periods. In Slump B, the greatest erosional zones are also located along the centre part of the headwall. Because of the small size of the slump differences in vertical variations are not as obvious as the ones observed in Slump A.

# 7 Discussion

## *7.1 Eroded sediment supply to the nearshore zone*

The large differences in volume losses estimated for slumps A and B show that calculations should be undertaken on individual slumps in future studies, with a particular emphasis on the type and size of slump. In addition, the supply of sediment to the nearshore zone is often considered to be related exclusively to wave-driven coastal erosion. However, the occurrence of retrogressive thaw slumps and the flow of liquefied mud can greatly modify the estimated amounts of sediment supplied to the nearshore zone. In the case of Slump A, coastal erosion on a 20 m high cliff at a rate of 1 m/yr for a 600 m long coastal strip during the 1970-2004 period, would yield 420 000 $m^3$ of volume loss (i.e. sediment + ice). With volumetric ice contents typically around 60% on coasts not affected by retrogressive thaw slumps, eroded sediment to the nearshore zone would account for 180 600 $m^3$ of sediment and 259 400 $m^3$ of ice. Slump A provides around 355 000 $m^3$ which is considerably greater than the volumes of sediment provided by typical cliff erosion. Similarly for Slump B, the sediment volume removed by coastal erosion is estimated at 51 000 $m^3$ for the 1970-2004 period, with an additional 22 246 $m^3$ of eroded sediment from the slump itself.

### *7.2 Retrogressive thaw slump polycyclicity*

Slump B's headwall retreat is mainly in a landward direction, whereas in Slump A the migration of the headwall is oblique to the coastline. The complex behaviour of Slump A is associated with its large size and the polycyclic nature of slump activity. Volumetric erosion for the 1970-2004 shows volume losses on the slump floor as well as the headwall. This reflects the development of smaller slumps within the floor of Slump A. This polycyclic behaviour is explained by the incomplete melting of massive ice bodies located in the main headwall as it retreated, due to the accumulation of sediment at the base by the mudflows (De Krom, 1990). The migration of the headwall, as well as the accumulated sediment load on the slump floor, leads to pools of liquefied mud that flow along channels downslope towards the coast. Concealed massive ice bodies in the slump floor are subsequently re-exposed by gullying processes, eventually leading to the occurrence of new retrogressive thaw slumps. The identification of zones marked by little to no erosion during the 1970-2004 period, and located within the muddy floor of Slump A can therefore be seen as an indication of potential future retrogressive thaw slump activity (Figure 11). The larger values of sediment loss associated from the overburden are thought to be linked to these low relief difference zones and likely reflect lower thicknesses of massive ice.

Polycyclicity requires wide and relatively flat surfaces to develop so mud lobes within the slump floor are mobile enough to conceal and expose zones of the floor cyclically. The floor steepness of Slump B, its small size and high elevation above the ground in relation to Slump A, lead to a more efficient evacuation of the mudflows and therefore to the more efficient melting of the headwall.

As mentioned previously, slumps A and B developed within the limits of former retrogressive thaw slumps that have been stable for over 50 years (Lantuit and Pollard, 2005), which means that the current study is concerned with a second generation of slump occurrence. Thus it is possible that massive ice bodies up to 20 m can be concealed during a long period after slumping activity, since no trace of volume loss is shown in the zones located above the headwalls since 1952.

## 8 Conclusion

This study is the first attempt to quantify sediment and ground ice volume losses associated with retrogressive thaw slump activity. Since retrogressive thaw slump frequency appears to be increasing on Herschel Island, total volume losses associated with these major thermokarst landforms are expected to increase during the 21$^{st}$ century. The DEMs extracted using stereophotogrammetric methods show that sediment eroded from retrogressive thaw slumps on arctic coasts are of the same order of magnitude as those from coastal erosion within the same section of coast. Given the current emphasis on estimations of eroded sediment from arctic coasts to the Arctic Ocean (Rachold *et al.*, 2003), it seems appropriate to reconsider the role of retrogressive thaw slumps and ultimately of ground ice in these calculations. Calculations on the Herschel Island shoreline show that along a 600 m section of coast, retrogressive thaw slump-related eroded sediment is approximately 355 042 m$^3$ which is greater than the 180 600 m$^3$ expected to be supplied by coastal cliff erosion alone.

In addition, stereophotogrammetric methods prove to be a valuable tool for the detection of zones at risk associated with polycyclic retrogressive thaw slumps. The high costs associated with high resolution satellite imagery can be seen as a deterrent for the use of such methods to investigate landslide dynamics. Nevertheless, they prove to be an economic alternative to field based surveys in remote arctic locations. The expected increased frequency of retrogressive thaw slump activity associated with global warming represents an imminent threat to arctic communities located in ice-rich regions such as the Canadian Western arctic. In this sense, stereophotogrammetric tools can serve as powerful monitoring tools to detect retrogressive thaw slumps.

## 9 Acknowledgements

This research was supported by the Natural Science and Engineering Research Council of Canada (NSERC). Support from the Polar Continental Shelf Project (PCSP) and the Aurora Research Institute (ARI) for the field component was greatly appreciated. Hugues Lantuit is supported by the Warren fellowship in GIS, McGill University and the Government of Canada Award Program administered by the International Council for Canadian Studies (ICCS) on behalf of the Department of Foreign Affairs and International Trade of Canada (DFAIT). The imagery is generously provided by the McGill Electronic Data Resources Service (EDRS). The field assistance of Ms. N. Couture, Ms. J. Turner and Mr. T. Haltigin is gratefully acknowledged. The authors wish to express sincere appreciation to the Yukon Territorial Government, to the Yukon Parks, Yukon Department of Renewable Resources and to the Environmental Impact Screening Committee (EISC), and to the Inuvialuit Renewable Resource Committees for their support and encouragement of this project. The authors also wish to thank C. Davey from McGill University for his helpful comments on this paper.

## 10 References

Brown, J., Ferrians, Jr. O.J., Heginbottom, J.A. and Melnikov, E.S.: Circum-Arctic Map of Permafrost and Ground-Ice Conditions. Boulder, CO: National Snow and Ice Data Center/World Data Center for Glaciology. Digital Media. 1998.

De Krom, V.: Retrogressive thaw slumps and active layer slides on Herschel Island, Yukon., M.Sc. Thesis, McGill University, Montréal, Québec, 157 pp, 1990.

Everdingen, R.van.: Multi-language glossary of permafrost and related ground-ice terms., Boulder, CO: National Snow and Ice Data Center/World Data Center for Glaciology, ed. 1998 revised January 2002

Harry, D.G., French, H.M., and Pollard, W.H. Massive ground ice and ice-cored terrain near Sabine Point, Yukon coastal plain. Can. J. Earth., 25, 1846--1856, 1988

Huscroft, C.A, Lipovsky P. and Bond J.D.: Permafrost and landslide activity: Case studies from southwestern Yukon Territory, In: Yukon Exploration and Geology 2003, D.S. Emond and L.L. Lewis (eds.), Yukon Geological Survey: 107--119, 2004.

Kokelj, S.V., Smith, S.A.S and Burn, C.R.: Physical and chemical characteristics of the active layer and permafrost, Herschel Island, Western arctic Coast, Canada, Permafr. P. P., 13, 171--185, 2002.

Lantuit, H., Couture, N., Pollard, W.H., Haltigin, T., De Pascale, G. and Budkewitsch, P.: Short-term evolution of coastal polycyclic retrogressive thaw slumps on Herschel Island, Yukon Territory., Berichte zur Polarforschung, *in press*.

Lantuit, H. and Pollard, W.H.: Fifty years of coastal erosion and retrogressive thaw slump activity on Herschel Island, southern Beaufort Sea, Yukon Territory., In : Mapping ground-ice related coastal erosion on Herschel Island, southern Beaufort Sea, Yukon Territory, Canada., M.Sc. Thesis, McGill University, Montréal, Quebec, 134 pp, 2005

Lewkowicz, A.G.: Headwall retreat of ground-ice slumps, Banks Island, Northwest Territories., Can. J. Earth., 24, 1077--1085, 1987.

Lewkowicz, A.G.: Climatic Change and the Permafrost Landscape., in Woo, M.K. and Gregor, D.J., 1991. arctic environment: Past, Present and Future, proceedings of a symposium, Nov 14-15, 1991, Dpt. Of Geography, McMaster University, Hamilton, 91--104, 1991.

Mackay, J.R.: Segregated epigenetic ice and slumps in permafrost, mackenzie delta, N.W.T., Geographical Bulletin, 8, 59--80, 1966.

Mackay, J.R.: The origin of massive icy beds in permafrost, western arctic coast, Canada., Can. J. Earth., 8, 397--422, 1971.

Mackay, J.R.: The World of Underground Ice. Annals Am. Assoc. Geographers, 62, 1--22, 1972.

McGillivray, D.G., Agnew, T.A., McKay, G.A., Pilkington, G.R. and Hill, M.C.: Impacts of climatic change on the Beaufort sea-ice regime: Implications for the arctic petroleum industry., Climate Change Digest CCD 93-01, Environnement Canada, Downsview, Ontario, 36pp, 1993.

Pollard, W.H.: The nature and origin of ground ice in the Herschel Island area, Yukon Territory., Proc., Fifth Canadian Permafrost Conference, Québec. 23--30, 1990.

Pollard, W.H. and French, H.M.: A first approximation of the volume of ground ice, Richards Island, Pleistocene Mackenzie Delta, N.W.T., Can. Geotech., 17, 509--516, 1980

Rachold, V., Eicken, H., Gordeev, V.V., Grigoriev, M.N., Hubberten, H-W., Lisitzin, A.P., Shevchenko, V.P. and Schirrmeister, L.: Modern terrigenous organic carbon input to the arctic Ocean., In: Stein, R. and Macdonald, R.W. (Eds.) Organic Carbon Cycle in the arctic Ocean: Present and Past. Springer Verlag, Berlin, 33--55, 2003.

Rampton, V.N.: Quaternary Geology of the Yukon Coastal Plain., Geological Survey of Canada Bulletin, 317, 49 pp, 1982.

Serreze, M.C., Walsh, J.E., Chapin, F.S.III, Osterkamp, T.E., Dyurgerov, M., Romanovsky, V.E., Oechel, W.C., Morison, J., Zhang, T., and Barry, R.G.: Observational evidence of recent change in the northern high-latitude environment., Clim. Change, 46, 159--207, 2000

Toutin, T., Chenier, R., Carbonneau, Y.: 3D geometric modelling of Ikonos GEO images. Proc. Joint ISPRS Workshop''High Resolution Mapping from Space 2001,'' Hannover, 19 – 21 September. Institute of Photogrammetry & Geoinformation, University of Hannover, 9 pp. (on CD ROM), 2001.

Valadan Z. and Toosi, K.N.: Rigorous and non-rigorous photogrammetric processing of IKONOS-1 geo image., Proc. Joint ISPRS Workshop "High resolution mapping from space 2003", October 2003, Hannover, Germany, 6pp, (on CD-ROM), 2003.

Wolfe, S.A.; Kotler, E.; and Dallimore, S.R.: Surficial characteristics and the distribution of thaw landforms (1970 to 1999), Shingle Point to Kay Point, Yukon Territory., Geological Survey of Canada, Open File 4088, 2001.

Young, S. and Judge, A.S.: Canadian permafrost distribution and thickness data collection: a discussion; Proc., National Student Conference on Northern Studies, W.P Adams and P.G. Johnson eds., 223--228, 1986.

**Table 1**
Eroded sediment volumes from retrogressive thaw slumps A and B

| | | Volumes for slump A ($m^3$) | Volumes for slump B ($m^3$) |
|---|---|---|---|
| 1952-1970 | Total volume loss | 585 953 | none |
| | Total eroded sediment volume | 104 381 | none |
| | Eroded sediment from overburden | 51096 | none |
| | Eroded sediment from massive ice | 53286 | none |
| 1970-2004 | Total volume loss | 1 566 909 | 105 999 |
| | Total eroded sediment volume | 355 042 | 22 246 |
| | Eroded sediment from overburden | 222 294 | 12986 |
| | Eroded sediment from massive ice | 132 748 | 9261 |

**Figure 1**
Typical bowl-shaped retrogressive thaw slump in Thetis Bay, Herschel Island, July 1986.

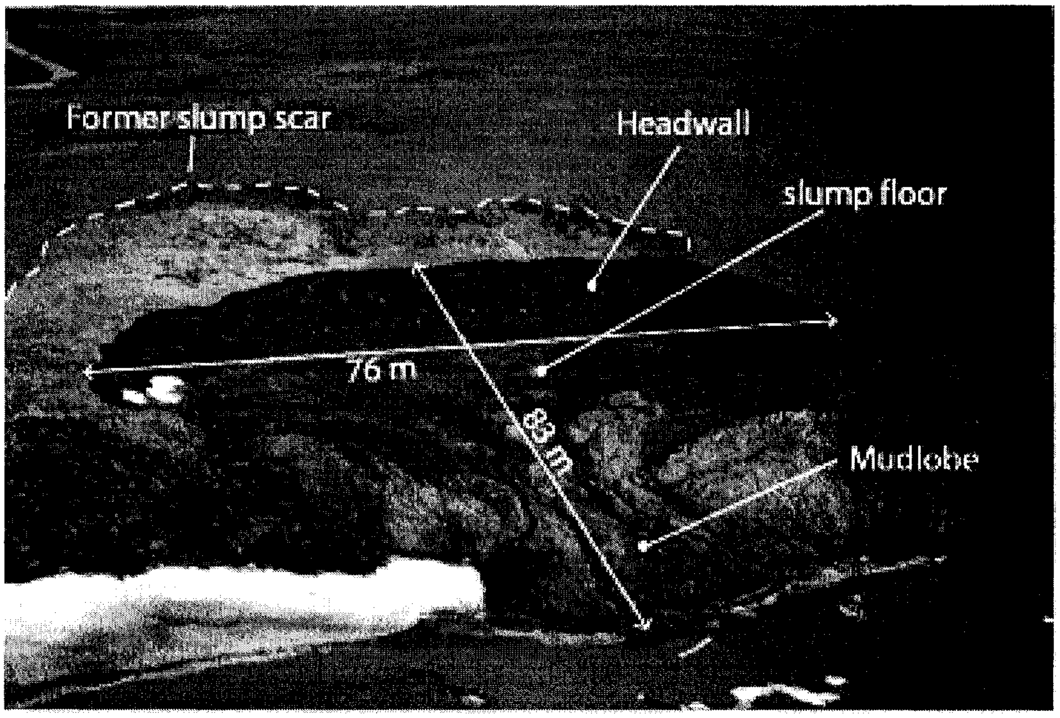

**Figure 2**
Conceptual scheme of retrogressive thaw slump. Inset B focuses on the slump headwall. Inset C is a cross-section of the slump.

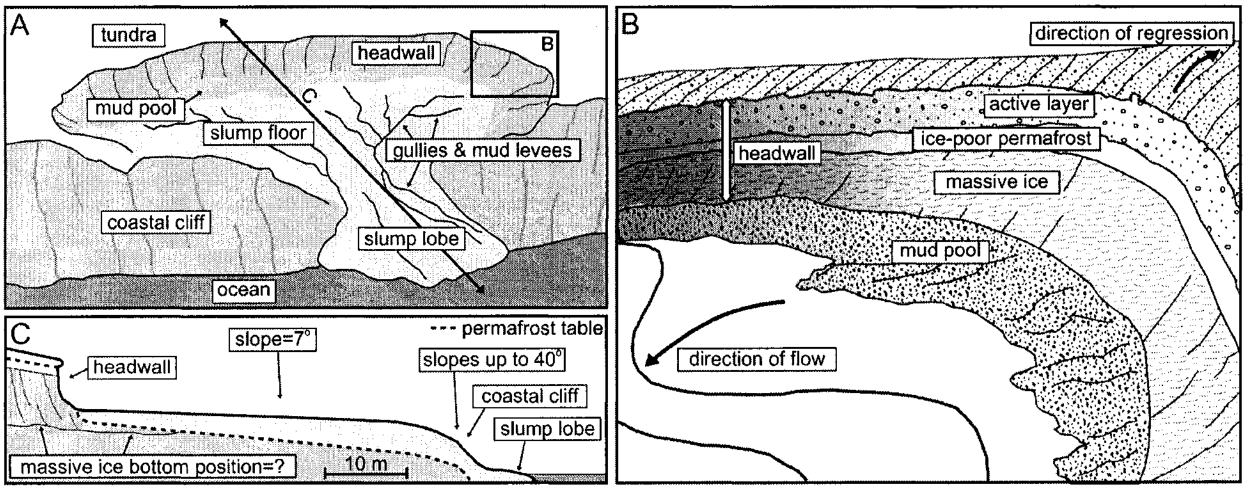

**Figure 3**
General study area is Herschel Island; the map inset displays the location of slumps A and B.

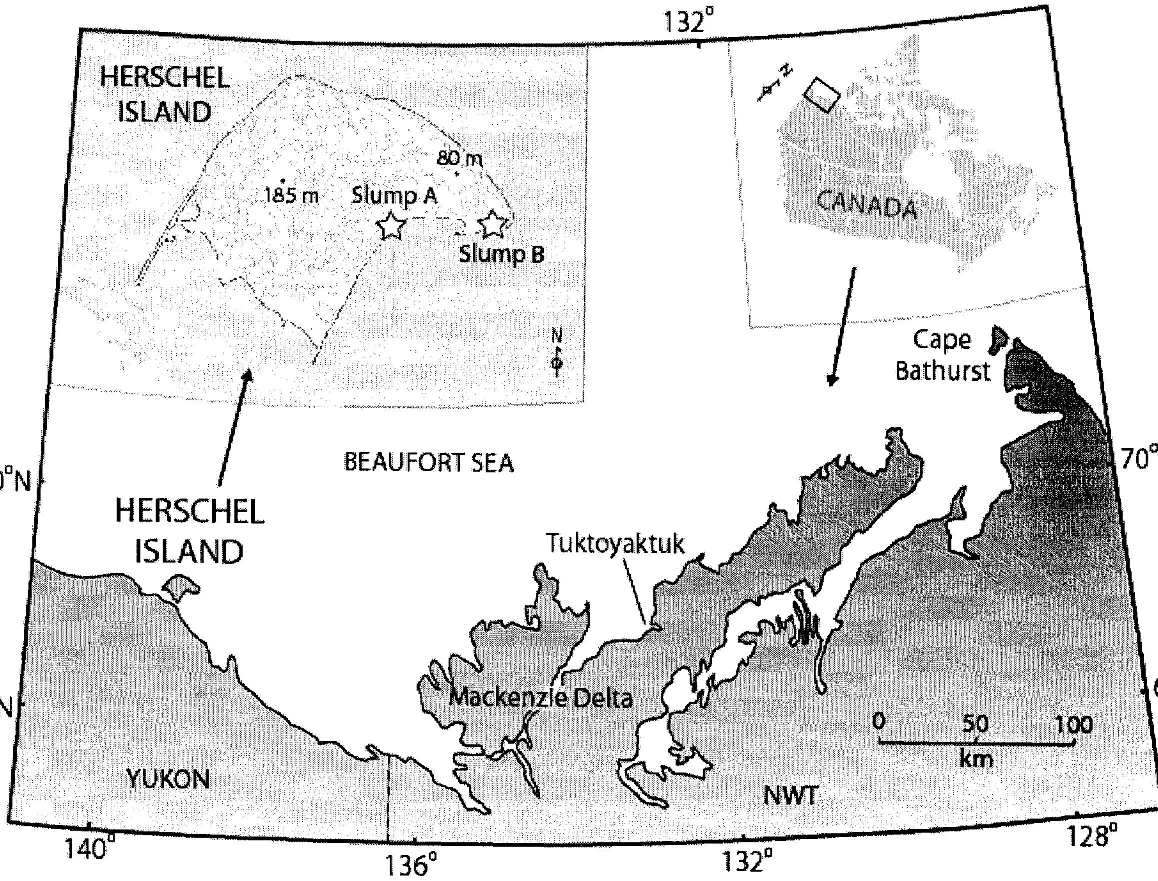

**Figure 4**
Location of main retrogressive thaw slump activity and study sites on Herschel Island

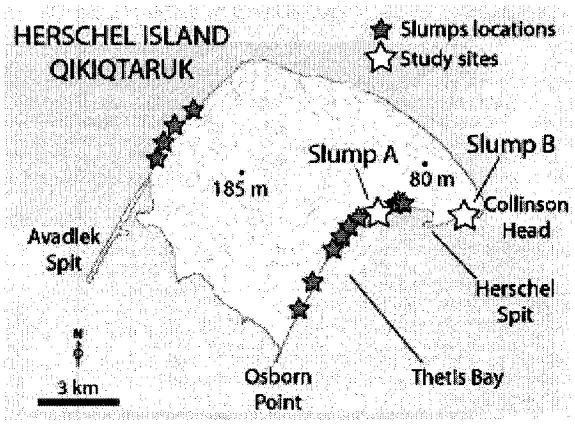

**Figure 5a**
2004 Ikonos panchromatic view of slump A with KDGPS points surveyed two days later overlaid

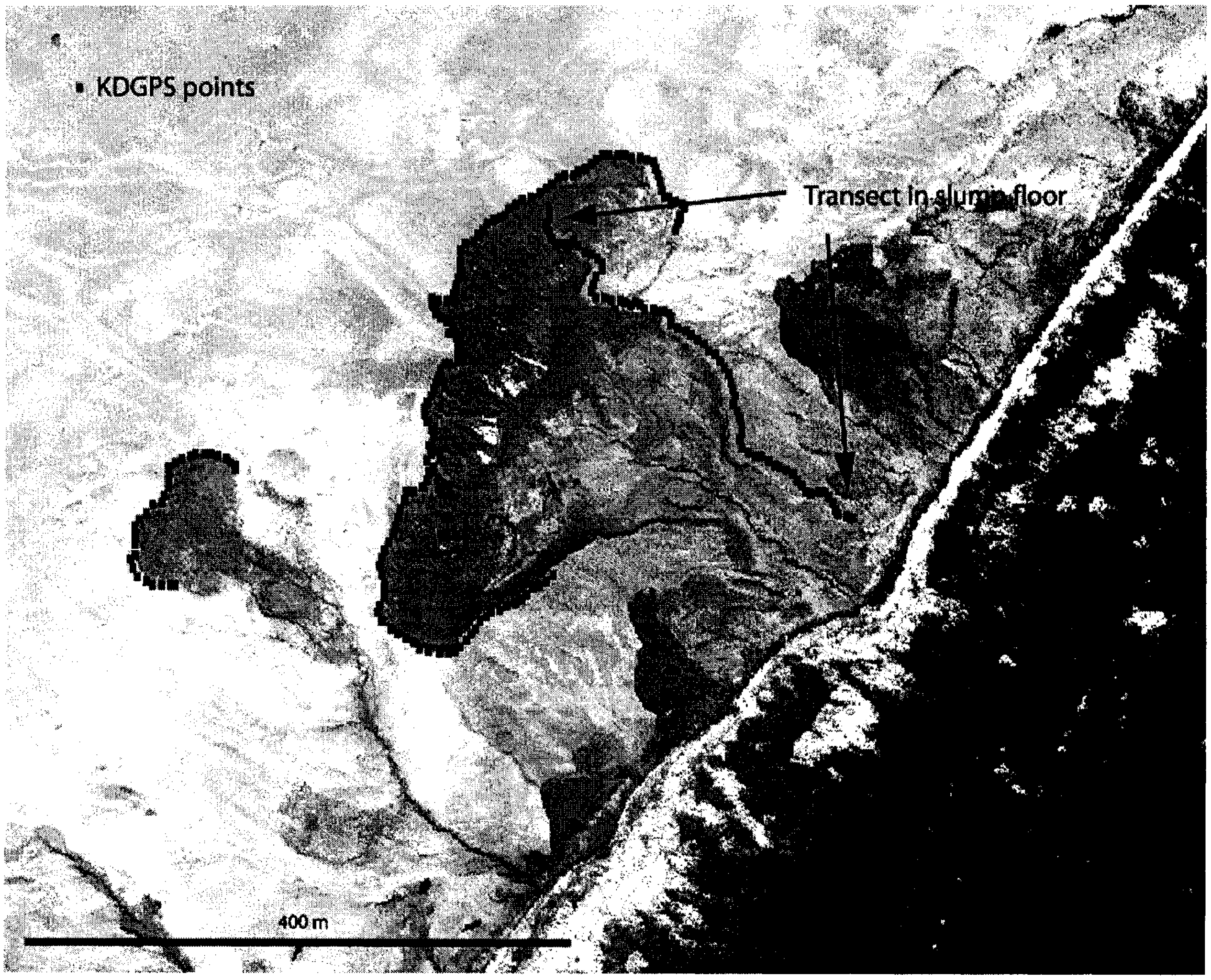

**Figure 5b**
2004 Ikonos panchromatic view of slump B with KDGPS points surveyed a day later overlaid

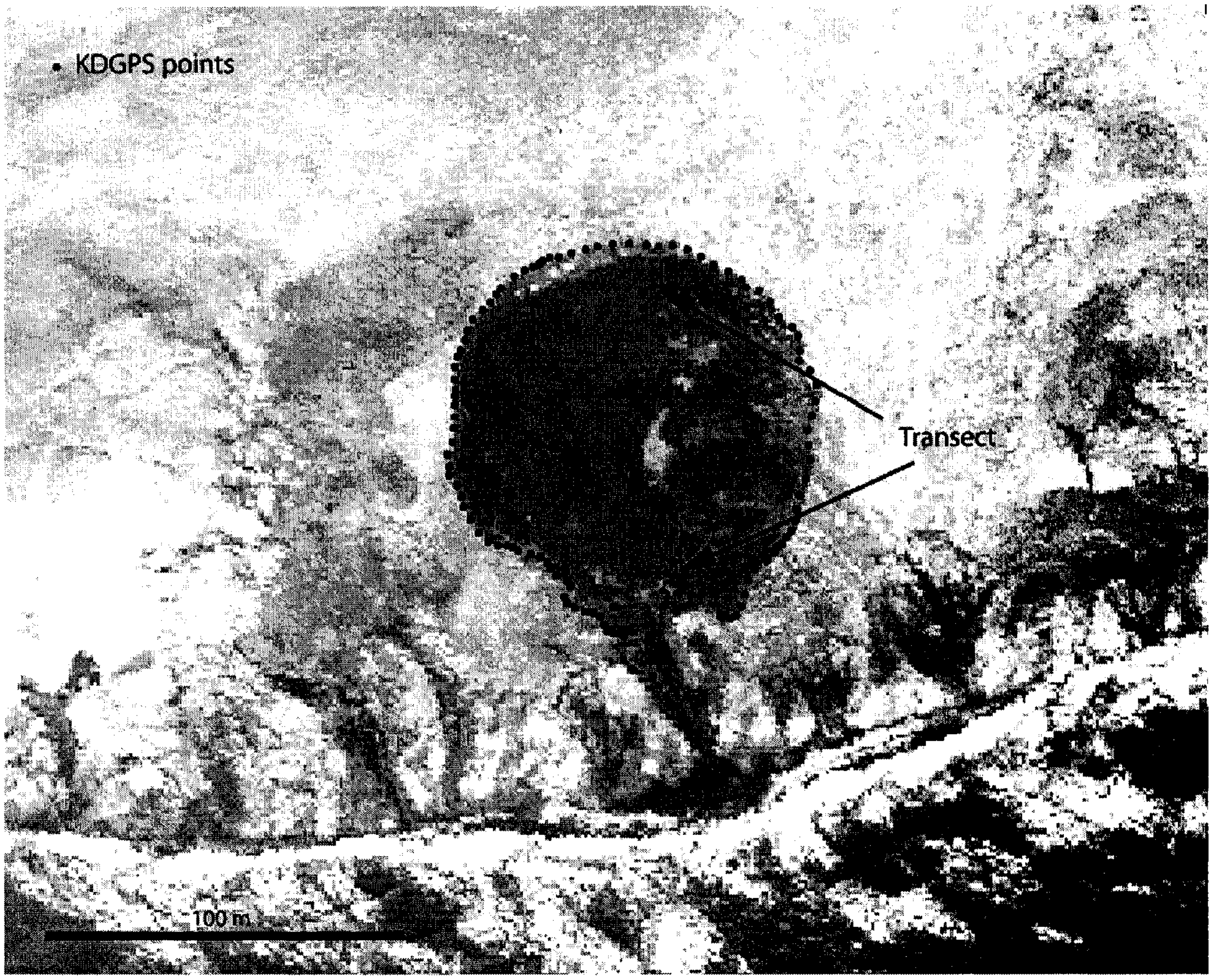


**Figure 6**
Slump floor profile of slump A from KDGPS points and DEM. The x distances indicate the distance from the top edge of the headwall measured on the Ikonos imagery

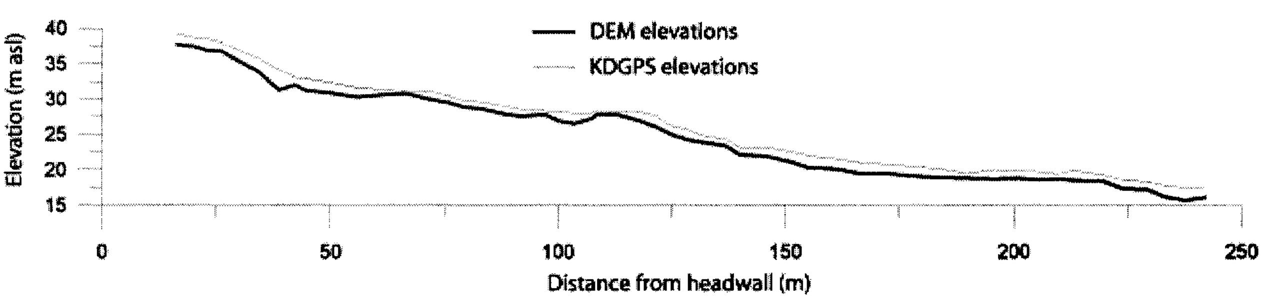

**Figure 7**
Slump floor profile of slump B from KDGPS points and DEM. The x distances indicate the distance from the top edge of the headwall measured on the Ikonos imagery

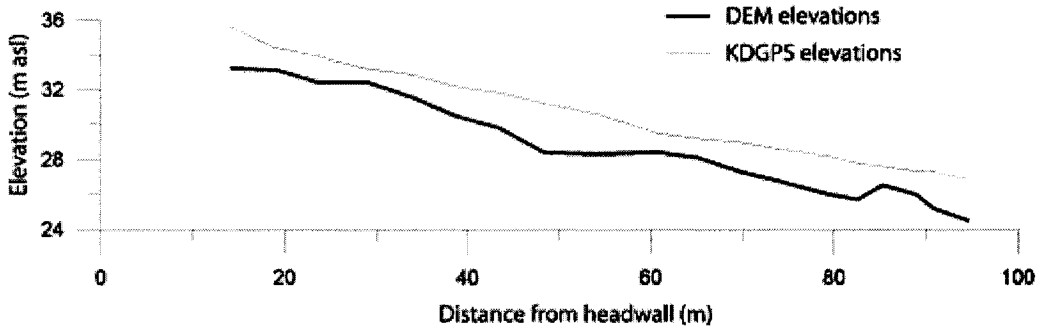


**Figure 8**
Scatter plot of KDGPS versus DEM elevations along the transect in slump A. Best least squares fit regression line is superimposed

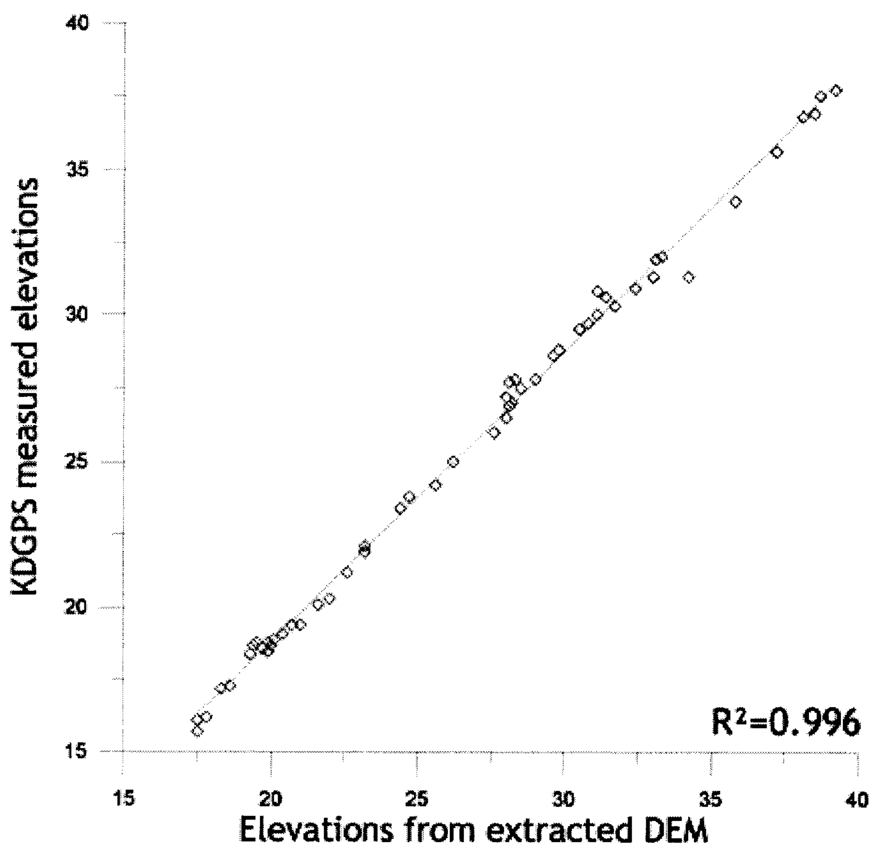

**Figure 9**
Scatter plot of KDGPS versus DEM elevations along the transect in slump B. Best least squares fit regression line is superimposed

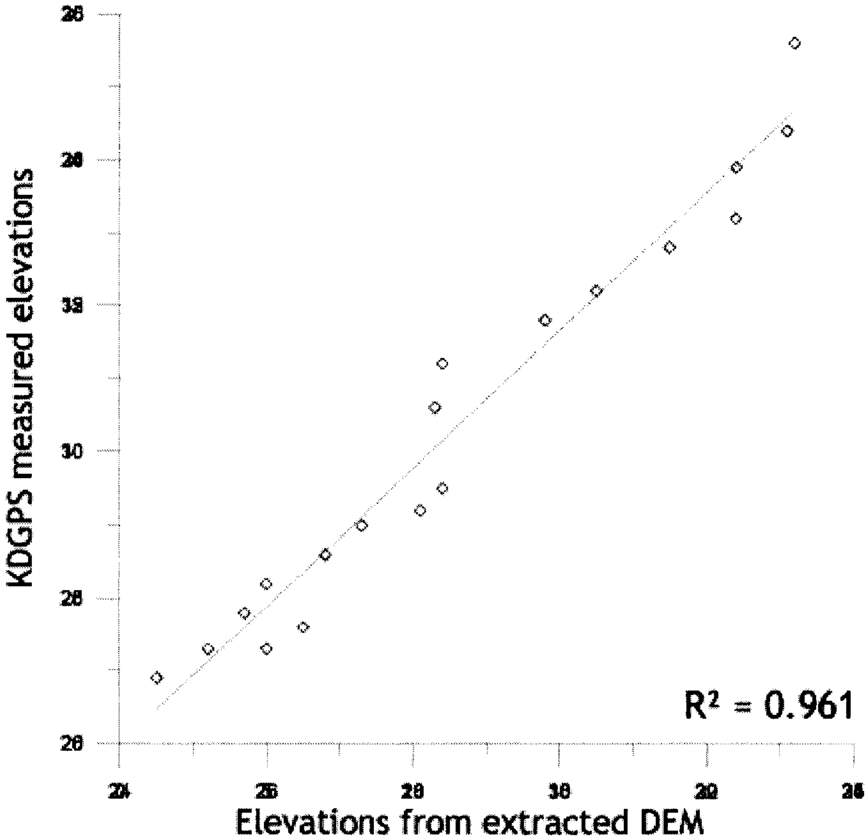

**Figure 10**
Volume losses map for 1952-1970 in slump A. Note the presence of discrete spots of greatest erosional values within the slump floor, probably pinpointing at the occurrence of two stages of slump activity (polycyclicity).

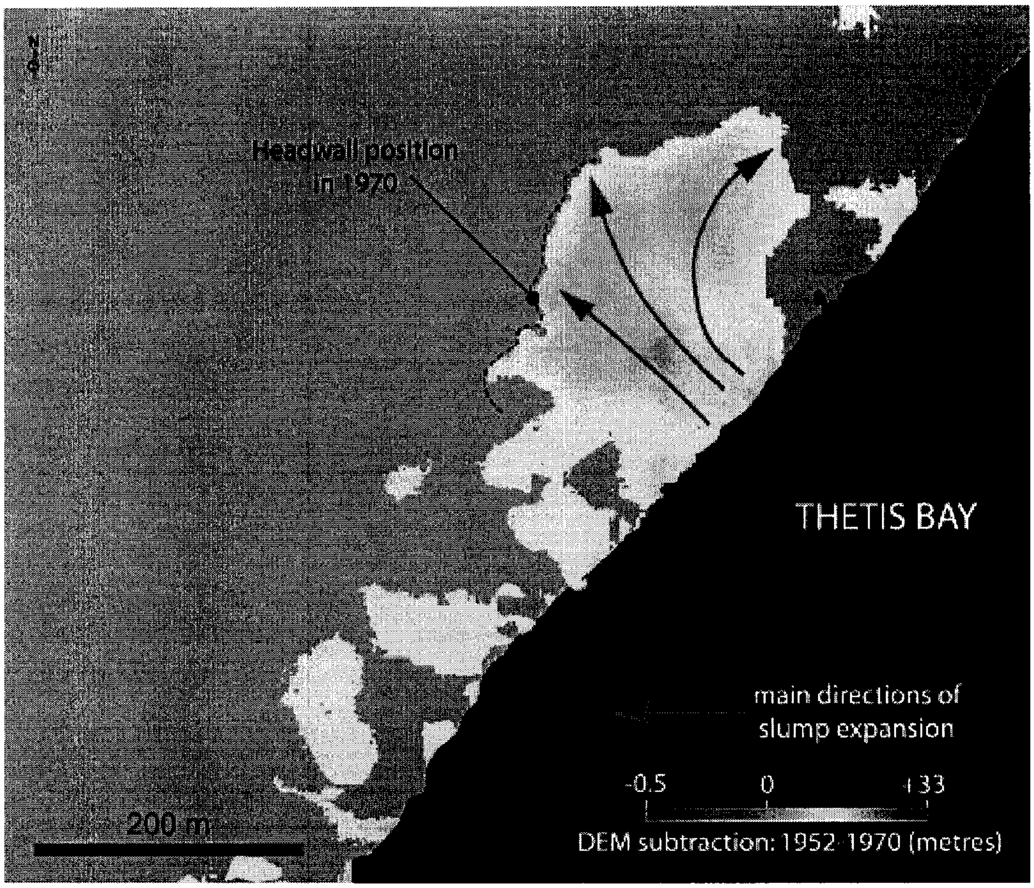

**Figure 11**
Volume losses map for 1970-2004 in slump A. Note the location of the greatest erosion immediately below the current headwall. The more littoral part of the slump is characterized by the presence of stable zones (blue) and zones currently eroding (greenish colors).

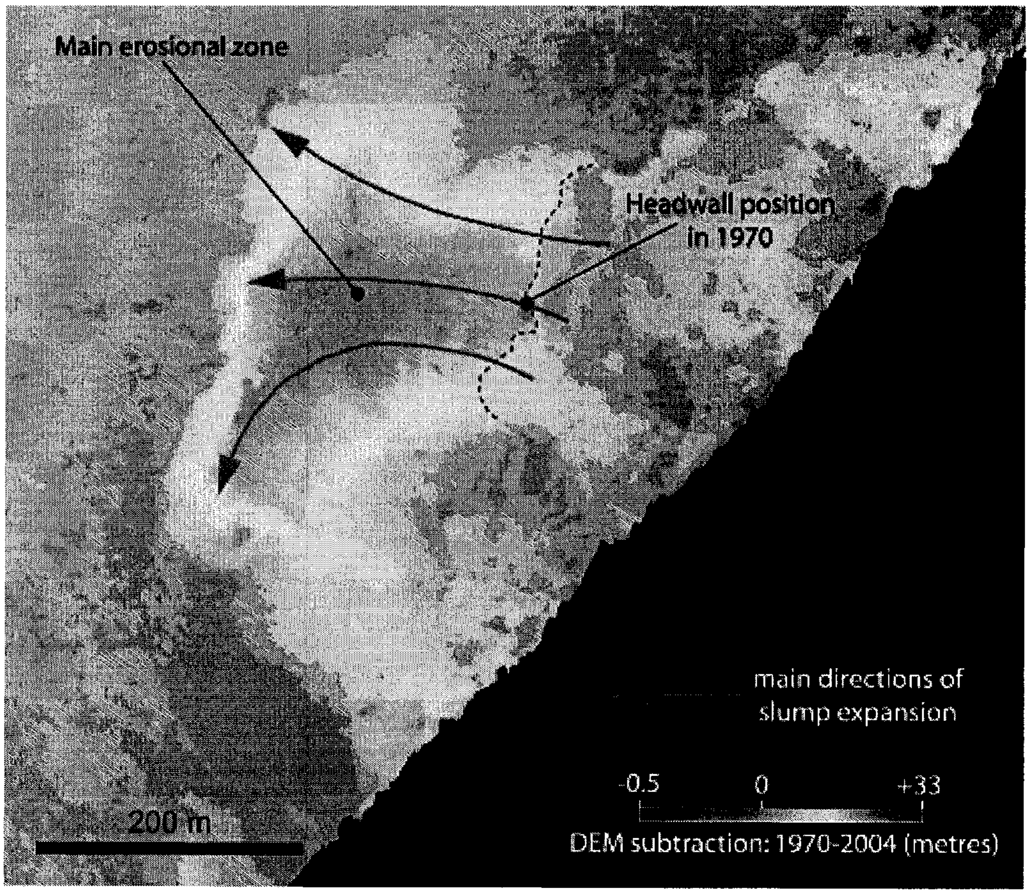

**Figure 12**
Volume losses map for 1970-2004 in slump B. Arrows indicate the direction of slump expansion. Note the constant width of the slump and the fairly homogeneous values for DEM subtraction. Those indicate the likely presence of a continuous massive lens which was melted in a headwall of constant height.

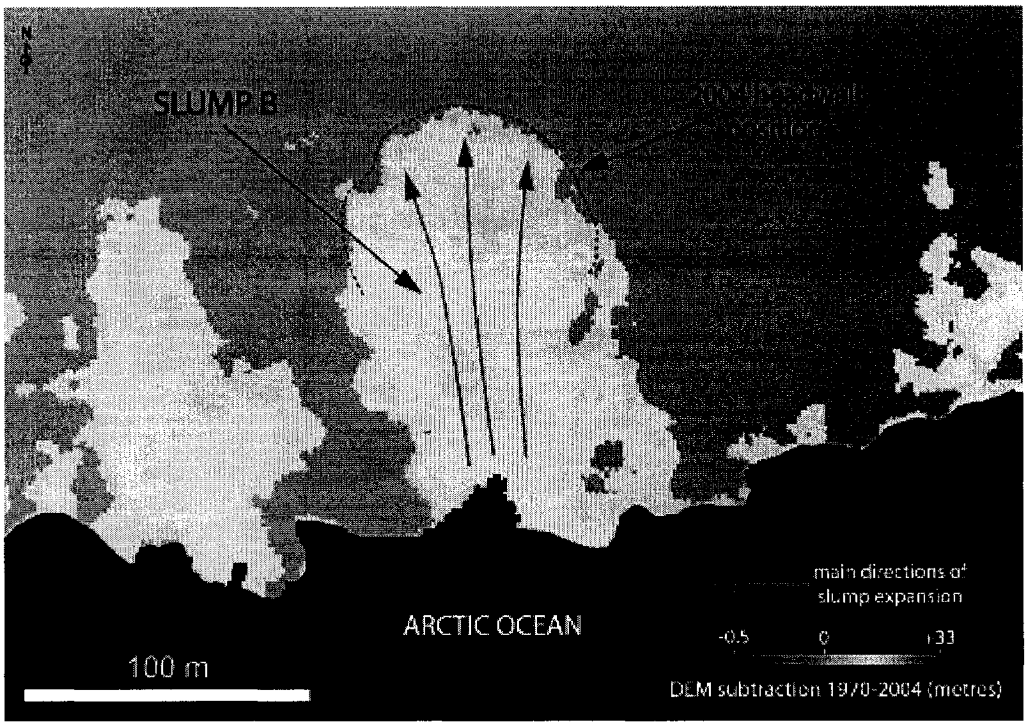

## CONCLUSION

The following conclusions are drawn from this thesis:

1) Shoreline erosion has exhibited an overall decrease over the 1952-2000 period on Herschel Island, Yukon Territory. Mean annual coastal retreat rates decreased from 0.74 m/yr over the 1952-1970 period to 0.55 m/yr over the 1970-2000 period on the shorelines exposed to ocean dynamics. These results are consistent with recent estimates of coastal retreat rates in the southern Beaufort Sea by Solomon (2004).

2) The highest coastal retreat rates are on shoreline sections exposed to the north-west, which is the main direction of storm attack in the region (Harper and Penland, 1982, Hudak and Young, 2002).

3) Although generally decreasing, coastal retreat rates have been increasing on south, south-south-east and south-east exposed shoreline sections, which are marked by high ice contents (Pollard, 1990) and the occurrence of most thermokarst features such as retrogressive thaw slumps.

4) The discrepancy between annual headwall retreat rates of retrogressive thaw slumps and coastal retreat rates has led to the development of large retrogressive thaw slumps on south, south-east and south-south-east exposed shoreline sections.

5) The number and the total area of retrogressive thaw slumps have dramatically increased between 1952 and 1970 on Herschel Island (+125% and +160% respectively).

6) Polycyclic retrogressive thaw slumps develop in a periodic fashion illustrated by a general relationship between retrogressive thaw slump generation and maximum inland extent, constant throughout the twentieth century, despite the intensified presence of active retrogressive thaw slumps on south to south-east exposed shorelines.

7) Calculations on the Herschel Island shoreline show that along a 600 m section of coast, retrogressive thaw slump-related eroded sediment is approximately 355 042 $m^3$ which is greater than the 180 600 $m^3$ expected to be supplied by coastal cliff erosion. Thus it seems appropriate to reconsider the role of retrogressive thaw slumps and ultimately of ground ice in calculations of eroded sediment on coastal sections.

8) Stereophotogrammetric methods proved to be a valuable tool for the detection of zones at risks associated with polycyclic retrogressive thaw slumps.

---

The high costs associated with high resolution satellite imagery can be seen as a deterrent for the use of such methods to investigate coastal and landslide dynamics. Nevertheless, they prove to be an economic alternative to field based surveys in the arctic remote locations. The expected increased threat due to coastal erosion and enhanced frequency of retrogressive thaw slump activity associated with global warming represents an imminent threat to arctic communities located in ice-rich regions such as the Canadian western Arctic. In this sense, photogrammetric and stereophotogrammetric tools can serve as powerful monitoring and detection tools.

## REFERENCES

Aré FE. 1964. Influence of the heat-transfer properties of frozen rocks on arctic coast destruction. (O vliyanii teplofizicheskikh svoistv merzlykh porod na razrushenie beregov arkticheskikh morey) in: Teplovye protsessy v merzlykh gornykh porodakh, Moskva, Nauka. 111-116.

Aré, FE. 1988. Thermal abrasion of sea coast. Polar Geography and Geology 12. VH. Winston& Sons, 157 pp.

Blasco SM, Shearer JM, Campbell P, Wright B and Melling H. 2004. Reduction in sea ice scour impact rates on the seabed 1979 to 2003, Canadian Beaufort Sea. Eos Transactions. Joint Assembly of the CGU, AGU, SEG and EEGS, Montreal, Canada, May 17-21, 2004. 85(17): C43A-10.

Bouchard M, 1974. Géologie des dépôts meubles de l'île Herschel, Territoire du Yukon. M.Sc. Thesis, Université de Montréal: Montréal, Quebec; 70 pp.

Brown RJE. 1970. Permafrost in Canada: Its influence on northern development. University of Toronto Press, Toronto, 234 pp.

Brown J, Ferrians Jr. OJ, Heginbottom JA and Melnikov ES. 1998. Circum-Arctic Map of Permafrost and Ground-Ice Conditions. Boulder, CO: National Snow and Ice Data Center/World Data Center for Glaciology. Digital Media

Bruun P. 1962. Sea level rise as a cause of shoreline erosion. Journal of Waterways and Harbours 1: 116-180.

Burn CR. 2000. The thermal regime of a retrogressive thaw slump near Mayo, Yukon Territory. Canadian Journal of Earth Sciences 37: 967-981.

Campeau S, Héquette A and Pienitz R. 2000. Late Holocene diatom biostratigraphy and sealevel changes in the southeastern Beaufort Sea. Canadian Journal of Earth Sciences 37: 63-80.

Carter TR, Hulme M, Crossley JF, Malyshev S, New MG, Schlesinger ME and Tuomenvirta H. 2000. Climate Change in the 21st Century - Interim Characterizations based on the New IPCC Emissions Scenarios. The Finnish Environment 433, Finnish Environment Institute: Helsinki; 148 pp.

Chapman WL. and Walsh JE. 1993. Recent Variations of Sea Ice and Air Temperature in High Latitudes. Bulletin of the American Meteorological Society, 74: 2-16.

Costard F, Aguirre-Puente J, Greeley R and Makhloufi N. 1999. Martian fluvial-thermal erosion: Laboratory simulation. J Geophys. Res. Planets. 104-E6: 14091-14098.

Dallimore SR, Wolfe S and Solomon SM. 1996. Influence of Ground Ice and Permafrost on Coastal Evolution, Richards Island, Beaufort Sea Coast, NWT. Canadian Journal of Earth Sciences 33: 664-675.

De Krom V. 1990. Retrogressive thaw slumps and active layer slides on Herschel Island, Yukon. M.Sc. Thesis, McGill University: Montréal, Québec; 157 pp.

Dyke LD. 1991. Temperature changes and thaw of permafrost adjacent to Richards Island, Mackenzie Delta, N.W.T. Canadian Journal of Earth Sciences. 28: 1834-1842

Forbes DL. 1980. Late Quaternary sea levels in the southern Beaufort Sea. In Current Research, Geological Survey of Canada. Paper 80-1B: 75-87.

Forbes DL. 1989. Discussion – Maximum storm surge elevations in the Tuktoayktuk region of the Beaufort Sea. Letter to the editor, Arctic, 42: 182.

Forbes DL and Taylor RB. 1994. Ice in the shore zone and the geomorphology of cold coasts. Progress in Physical Geography 18: 59-96.

French HM. 1996. The Periglacial Environment. 2nd Edition. Longman Group Limited, London and New York, 309 pp.

Gillie RD. 1988. Beaufort Sea artificial island data. Report No. 096, Environmental Studies Resolving Funds. Ottawa. Ontario. 30pp.

Harper JR. 1990. Morphology of the Canadian Beaufort Sea Coast. Marine Geology 91: 75-91.

Harper JR and Penland PS. 1982. Beaufort Sea sediment dynamics. Technical Report for Geological Survey of Canada. Woodward-Clyde Consultants: Victoria, British Columbia; 198 pp.

Héquette A and Barnes PW. 1990. Coastal retreat and shoreface profile variations in the Canadian Beaufort Sea. Marine Geology 91: 113-132.

Héquette A, Desrosiers M, Hill PR and Forbes DL. 2001. The influence of coastal morphology on shoreface sediment transport under storm-combined flows, Canadian Beaufort Sea. Journal of Coastal Research. 17: 507-516.

Hill PR., Héquette A and Ruz M-H. 1993. Holocene sea-level history of the Canadian Beaufort Shelf. Canadian Journal of Earth Sciences 30: 103–108.

Hoque MA and Pollard WH. *in press*. Modeling block failures in vertical cliffs of arctic coasts underlain by permafrost. Berichte zur Polarforschung.

Hudak DR. and Young JMC. 2002. Storm climatology of the southern Beaufort Sea. Atmosphere-Ocean 40: 145-158.

IPCC. 2001. Climate Change 2001: The Scientific Basis. Cambridge University Press. Cambridge, UK.

Johnson K, Solomon SM, Berry D and Graham P. 2003. Erosion progression and adaptation strategy in a northern coastal community. Proceedings - 8th International Conference on Permafrost, Zurich, Switzerland, July 20-25, 2003. Edited by . Phillips, S.M. Springman and L.U. Arenson; International Permafrost Association 8:489-494.

Kane DL, Hinzman LD and Zarling JP. 1991. Thermal response of the active layer to climatic warming in a permafrost environment. Cold Regions Science and Technology. 19: 111-122.

Kasser M and Egels Y. 2001 Digital Photogrammetry Ed. Taylor & Francis. 380 pp

Komar PD. 1998. Beach processes and sedimentation, 2nd Ed. Prentice-Hall, Englewood Cliffs, N.J., 544pp.

Kobayashi N. 1985. Formation of thermoerosional niches into frozen bluffs due to storm surges on the Beaufort Sea coast. Journal of Geophysical Research, 90(C6), 11983-11988.

Kobayashi N, Vidrine JC, Nairn RB and Solomon SM. 1999. Erosion of frozen cliffs due to storm surge on Beaufort sea coast. Journal of coastal research 15: 332-344.

Lantuit H and Pollard WH. 2005. Fifty years of coastal erosion and retrogressive thaw slump activity on Herschel Island, southern Beaufort Sea. Unpublished manuscript. In Lantuit H. 2004. Mapping permafrost and ground-ice related coastal erosion on Herschel Island, southern Beaufort Sea, Yukon Territory, Canada., M.Sc. thesis, Dept. of Geography, McGill University, Montréal, Canada, 134 pp.

Lewkowicz AG. 1987. Headwall retreat of ground-ice failures, Banks Island, Northwest Territories. Canadian Journal of Earth Sciences 24: 1077-1085.

Lillesand TM and Kiefer RW. 1979. Remote Sensing and Image Interpretation. John Wiley and Sons, Inc, 612 pp.

Mackay JR. 1959. Glacier ice-thrust features of the Yukon coast. Geographical Bulletin. 13: 5-21.

MacKay JR. 1960. Notes on small boat harbours of the Yukon Coast. Geography Bulletin 15: 19-30.

MacKay JR. 1963. Notes on the shoreline recession along the coast of the Yukon Territory. arctic 16: 195-197.

MacKay JR. 1971. The origin of massive icy beds in permafrost, western arctic coast, Canada.

Canadian Journal of Earth Sciences 8 (4):.397-422.

Mackay JR. 1972. The world of underground ice. Annals of the Association of American Geographers 62: 1-22.

Mackay JR. 1986. Fifty years of coastal retreat west of Tuktoyaktuk, District of Mackenzie in Current Research, Part A, Geological Survey of Canada, Paper 86-1A: 727-735.

Makhloufi N, Costard F, Aguirre-Puente J, Costard J, Posado-Cano R and Guillemet G. 1999. Laboratory simulation of thermal erosion : possible application to the pollution problems. Polar Records. 35 (192): 67-72.

McDonald BC and Lewis CP. 1973. Geomorphologic and Sedimentologic Processes of Rivers and Coast, Yukon Coastal Plain. Environmental-Social Committee, Northern Pipelines, Canada; Rept. No. 73-39, 245 pp

McGillivray DG, Agnew TA, McKay GA, Pilkington GR. and Hill MC. 1993. Impacts of climatic change on the Beaufort sea-ice regime: Implications for the arctic petroleum industry. Climate Change Digest CCD 93-01, Environnement Canada: Downsview, Ontario; 36pp.

Maxwell B. 1997. Responding to global climate change in Canada's arctic. Vol. II of the Canada Country Study: Climate impacts and adaptation. Environnement Canada. Downsview, Ontario. 82pp.

Melnikov I, Sherr B, Wheeler P and Welch H. 1998. Preliminary biological and chemical oceanographic evidence for a long-term warming trend in the arctic Ocean (current materials of the SHEBA ice camp, Beaufort Sea) in Report on study of the arctic Change workshop held November 10-12, 1997, University of Washington, Seattle, Washington. 68pp.

Muller SW. 1945. Permafrost of Perennially Frozen Ground and Related Engineering Problems.

U.S. Geological Survey Special Report Strategic Engineering Study 62. Washington, D.C., U.S. Government Printing Office.

Ogorodov SA. 2003. Coastal dynamics in the Pechora Sea under technogenic impact. Berichte zur Polar- und Meeresforschung (Reports on Polar and Marine Research) 443: 74-80.

Osterkamp TE., and Romanovsky VE. 1999. Evidence for warming and thawing of discontinuous permafrost in Alaska. Permafrost and Periglacial Processes, 10(1): 17-37.

Pollard WH. 1989. Buried snowbank ice in the central and northern Yukon Territory. Proceedings, Twenty-Fifth Eastern Snow conference, Québec; 292-297.

Pollard WH. 1990. The nature and origin of ground ice in the Herschel Island area, Yukon Territory. Proceedings, Fifth Canadian Permafrost Conference, Québec; 23-30.

Pollard WH. 1998. arctic Permafrost and Ground ice. In: Weatherhead, E. And Morseth, C.M. (eds.) Chapter 11: Climate Change, Ozone and ultraviolet Radiation. arctic Monitoring and Assessment Program Report.

Pollard W, Omelon C, Couture N, Solomon S. and Budkewitsch P. 2002. Ice content and sensitivity analysis based on landscape interpretation for several sites along the Beaufort Sea coast. Berichte zur Polarforshung und Meeresforschung, 413, 48-52

Rachold V, Eicken H, Gordeev VV, Grigoriev MN, Hubberten H-W, Lisitzin AP, Shegchenko VP and Schirrmeister L (2003). Modern terrigenous organic carbon input to the arctic Ocean. In: Stein, R and Macdonald, R W (Eds.) Organic Carbon Cycle in the arctic Ocean: Present and Past. Springer Verlag, Berlin; 33-55.

Rampton VN. 1982. Quaternary geology of the Yukon coastal plain. Geological Survey of Canada, Bulletin 317.

Reimnitz E and Barnes PW. 1987. Sea-ice influence on arctic coastal retreat. Proceedings, Coastal Sediments 87 (New Orleans). New-York, American Society of Civil Engineers, 1578-91.

Reimnitz E, Barnes PW and Harper JR. 1990. A review of beach nourishment from ice transport of shoreface materials, Beaufort Sea, Alaska. Journal of Coastal Research. 6: 439-470.

Ritter, DF. 1978. Process Geomorphology. WmC Brown Publishers: Dubuque, Iowa. 579pp.

Serreze MC, Walsh JE, Chapin FS III, Osterkamp TE, Dyurgerov M, Romanovsky VE, Oechel WC, Morison J, Zhang T and Barry RG. 2000 Observational evidence of recent change in the northern high-latitude environment. Climatic Change 46: 159-207.

Shumskii PA. 1964. Principles of structural glaciology. (translated from Russian). Dover Publications, New York, 497 pp.

Shumskii PA. and Vtyurin BI. 1966. Underground ice. in Proceedings of the Permafrost International Conference, National Academy of Sciences, Washington, D.C. NRC Publication 1287, 108-113.

Smith CAS, Kennedy CE, Hargrave AE and McKenna KM. 1989. Soil and vegetation of Herschel Island, Yukon Territory. Yukon Soil Survey Report No. 1. Land Resource Research Centre, Agriculture Canada: Ottawa.

Solomon SM. 2002. Tuktoyaktuk Erosion Risk Assessment Report. Geological Survey of Canada, Natural Resources Canada.

Solomon SM. 2004. Spatial and temporal variability of shoreline change in the Beaufort-Mackenzie region, Northwest Territories, Canada. Geo-Marine Letters. In press.

Solomon SM, Forbes DL and Kierstead B. 1994. Coastal Impacts of Climate Change: Beaufort Sea Erosion Study. Canadian Climate Centre, Report 94-2 Environment Canada: Downsview, Ontario, Canada; 34 pp

Solomon SM and Covill R. 1995. Impacts of the September 1993 storm on the Beaufort Sea. Proceedings, 1995 Canadian Coastal Conference, 2: 779-795.

Solomon SM and Manson G. 2003. Coastal Processes and Climate Change along the Canadian Beaufort Sea. Presentation. SEARCH Open Science Meeting, October 27-30, 2003, Seattle, USA.

Van Everdingen R. ed. 1998 revised January 2002. Multi-language glossary of permafrost and related ground-ice terms. Boulder, CO: National Snow and Ice Data Center/World Data Center for Glaciology.

Vassiliev A, Kanevskiy M, Cherkashov G and Vanshtein B. 2004. Coastal Dynamics at the Barents and Kara Sea key sites. Geo-Marine Letters. *Online edition.*

Williams PJ. 1995. Permafrost and climate change: geotechnical implications. Philosophical Transactions, Royal Society of London 352 (1699): 347-358.

Wolfe SA, Kotler E and Dallimore SR. 2001. Surficial characteristics and the distribution of thaw landforms (1970 to 1999), Shingle Point to Kay Point, Yukon Territory. 1970 to 1999), Shingle Point to Kay Point, Yukon Territory.